CARBON DYNAMICS OF AGRICULTURAL AND FOREST ECOSYSTEMS AND REMOTE SENSING

Evaluating Carbon Dynamics of Agricultural and Managed Forest Ecosystems Using Remote Sensing

By Nur Hussain

A Thesis
Submitted to the School of Graduate Studies
In Partial Fulfillment of the Requirements
For the Degree
Doctor of Philosophy

McMaster University © Copyright by Nur Hussain, 2024 DOCTOR OF PHILOSOPHY (2024) McMaster University

(Earth Science) School of Earth, Environment, & Society

Hamilton, Ontario, Canada

TITLE: Evaluating Carbon Dynamics of Agricultural and Managed Forest

Ecosystems Using Remote Sensing

AUTHOR: Nur Hussain

SUPERVISOR: Professor M. Altaf Arain

NUMBER OF PAGES: 178

DEDICATED TO MY PARENTS

AZIZUR RAHMAN AND NASIMA KHATUN

ABSTRACT

Climate change is significantly impacting terrestrial ecosystems through altered environmental conditions and enhanced atmospheric CO₂, which has increased by about 40% since the preindustrial period. Forests, covering about 30% of global land, play a vital role in the carbon (C) cycle by sequestering 15.6 billion tonnes of CO₂ equivalent annually from the atmosphere. The agricultural sector is also a major contributor to atmospheric CO₂, however, it has a net source of C and emits 9.3 billion tonnes of CO₂ equivalent annually, which is about 11% of global emissions. In recent years, advanced remote sensing and eddy covariance (EC) techniques have become vital systems for assessing CO₂ exchanges and providing real-time monitoring capabilities for both forest and agricultural ecosystems. Integration of these techniques would enhance our understanding of C exchanges and their major controls in these ecosystems. It will help to explore how these ecosystems may be impacted by climate change and natural and human-induced disturbance events and develop climate-tailored forest and agricultural management practices to increase their carbon sequestration capabilities.

In this study, high-resolution remote sensing and EC flux measurements made in an agricultural field in Southern Ontario, Canada were used to determine C sequestration or loss capabilities of different crops in the Great Lakes region and explore how they may be impacted by extreme weather events. This study also explored the best forest management practices that can be adopted to enhance carbon sequestration in the temperature conifer plantation forests in the agricultural landscape of Southern Ontario. Furthermore, it determined how the native (deciduous) forest ecosystems of the Great Lakes region may be impacted by natural disturbances (i.e. insect infestation). These agricultural and forest sites are part of the Turkey Point Environmental

Observatory (TPEO) and associated with the Global Water Futures (GWF) program, US-Canada Global Centre for Climate Change and Transboundary Waters, Ameriflux and the global Fluxnet.

In the agricultural site, EC fluxes were continuously measured from 2020 to 2023, when the site was planted with corn, sweet potato and tobacco crops. Net ecosystem production (NEP) of the agricultural site was 485 (corn), 249 (corn), -120 (sweet potato) and 7 (tobacco) g C m⁻² yr⁻¹, respectively from 2020 to 2023. The reduction in NEP for corn in 2021 can be attributed to both the drought conditions in May and August, where precipitation was significantly below the 30-year normal (38 mm in May and 46 mm in August), causing stress during critical growth periods, and the inherent differences in carbon dynamics associated with crop types and their responses to climatic extremes. Corresponding annual evapotranspiration (ET) values were 680, 727, 732 and 715 mm yr⁻¹, which accounted for approximately 60%, 72%, 77% and 73% of the annual total precipitation. Study results showed that overall, the site was a net C sink when corn was planted in 2020 and 2021, a net source of C when sweet potatoes were planted in 2022 and C neural when tobacco was planted in 2023. The grain yields (GY) were 537, 491, 118 and 124 g C m⁻² in 2020, 2021, 2022 and 2023 resulting in annual net ecosystem carbon balance (NECB) of -52 (corn), -242 (corn), -238 (Sweet potato) and -117 (tobacco) g C m⁻² year⁻¹.

High-resolution Sentinel-2 satellite ($10 \times 10 \text{ m}^2$) and drone-observed remote sensing data along with EC fluxes were used to evaluate the effect of five different variable retention harvesting (VRH) treatments on the growth and C uptake of a 90-year-old red pine (*Pinus resinosa Ait.*) plantation (1931) forest, in Southern Ontario, Canada. VRH emulates natural post-disturbance canopy structures to enhance biodiversity and resilience. Treatments included 33% aggregate

(33A), 55% aggregate (55A), 33% dispersed (33D), 55% dispersed (55D), and an unharvested control (CN), each replicated four times in 1 ha plots. From 2010 to 2020, mean daily Normalized Difference Vegetation Index (NDVI) values ranged from 0.25 to 0.86, with 55D showing the highest NDVI values. Satellite-derived annual GPP correlated with observed annual GPP ($R^2 = 0.88$, p = 0.032) in an adjacent white pine plantation forest. These GPP estimates indicated that VRH treatment with dispersed residual canopies retaining over half the initial basal area (i.e 55D) was the most optimized management strategy that can be deployed for forest growth and C uptake to mitigate climate change. Overall, the mean annual GPP for the 20-ha site was 1651 ± 89 g C m⁻² year⁻¹, ranging from 1407 to 1864 g C m⁻² year⁻¹.

Finally, high-resolution Sentinel-2 satellite remote sensing and EC observation were employed to investigate the impact of 2021 spongy moth (*Lymantria dispar*) infestation on forest productivity and C losses in the deciduous and mixed forests across Southern Ontario. Results showed a significant reduction in leaf area index (LAI) and GPP values. Growing season mean LAI values for deciduous (mixed) forests across the region were 3.66 (3.18), 2.74 (2.64), and 3.53 (2.94) m² m⁻² in 2020, 2021, and 2022, respectively, indicating approximately 24 (14)% reduction in LAI compared to pre- and post-infestation years. Similarly, growing season GPP values in deciduous (mixed) forests across the region were 1338 (1208), 868 (932), and 1367 (1175) g C m⁻², respectively in 2020, 2021, and 2022, showing about 35 (22)% reduction in GPP in 2021 compared to pre- and post-infestation years. This infestation-induced reduction in GPP of deciduous and mixed forests, when upscaled to the whole study area (178,000 km²), resulted in 21.1 (21.4) Mt of C loss compared to 2020 (2022), respectively from Sothern Ontario alone. It shows the large scale of C losses caused by 2021 infestation in Canadian Great Lakes region.

This dissertation improved our understanding of C exchanges in the forest and agriculture ecosystem within the Great Lakes region of North America. The methods developed in this study offer valuable tools to assess and quantify C uptake capabilities and natural disturbance impacts on the regional C balance of forest ecosystems by integrating field observations, high-resolution remote sensing data and models. Study results will also help in developing sustainable forest management practices to achieve net-zero C emission goals through nature-based climate change solutions.

ACKNOWLEDGEMENTS

I extend my sincere appreciation to Dr. Altaf Arain, my supervisor, for affording me the opportunity and financial support to pursue my Ph.D. within his esteemed research group at McMaster University. I am deeply thankful for his unwavering guidance, enduring patience, and continual encouragement throughout the years. I am particularly grateful for his invaluable advice and steadfast support in preparing me for the path ahead.

Gratitude is also extended to the esteemed members of my Ph.D. committees, Dr. Shusen Wang and Dr. Alemu Gonsamo, for generously offering their time, encouragement, and insightful guidance. I wish to thank William C. Parke for his counsel in the study of the impact of Variable Retention Harvesting Treatments on carbon uptake. I express my thanks to Natural Resources Canada – Canada Centre for Remote Sensing for providing the drone instrument and to the dedicated team of Francis Canisius and Sylvain G. Leblanc for their assistance in operating the drone and facilitating data collection.

Grateful recognition is given to everyone associated with the McMaster Hydrometeorology and Climatology Research Group at McMaster University, including Dr. Shawn, Tariq Deen, Muhammad Rizwan, Elizabeth Arango Ruda, Daniel Mutton, Farbod Tabaei, Lejla Latifovic, Noah Stegman, and Liam Kreibich, for the enriching experiences over the years. Special thanks are reserved for Jay Brodeur for contributing to Flux data analysis management. I thank Frank de Leebeck for generously granting access to his agricultural farm and property. Additional thanks to my friends Mehedi Hassan, Fehzan Saleem, Md Rasel Sheikh and Araf Al Rafi. I appreciate the solid support from SGES staff and faculty, specifically to Salomé Santos-Blaguski.

I am profoundly grateful to my closest friends and family for their enduring encouragement and belief in the possibility of this journey. To my parents, I extend heartfelt thanks for supporting my pursuit of education despite the geographical distance and for your boundless love. Lastly, a special thank you to my beloved wife, Sumaya Rahman Prova. Your belief in me, constant encouragement, and unwavering support have been instrumental at every step of this challenging journey.

TABLE OF CONTENTS

TITLE PAGE	i
DESCRIPTIVE NOTE	ii
DEDICATION	iii
ABSTRACT	iv
ACKNOWLEDGEMENTS	vii
TABLE OF CONTENTS	ix
LIST OF FIGURES	xii
LIST OF TABLES	XV
PREFACE	XV
CHAPTER 1: INTRODUCTION	1
1.1 Changing Climate	1
1.2 Agricultural Ecosystem and Climate Change	1
1.3 Forest Ecosystem and Climate Change.	2
1.4 Extreme Weather Event and Climate Change	3
1.5 Novelty of Study	4
1.6 Objectives of study	6
1.7 Study Sites	7
1.8 Overview of Methodology	7
1.9 References.	11
CHAPTER 2: CARBON, WATER AND ENERGY FLUXES IN AN	
AGRICULTURAL FIELD IN THE GREAT LAKES REGION IN CANADA	17
2.1 Abstract	17
2.2 Introduction.	18
2.3 Methods	21
2.3.1 Site description.	21
2.3.2 Flux and meteorological data measurements, quality control and gap filling	22

2.4 Results	25
2.4.1 Meteorological Conditions	25
2.4.2 Energy flux dynamics	26
2.4.3 Carbon flux dynamics	28
2.4.4 Water flux dynamics	30
2.4.5 Water and light use efficiency	31
2.4.6 Environmental controls on carbon and water fluxes	32
2.5 Discussion.	33
2.5.1 Energy and water flux dynamics	33
2.5.2 Carbon flux dynamics	35
2.6 Conclusion.	39
2.7 Acknowledgment	41
2.8 References	42
CHAPTER 3: EVALUATING THE EFFECTIVENESS OF DIFFERENT VARIABLE RETENTION HARVESTING TREATMENTS ON FOREST CARBON LIPTAKE USING REMOTE	
UPTAKE USING REMOTE	
SENSING	67
3.1 Abstract	67
3.2 Introduction	68
3.3 Methods	71
3.3.1 Site description	71
3.3.2 Data Set	72
3.3.2.1 Satellite data	72
3.3.2.2 Drone instrumentation and data retrieval	73
3.3.2.3 Eddy covariance flux and meteorological	74
3.3.3 Satellite GPP estimates	74
3.3.4 Statistical analysis	74
3.4 Results	76
3.4.1 Climate	76
3.4.2 Effects of variable retention harvesting on forest growth	77

3.4.3 Effect of variable retention harvesting treatments	79
3.5 Discussion.	80
3.5.1 Effect of variable retention harvesting on forest growth	80
3.5.2 Study limitations	83
3.6 Conclusions	84
3.7 Acknowledgment	85
3.8 References.	86
3.9 Supplementary	96
3.9.1 Remote Sensing Indices	96
3.9.2 Remote Sensing GPP	96
CHAPTER 4: ASSESSMENT OF SPONGY MOTH INFESTATION IMPACTS ON	
FOREST PRODUCTIVITY AND CARBON LOSS USING THE SENTINEL-2	
SATELLITE REMOTE SENSING AND EDDY COVARIANCE FLUX DATA	110
4.1 Abstract	110
4.2 Introduction	111
4.3 Materials and Methods	114
4.3.1 Study area	114
4.3.2 Remote sensing and observed eddy covariance flux datasets	116
4.3.3 Land use and land cover (LULC) classification	117
4.3.4 Retrieval of leaf area index (LAI)	118
4.3.5 Remote sensing-based gross primary productivity (GPP)	119
4.3.6 Statistical analysis	120
4.4 Results	122
4.4.1 Climatic conditions	122
4.4.2 Dynamics of remote sensing-based leaf area index (LAI)	123
4.4.3 Impact of spongy moth infestation on (GPP)	123
4.5 Discussion	126
4.6 Conclusion	129
4.7 Acknowledgement	130
4.8 References	131

CHAPTER 5: SUMMARY AND CONCLUSIONS	155
5.1 Summary of Results and Their Significance	155
5.2 Study Limitations	157
5.3 Suggestions for Future Research	157
5.4 Conclusions	159
5.5 References	160

LIST OF FIGURES

Figure 2.1	The annual course of the meteorological conditions at Turkey Point	
	Agricultural site for 2020 to 2023	59
Figure 2.2	Daily values of turbulent fluxes $(H + LE)$ vs radiative fluxes $(Rn - G)$	60
Figure 2.3	The monthly mean energy fluxes for 2020, 2021, 2022 and 2023	61
Figure 2.4	Daily values of net ecosystem productivity, NEP (a-d) and	
	evapotranspiration, ET (e-h) values for 2020, 2021, 2022 and 2023	62
Figure 2.5	The cumulative values of (a) GEP and RE and (b) NEP for 2020, 2021,	
	2022 and 2023	63
Figure 2.6	Water use efficiency (WUE) from 2020 to 2023.	64
Figure 2.7	The relationship between Gross Primary Production (GEP) and	
	Photosynthesis Active Radiation (PAR) across different crops	65
Figure 2.8	Principal component analysis (PCA) of environmental controls with	
	panels: (a) for GEP, (b) for NEP, (c) for RE, and (d) for ET	66
Figure 3.1	a) Location map of Canada	
	b) Southern Ontario regional map and	
	c) Aerial view of the VRH treatment plots	100
Figure 3.2	Workflow of the data analysis to estimate satellite GPP	101
Figure 3.3	Time series of meteorological variables from 2010 to 2020	102
Figure 3.4	Yearly cumulative total precipitation (P) from 2010 to 2020	103
Figure 3.5	Spatiotemporal patterns of mean daily NDVI by moth	104
Figure 3.6	a) Time series of mean daily NDVI	
	b) time series of mean daily GPP	105
Figure 3.7	NDVI contribution to principal component analysis (PCA) for each	
	variable retention harvesting treatment from 2014 to 2020	106
Figure 3.8	Comparison of mean daily NDVI for all VRH treatments	107
Figure 3.9	a-e) Satellite-derived gross primary productivity (GPP) and	
	f) GPP from eddy covariance flux measurements	108
Figure 3.10	a) Mean daily GPP for each treatment and	
	b) box plot of post-harvest daily mean GPP	109

Figure 4.1	Study area map	146
Figure 4.2	Defoliated tree due to spongy moth infestation	147
Figure 4.3	The relationship between Satellite-derived and Eddy Covariance (EC)	
	flux tower-based observed daily GPP values	148
Figure 4. 4	Daily mean values of	
	a) photosynthetically active radiation (PAR),	
	b) air temperature (Ta) and soil temperature (Ts) at 5cm depth,	
	c) vapor pressure deficit (VPD) and	
	d) precipitation (P) and volumetric water content (VWC)	149
Figure 4.5	Daily cumulative precipitation (P) from 2020 to 2022	150
Figure 4.6	Monthly mean LAI values over the study area	151
Figure 4.7	a-d) Daily GPP values	
	e-h) Cumulative GPP values over the growing season	152
Figure 4.8	The daily standardized anomaly in GPP	153
Figure 4.9	The spongy moth outbreak areas in 2021.	154

LIST OF TABLES

Table 2.1	Monthly and annual total precipitation (P) values and Temperature (T) in	
	2020, 2021, 2022 and 2023	55
Table 2.2	Annual and growing season (GS) total GEP, NEP, RE and ET. GEP, NEP,	
	RE, Grain yield (GY) and net ecosystem carbon balance (NECB) values	
	in g C m ⁻² and ET values in mm.	56
Table 2.3	Correlation coefficients of climatic variables (PAR, Ta, Ts, VPD, VWC)	
	with biomass production (GEP), carbon uptake (NEP), and water balance	
	of ET across different crops from 2020 to 2023.	57
Table 2.4	Annual NEP of the corn crop in different study sites of North America	58
Table 3.1	Mean annual photosynthetically active radiation (PAR), air temperature	
	(Tair), daily mean vapor pressure deficit (VPD) and total annual	
	precipitation (P) and growing season	98
Table 3.2	a) Daily mean NDVI (+ 1 SD) for the growing season,	
	b) Annual total GPP (g C m-2 y-1) for each treatment and	
	c) Observed annual total GPPEC (g C m-2 y-1) using EC flux	99
Table 4.1	Confusion matrices-based accuracy assessment of land use and land	
	cover (LULC) classification.	141
Table 4.2	Input parameters set for the PROSAIL model.	142
Table 4.3	Equations have been used for ecosystem properties	143
Table 4.4	Mean daily GPP of different vegetation types in the growing season	145

PREFACE

This doctoral dissertation includes three main chapters that has either been published as a paper in peer-reviewed journal or manuscripts that has either been submitted or are ready for submission to a journal. These papers or manuscripts used remote sensing data and EC fluxes from the Turkey Point Environmental Observatory (TPEO). Although there is some overlap in the information, such as the description of study sites and methodology, each chapter has specific objectives supporting main study gaol of providing the insight into carbon uptake capabilities and dynamics of the agricultural and forest ecosystems of the Great Lakes region. Summary of all four main chapters and contributions from the PhD candidate and any collaborators or co-authors are summarized in the following section.

Chapter 2

Title: Carbon, water and energy fluxes in an agricultural field with crop rotations in the Great Lakes region

Authorship: M. Altaf Arain, Nur Hussain, Liam Kreibich, Jason Brodeur and Zoran Nesic

Status: To be submitted to Agriculture and Forest Meteorology in Fall 2024.

Candidate's Contribution: As Principal Investigator (PI) of the project, M Altaf Arain secured funding and established this agricultural flux tower site in the summer of 2020. Nur Hussain, PhD candidate played a key role in flux and meteorological data collection and data analysis. The candidate wrote the first draft of the manuscript. Altaf Arain contributed to fieldwork and solely maintained the operation of this flux site during the COVID-19 pandemic. He also offered valuable ideas for data analysis and plotting figures and edited several versions of the draft manuscripts. Liam Kreibich took over field work responsibilities and helped in data collection in 2023. Jason

School of Earth, Environment, & Society

Ph.D. Thesis – Nur Hussain

Brodeur contributed in data analysis and data quality control. Zoran Nesic helped with the

establishment and operation of flux sites and data quality control.

Chapter 3

Title: Evaluating the effectiveness of different variable retention harvesting treatments on forest

carbon uptake using remote sensing.

Authorship: Nur Hussain, M. Altaf Arain, Shusen Wang, William C. Parker and Ken A. Elliott

Status: Published.

Full Reference: Hussain, N., Arain, M. A., Wang, S., Parker, W. C., & Elliott, K. A. (2024).

Evaluating the effectiveness of different variable retention harvesting treatments on forest carbon

uptake using remote sensing. Remote Sensing Applications: Society and Environment, 33, 101124.

Candidate's Contribution: Nur Hussain, PhD candidate, collected and analyzed remote sensing

data and wrote first draft of the manuscript. M. Altaf Arain provided valuable ideas for data

analysis and edited draft manuscripts. William C. Parker, Ken A. Elliott and Shusen Wang

provided valuable suggestions to enhance the quality of the manuscript and helped in editorial

work.

Chapter 4

Title: Assessment of spongy moth infestation impacts on forest productivity and carbon loss using

the Sentinel-2 satellite remote sensing and eddy covariance flux data.

Authorship: Nur Hussain, Alemu Gonsamo, Shusen Wang and M. Altaf Arain

xvii

Status: Published.

Full Reference: Hussain, N., Gonsamo, A., Wang, S., & Arain, M. A. (2024). Assessment of spongy moth infestation impacts on forest productivity and carbon loss using the Sentinel-2 satellite remote sensing and eddy covariance flux data. Ecological Processes, 13(1), 37.

Candidate's Contribution: Nur Hussain, PhD candidate, played a primary role in collecting and analyzing remote sensing data and wrote the first draft of the manuscript. Altaf Arain contributed in the collection of flux and meteorological data and provided insight in data analysis. He also edited draft manuscripts and provided feedback during the writing process. Alemu Gonsamo offered valuable suggestions and ideas to enhance the scientific contributions of the manuscript.

CHAPTER 1

INTRODUCTION

1.1 Changing Climate

In the last few decades, the global climate has changed rapidly. According to the Intergovernmental Panel on Climate Change (IPCC) Fifth Assessment Report, the global temperature increased by 0.85 °C between 1880 and 2015. From 1951 to 2015, the rate of change was 0.12 °C per decade, which is twice as much as from 1880 to 2015 (IPCC, 2014). Recently, North Hampshire has experienced fast warming due to global climate change (IPCC, 2013). The yearly average temperature in Northern Hampshire increased by almost twice the global average temperature increase rate (Vincent et al., 2015). In Canada, the entire country has seen an average increase of 1.78°C over the past 65 years, while the southern region of Canada has experienced an average warming of 1.68°C. These climate changes are negatively impacting ecosystems, especially forests and agriculture.

1.2 Agricultural Ecosystem and Climate Change

The increase in atmospheric CO₂ is a major contributing factor in human-induced climate warming (Myhre et al., 2013; Lynch et al., 2021). CO₂ levels in the air have increased by about 40% compared to levels before the industrialization (IPCC, 2013). The agriculture systems contribute substantially to this increase in atmospheric CO₂, releasing 9.3 billion tonnes of carbon dioxide equivalent (CO₂eq), constituting roughly 11% of the total annual global CO₂ emissions (Gilbert, 2012; Mbow et al., 2017; Lamb et al., 2021; Lynch et al., 2021). In Canada, agriculture significantly contributes to the country's overall CO₂ emissions, emitting approximately 10% of the total national emissions of 729 Mt CO₂eq (Fouli et al., 2021).

Although, Canadian agriculture systems have acted both, a C sink and a C source, depending on the geographic region and crop type (Gregorich et al., 2005; Laamrani et al., 2021), they have potential for playing an important role in curbing CO₂ emissions and serve as substantial C reservoirs to mitigate climate change, if adequate climate tailored management practices are deployed (Horowitz and Gottlieb, 2010).

1.3 Forest Ecosystem and Climate Change

Forest ecosystems cover about 30% of the land surface and they play a vital role in the global C cycle (Heino et al., 2015; Ontl et al., 2016; Reichstein and Carvalhais, 2019). These ecosystems, actively contribute to the global C cycle through photosynthesis and ecosystem respiration (FAO, 2010). The balance between these major CO₂ exchanges determines whether the forest is net C sink or a source and how efficiently photosynthesis is turned into net biomass growth and C uptake (DeLucia et al., 2007; Litton et al., 2007). On a larger scale, the increase in biomass from photosynthesis is characterize as gross primary production (GPP). Forests consistently show high levels of GPP, making them Earth's most substantial C absorbers and C reservoirs (Peters et al., 2007; Pan et al., 2011). Forests in North America are expected to contribute around 76% to the region's net terrestrial C storage (Hayes et al., 2012). Regarding Canada's forest ecosystems, their role in the C cycle varies across different time scales, ranging from annual to centennial. Historically, Canada's forests have demonstrated a pattern of C absorption, averaging 173 million metric tons of C (MtC) per year over much of the past century (Hengeveld et al., 2008), although this rate can be influenced by periodic disturbance events such as wildfires or insect infestations.

Global climate change poses a major challenge to terrestrial ecosystems (Gabaldón-Leal et al., 2016; IPCC, 2014). Warming climate have led to significant changes in forest ecosystems (Seppälä, 2009). It has contributed to lower growth rates and increased tree mortality due to drought, heat, and soil moisture scarcity. These threats may be further intensified by additional ecological shifts, such as elevated concentrations of low-altitude ozone, the deposition of nitrogenous pollutants, the emergence of exotic pests and pathogens, environmental disruption, and heightened disturbances like fires (Keenan, 2015). The continued impacts of climate change could significantly contribute to the degradation of forests. Anticipated future changes may lead to the relocation of tree species, transformations in ecological regions, alterations in terrestrial ecosystem function, and the potential restructuring of ecosystems' productivity following disturbances related to ongoing climate change. In Canada, the composition of forest cover has undergone rapid changes in recent decades due to both human activities and other disruptions, leading to spatial and temporal variations in Canada's forested areas caused by anthropogenic activities.

1.4 Climate Change and Extreme Weather Event

Extreme weather events include unusually high temperatures, heavy rainfall, and prolonged and severe droughts. Climate warming can lead to increase in the frequency and intensity of extreme weather events such as storms, flooding, droughts, and wildfires, as well as insect outbreaks of pests and diseases (IPCC, 2014; Beach et al., 2015). It can also cause major changes in the spatial and temporal distribution of precipitation. These changes are likely to affect the future productivity of agriculture and forestry (Diffenbaugh et al., 2012).

However, extreme weather events are expected to become more severe in the future. They will cause forest degradation through multiple way such as increased wildfires and infestations. Both of these natural disturbances have significantly impacted C fluxes and C storage in Canada's forests in recent years, in particular insect infestations which has impacted large areas in the both western (mountain pine beetle) and eastern (Spongy moth) parts of the country (Kurz et al., 2002). In eastern Canada, 595 million hectares of potential areas are climatically suitable for the future spongy moth outbreak, which may substantially impact terrestrial C sequestration (Gray, 2004). However, temporary and unpredictable nature poses natural disturbances, particular insect infestation poses challenges for their effective monitoring and management (De Beurs & Townsend, 2008).

Research conducted in this PhD dissertation has helped to enhance our understanding of C exchange processes in agricultural and forest ecosystems, develop advanced monitoring capabilities by integrating micrometeorology and remote sensing techniques and provide an assessment of the best forest management practices to enhance growth and C sequestration in changing climate.

1.5 Novelty of the Study

Agriculture, the primary land use in Southern Ontario, plays a crucial role in the national economy and is vulnerable to climate extremes (Gabriel et al., 1993; Smith, 2015; Yusa et al., 2015; Lesk et al., 2016; Zafiriou et al., 2023). The agriculture sector contributed about 15% of the national net farm income (Statistics Canada, 2018). Corn is the main crop, grown on an average of 887,000 hectares each year (OMAFRA, 2017), which can improve the regional ecosystem, aid in climate change mitigation, and contribute to C sequestration. Southern

Ontario is an important ecological and economic (both agricultural and industrial) region of the country. This PhD study provided valuable insights into C flux dynamics in different crops in this region. Continuous monitoring of energy, water, and C fluxes, along with climatic variables across various crops, will provide crucial data for formulating strategies to tackle climate change through C sequestration in agricultural fields. Additionally, it will offer insights into the impacts of extreme weather events on crop ecosystems and food production and food security in the Great Lakes region.

In addition, nature-based climate solutions, encompassing enhanced forest C uptake through management and conservation, are proposed as cost-effective measures to address climate change (Kaarakka et al., 2021; Creutzig et al., 2022; Marvin et al., 2023). In Canada, 66% of forests undergo active management, with variable retention harvesting (VRH) being suggested as a key approach to manage these forests (Natural Resources Canada (NRC), 2016). VRH, originally designed to reduce clearcutting and promote stand regeneration, has been extensively studied for its impacts on biodiversity and ecosystem processes. Remote sensing techniques provide a valuable opportunity for assessing changes in forest structure and evaluating the effectiveness of management practices in enhancing growth and C sequestration. This PhD dissertation have provided framework for the integration ground-based flux tower and remote sensing techniques to provide an assessment of the best forest management practices to enhance growth and C sequestration in changing climate. It also used this framework to provide a regional assessment of C losses due to record 2021 Spongy month infestation in southern Ontario, providing vital data for C budget assessments for forest managers and policy makers.

1.6 Objectives of the study

Forest and agricultural ecosystems are a major player in the global carbon cycle. They face many challenges due to climate change and extreme weather events such as heat, drought, and soil moisture scarcity. The primary study objective of this study is to examine the influence of climate variability on C exchanges in agricultural and managed forest ecosystems in southern Ontario in the Great Lakes region. Specific objectives include:

- (1) Continuously measure C fluxes and meteorological variables in an agricultural site in Southern Ontario and evaluate how these C exchanges may respond to extreme weather conditions such as drought and heat waves. Determine major environmental controls and investigate seasonal and annual dynamics of crop productivity, C sequestration and water use efficiency.
- (2) Evaluate the impact of different forest management regimes or thinning patterns on the growth and productivity of a managed forest ecosystem. Explore the effectiveness of various forest management treatments such as variable retention harvesting (VRH) in enhancing forest C uptake and resilience to extreme weather events and climate change.
- (3) Determine seasonal variations and trends in the leaf area index (LAI) using high-resolution remote sensing data. Also, determine forest photosynthetic uptake and GPP using observed eddy covariance flux and remote sensing data and quantify C losses across the region because of this widespread and severe spongy moth infestation of 2021.

1.7 Study Sites

This dissertation involved making flux and meteorological measurements at the Turkey Point Environmental Observatory (TPEO), located near the northern shore of Lake Erie in southern Ontario, Canada. Eddy covariance (EC) flux measurements of CO₂, water vapor, and energy, were made at a newly established agricultural flux tower site known as TPAg or CA-TPAg (Ameriflux notation) from 2020 to 2023. Similar EC flux, meteorological, and ecological measurements were also made in three different ages (84-, 49-, and 21-year old as of 2023) of conifer forest since 2002 and a deciduous (>90-year old) forest since 2012. TPEO is one of the few sites in Ameriflux and global Fluxnet with long-term (>20 years) flux data availability. The addition of the agricultural site at TPAg has expanded the representation of TPEO to all major biomes in the Great Lakes region, covering coniferous and deciduous forests, as well as agricultural crops. The forest sites are abbreviated as TP02, TP74, TP39, and TPD, referring to 'Turkey Point' followed by the year of stand establishment (i.e., 2002, 1974, 1939), with TPD (Turkey Point Deciduous) as an exception. Turkey Point Observatory is part of the Global Water Futures (GWF) program, Ameriflux, global Fluxnet and US-Canada Global Centre for Climate Change and Transboundary Waters. In the global Fluxnet archives and literature, the Turkey Point Observatory sites are denoted as CA-TP1, CA-TP3, CA-TP4, and CA-TPD for the 17-, 45-, 80-year-old pine forests, and >90-year-old deciduous forest, respectively. Detailed information on site characteristics, instrumentation, and measurements is provided in the individual chapters.

1.8 Overview of Methodology

Half-hourly measurements of CO₂ flux (Fc) and energy fluxes (H, LE, G, and Rn) were conducted from June 2020 to December 2022 using an open-path Eddy Covariance (EC)

system with a sonic anemometer (model CSAT3, Campbell Scientific Inc.) and an infrared gas analyzer (IRGA, model LI-7500, Li-COR Inc.) in the agricultural site. Similar flux data were measured int the forest sites using closed-path EC system (comprising Li-7200 or Li-7000 gas analyzers and CSAT3 sonic anemometer), since 2023 in conifer forests and since 2012 in deciduous forest. Solar radiation, photosynthetically active radiation (PAR), air temperature, relative humidity, wind speed and direction, atmospheric pressure, precipitation and soil temperature and soil water content at several depths were also measure at all these sites.

To determine environmental controls on daily variation of C fluxes and evapotranspiration (ET), the gap-filled and non-gap-filled data were used. EC flux and meteorological data were quality controlled by using the Biometeorological Analysis, Collection, and Organizational Node (BACON) software developed by our Lab (Brodeur, 2014). The marginal distribution sampling (MDS) method by Reichstein et al. (2005) fills gaps in NEE time series using covariance with meteorological variables and auto-correlation over time. It averages NEE measurements under similar environmental conditions within a set period, expanding the search if no suitable data are found. This study modified the method to estimate NEE for all half-hour intervals, including those with data, to create a complete time series and evaluate gap-filling performance comprehensively. Small gaps in meteorological data within a few hours were filled using linear interpolation from the same site. For larger data gaps, missing meteorological variables were estimated using backtracking linear regression with data from adjacent forest sites, based on information from the nearest flux station located approximately 700 meters away.

The partitioning of net ecosystem exchange (NEE) into respiration (RE) and gross ecosystem productivity (GEP) was carried out using the approach described by Peichl et al. (2010). RE was estimated as equivalent to NEE during nighttime (PAR < 100 μ mol m⁻² s⁻¹). These nighttime RE values were used to construct a continuous RE time series based on soil temperature at 5 cm (Ts_{5cm}) and soil moisture at 0-30 cm (θ _{0-30cm}), employing temperature response parameters (R₁₀ and Q₁₀) to describe the RE-Ts5cm relationship, adjusted by a soil moisture function as outlined by Brodeur (2014).

$$RE = R_{10} \times Q_{10}^{\frac{(Ts_5 - 10)}{10}} \times \frac{1}{[1 + \exp(a_1 - a_2 \theta_{0 - 30cm})]}$$
(1.1)

$$GEP = \frac{\alpha RARd \ Amax}{\alpha RARd - Amax} \times f(T_s) \times VPD \times f(\theta_{0-30 \text{cm}})$$
 (1.2)

where, R_{10} and Q_{10} are fitted temperature response parameters that characterize the relationship between RE and soil temperature (T_s). The function $\theta_{0-30\text{cm}}$ is a sigmoidal function representing the impact of soil moisture at 30 cm depth. The remaining terms account for the scaling effects of GEP in relation to Ts, vapor pressure deficit (VPD), and soil moisture at 0-30 cm ($\theta_{0-30\text{cm}}$).

Sentinel-2A and Sentinel-2B (S2), part of the COPERNICUS satellite systems, offer high-resolution datasets for global terrestrial ecosystem monitoring (Drusch et al., 2012; Löw & Koukal, 2020; Li et al., 2022). The Sentinel-2 multispectral instrument (MSI) system provides 13 spectral bands, including 10 m spatial resolution for visible and near-infrared (NIR) and 20 m spatial resolution for Short-Wave Infrared (SWIR) spectrum (Drusch et al., 2012; Maselli et al., 2020; Sun et al., 2021; Bossung et al., 2022). This study used Sentinel-2 data to calculate vegetation indices (VIs) like NDVI and LAI for biomass estimation and GPP for C uptake. LAI was estimated using the PROSAIL model, a combination of PROSPECT (Jacquemoud and

Baret, 1990; Feret et al., 2008) and SAIL models (Verhoef, 1984). GPP was estimated using the Sentinel-2-based LUE model to quantify the CO₂ uptake from different vegetation types. LUE can empirically estimate GPP (Zhang et al., 2017; Sun et al., 2019; Xie et al., 2019) using remote sensing data. Observed air temperature (Tair) and photosynthetic active radiation (PAR) data were used with satellite data in the LUE model to calculate GPP.

1.9 References

- Beach, R. H., Cai, Y., Thomson, A., Zhang, X., Jones, R., McCarl, B. A., ... & Boehlert, B. (2015). Climate change impacts on US agriculture and forestry: benefits of global climate stabilization. Environmental Research Letters, 10(9), 095004.
- Bossung, C., Schlerf, M., & Machwitz, M. (2022). Estimation of canopy nitrogen content in winter wheat from Sentinel-2 images for operational agricultural monitoring. Precision Agriculture, 1-24.
- Brodeur, J. (2014). Data-driven approaches for sustainable operation and defensible results in a long-term, multi-site ecosystem flux measurement program (Doctoral dissertation). McMaster University, Hamilton, ON-Canada.
- Creutzig, F., Niamir, L., Bai, X., Callaghan, M., Cullen, J., Díaz-José, J., ... & Ürge-Vorsatz, D. (2022). Demand-side solutions to climate change mitigation consistent with high levels of well-being. Nature Climate Change, 12(1), 36-46.
- De Beurs, K. M., & Townsend, P. A. (2008). Estimating the effect of gypsy moth defoliation using MODIS. Remote Sensing of Environment, 112(10), 3983-3990.
- De Lucia, E. H., Drake, J. E., Thomas, R. B., & Gonzalez-Meler, M. I. Q. U. E. L. (2007). Forest carbon use efficiency: is respiration a constant fraction of gross primary production? Global Change Biology, 13(6), 1157-1167.
- Diffenbaugh, N. S., Hertel, T. W., Scherer, M., & Verma, M. (2012). Response of corn markets to climate volatility under alternative energy futures. Nature climate change, 2(7), 514-518.
- Drusch, M., Del Bello, U., Carlier, S., Colin, O., Fernandez, V., Gascon, F., ... & Bargellini, P. (2012). Sentinel-2: ESA's optical high-resolution mission for GMES operational services. Remote sensing of Environment, 120, 25-36.
- FAO (Food Agric. Organ. UN). 2010. Global forest resources assessment 2010: main report. FAO For. Pap. 163, FAO, Rome.
- Feret, J. B., François, C., Asner, G. P., Gitelson, A. A., Martin, R. E., Bidel, L. P., ... & Jacquemoud, S. (2008). PROSPECT-4 and 5: Advances in the leaf optical properties model separating photosynthetic pigments. Remote sensing of environment, 112(6), 3030-3043.

- Fouli, Y., Hurlbert, M., & Kröbel, R. (2021). Greenhouse Gas Emissions from Canadian Agriculture: Estimates and Measurements. SPP Briefing Paper, 14, 35.
- Gabaldón-Leal, C., Webber, H., Otegui, M. E., Slafer, G. A., Ordóñez, R. A., Gaiser, T., ... & Ewert, F. (2016). Modelling the impact of heat stress on maize yield formation. Field Crops Research, 198, 226-237.
- Gabriel, A. O., & Kreutzwiser, R. D. (1993). Drought hazard in Ontario: A review of impacts, 1960–1989, and management implications. Canadian Water Resources Journal, 18(2), 117-132.
- Gilbert, N. (2012). One-third of our greenhouse gas emissions come from agriculture. Nature, 31, 10-12.
- Gray, D. R. (2004). The gypsy moth life stage model: landscape-wide estimates of gypsy moth establishment using a multi-generational phenology model. Ecological Modelling, 176(1-2), 155-171.
- Gregorich, E. G., Rochette, P., VandenBygaart, A. J., & Angers, D. A. (2005). Greenhouse gas contributions of agricultural soils and potential mitigation practices in Eastern Canada. Soil and Tillage Research, 83(1), 53-72.
- Hayes, D. J., Turner, D. P., Stinson, G., McGuire, A. D., Wei, Y., West, T. O., ... & Cook, R.
 B. (2012). Reconciling estimates of the contemporary North American carbon balance among terrestrial biosphere models, atmospheric inversions, and a new approach for estimating net ecosystem exchange from inventory-based data. Global Change Biology, 18(4), 1282-1299.
- Hengeveld, H., Braithwaite, L., Desjardins, R., Gorjup, J., & Hall, P. (2008). Enhancement of greenhouse gas sinks: a Canadian science assessment, Atmospheric Science Assessment and Integration, Environment Canada, Toronto, Ontario.
- Horowitz, J., & Gottlieb, J. (2010). The Role of Agriculture in Reducing Greenhouse Gas Emission. United States Department of Agriculture, 15 (September), 2-8
- Heino, M., Kummu, M., Makkonen, M., Mulligan, M., Verburg, P.H., Jalava, M., Räsänen, T.A., 2015. Forest loss in protected areas and intact forest landscapes: A global analysis. PLoS ONE, 10, e0138918. https://doi.org/10.1371/journal.pone.0138918.
- IPCC, (2013). Summary for Policymakers. In: Climate Change 2013: The Physical Science Basis. Contribution of Working Group I to the Fifth Assessment Report of the

- Intergovernmental Panel on Climate Change. Cambridge University Press, Cambridge, United Kingdom and New York, NY, USA.
- IPCC (2014). Climate Change 2014: Impacts, Adaptation and Vulnerability. Part A: Global and Sectoral Aspects. Contribution of Working Group II to the Fifth Assessment Report of the Intergovernmental Panel on Climate Change ed C B Field et al. (Cambridge: Cambridge University Press) p 1132.
- Jacquemoud, S., & Baret, F. (1990). PROSPECT: A model of leaf optical properties spectra. Remote sensing of Environment, 34(2), 75-91.
- Kaarakka, L., Cornett, M., Domke, G., Ontl, T., Dee, L. E., 2021. Improved forest management as a natural climate solution: A review. Ecol. Solut. Evid. 2, e12090. https://doi.org/10.1002/2688-8319.12090
- Keenan, R.J., 2015. Climate change impacts and adaptation in forest management: a review. Ann. For. Sci. 72, 145–167. https://doi.org/10.1007/s13595-014-0446-5
- Kurz, W. A., Apps, M., Banfield, E., & Stinson, G. (2002). Forest carbon accounting at the operational scale. The Forestry Chronicle, 78(5), 672-679.
- Laamrani, A., Voroney, P. R., Gillespie, A. W., & Chehbouni, A. (2021). Development of a land use carbon inventory for agricultural soils in the Canadian province of Ontario. Land, 10(7), 765.
- Lamb, W. F., Wiedmann, T., Pongratz, J., Andrew, R., Crippa, M., Olivier, J. G., ... & Minx, J. (2021). A review of trends and drivers of greenhouse gas emissions by sector from 1990 to 2018. Environmental research letters, 16(7), 073005.
- Lesk, C., Rowhani, P., & Ramankutty, N. (2016). Influence of extreme weather disasters on global crop production. Nature, 529(7584), 84-87.
- Litton, C. M., Raich, J. W., & Ryan, M. G. (2007). Carbon allocation in forest ecosystems. Global Change Biology, 13(10), 2089-2109.
- Li, M., Shamshiri, R. R., Weltzien, C., & Schirrmann, M. (2022). Crop Monitoring Using Sentinel-2 and UAV Multispectral Imagery: A Comparison Case Study in Northeastern Germany. Remote Sensing, 14(17), 4426.
- Löw, M., & Koukal, T. (2020). Phenology modelling and forest disturbance mapping with sentinel-2 time series in Austria. Remote Sensing, 12(24), 4191.

- Lynch, J., Cain, M., Frame, D., & Pierrehumbert, R. (2021). Agriculture's contribution to climate change and role in mitigation is distinct from predominantly fossil CO₂-emitting sectors. Frontiers in sustainable food systems, 300.
- Marvin, D. C., Sleeter, B. M., Cameron, D. R., Nelson, E., & Plantinga, A. J. (2023). Natural climate solutions provide robust carbon mitigation capacity under future climate change scenarios. Scientific Reports, 13(1), 19008.
- Maselli, F., Battista, P., Chiesi, M., Rapi, B., Angeli, L., Fibbi, L., ... & Gozzini, B. (2020). Use of Sentinel-2 MSI data to monitor crop irrigation in Mediterranean areas. International Journal of Applied Earth Observation and Geoinformation, 93, 102216.
- Mbow, H. O. P., Reisinger, A., Canadell, J., & O'Brien, P. (2017). Special Report on climate change, desertification, land degradation, sustainable land management, food security, and greenhouse gas fluxes in terrestrial ecosystems (SR2). Ginevra, IPCC, 650.
- Myhre, G., Shindell, D., Bréon, F.-M., Collins, W., Fuglestvedt, J., Huang, D., et al. (2013). Anthropogenic and natural radiative forcing, in Climate Change 2013: The Physical Science Basis. Contribution of Working Group 1 to the Fifth Assessment Report of the Intergovernmental Panel on Climate Change, eds T. F. Stocker, D. Qin, G.-K. Plattner, M. Tignor, S. K. Allen, and J. Boschung, et al. (Cambridge; New York, NY: Cambridge University Press), 659–740.
- NRC. (2016). The State of Canada's Forests. Annual Report 2016, Natural resources Canada, represented by the Minister of Natural Resources, Canada. https://cfs.nrcan.gc.ca/pubwarehouse/pdfs/37265.pdf
- OMAFRA-Ontario Ministry of Agriculture, Food and Rural Affairs. (2017). Insects and pests of field crops. Agronomy guide for field crops publication 811, 322-324.
- Ontl, T.A., Janowiak, M.K., Swanston, C.W., Daley, J., Handler, S., Cornett, M., Hagenbuch, S., Handrick, C., McCarthy, L., & Patch, N., 2020. Forest management for carbon sequestration and climate adaptation. J. For. 118, 86–101. https://doi.org/10.1093/jofore/fvz062.
- Pan, Y., Birdsey, R. A., Fang, J., Houghton, R., Kauppi, P. E., Kurz, W. A., ... & Hayes, D. (2011). A large and persistent carbon sink in the world's forests. Science, 333(6045), 988-993.

- Peichl, M., Arain, M. A., & Brodeur, J. J. (2010). Age effects on carbon fluxes in temperate pine forests. *Agricultural and Forest Meteorology*, *150*(7-8), 1090-1101.
- Peters, W., Jacobson, A. R., Sweeney, C., Andrews, A. E., Conway, T. J., Masarie, K., ... & Tans, P. P. (2007). An atmospheric perspective on North American carbon dioxide exchange: CarbonTracker. Proceedings of the National Academy of Sciences, 104(48), 18925-18930.
- Reichstein, M., Carvalhais, N. (2019). Aspects of Forest Biomass in the Earth System: Its Role and Major Unknowns. Surv. Geophys. 40, 693–707. https://doi.org/10.1007/s10712-019-09551-x
- Seppälä, R. (2009). A global assessment on adaptation of forests to climate change. Scandinavian Journal of Forest Research, 24(6), 469-472.
- Smith, P. G. (2015). Long-term temporal trends in agri-environment and agricultural land use in Ontario, Canada: transformation, transition and significance. Journal of Geography and Geology, 7(2), 32.
- Statistics Canada. (2018). Net Farm Income, CANSIM (Database), Table 002 0009.
- Sun, Y., Qin, Q., Ren, H., & Zhang, Y. (2021). Decameter cropland LAI/FPAR estimation from sentinel-2 imagery using google earth engine. IEEE Transactions on Geoscience and Remote Sensing, 60, 1-14.
- Sun, Z., Wang, X., Zhang, X., Tani, H., Guo, E., Yin, S., & Zhang, T. (2019). Evaluating and comparing remote sensing terrestrial GPP models for their response to climate variability and CO₂ trends. Science of the total environment, 668, 696-713.
- Verhoef, W. (1984). Light scattering by leaf layers with application to canopy reflectance modeling: The SAIL model. Remote sensing of Environment, 16(2), 125-141.
- Vincent, L. A., Zhang, X., Brown, R. D., Feng, Y., Mekis, E., Milewska, E. J., ... & Wang, X.
 L. (2015). Observed trends in Canada's climate and influence of low-frequency variability modes. Journal of Climate, 28(11), 4545-4560.
- Xie, X., Li, A., Jin, H., Tan, J., Wang, C., Lei, G., ... & Nan, X. (2019). Assessment of five satellite-derived LAI datasets for GPP estimations through ecosystem models. Science of The Total Environment, 690, 1120-1130.

- Yusa, A., Berry, P., Cheng, J. J., Ogden, N., Bonsal, B., Stewart, R., & Waldick, R. (2015). Climate change, drought and human health in Canada. International journal of environmental research and public health, 12(7), 8359-8412.
- Zafiriou, M., Lika, E., & Mussell, A. (2023). Competing Pressures on Land Use in Canadian Agriculture: To Intensify or Not to Intensify-That is the Question. The Canadian Agri-Food Policy Institute, Ottawa, Canada.
- Zhang, Y., Xiao, X., Wu, X., Zhou, S., Zhang, G., Qin, Y., & Dong, J. (2017). A global moderate resolution dataset of gross primary production of vegetation for 2000–2016. Scientific data, 4(1), 1-13.

CHAPTER 2

CARBON, WATER AND ENERGY FLUXES IN AN AGRICULTURAL FIELD IN THE GREAT LAKES REGION IN CANADA

2.1 Abstract

Eddy covariance (EC) flux measurements of energy, water vapor and carbon dioxide (CO₂) were made in a newly established agricultural flux tower site, hereafter known as CA-TPAg (Ameriflux notation) in the Great Lakes region in Southern Ontario, Canada from 2020 and 2023. This agriculture flux site has become part of the Turkey Point Environmental Observatory (TPEO), where EC flux, meteorological and ecological variables are being continuously made in three different ages (84-, 49- and 21-yr old as of 2023) of conifer forests since 2002 and a deciduous (>90-yr old) forest since 2012, enabling TPEO to become representative of the major biomes in the Great Lakes region. The agricultural site was planted with corn in 2020 and 2021, sweet potato in 2022 and tobacco in 2023. Study results showed that the mean daily evapotranspiration (ET) over the growing season was 3.12, 3.74, 3.78 and 2.96 mm d⁻¹ in 2020, 2021, 2022 and 2023 for corn, corn, sweet potato and tobacco, respectively. Corresponding annual ET values were 680, 727, 732 and 715 mm yr⁻¹, which accounted for approximately 60%, 72%, 77% and 73% of the annual total precipitation. The observed annual gross ecosystem productivity (GEP) values were 1289, 1359, 705 and 885 g C m² yr⁻¹ in 2020, 2021, 2022 and 2023, respectively, while corresponding annual ecosystem respiration (RE) values were 804, 1110, 825 and 878 g C m² yr⁻¹. Overall, the site was a carbon (C) sink with annual NEP values of 485 and 249 g C m² yr⁻¹, respectively when corn was planted in 2020 and 2021. It was a C source with annual NEP value of -120 g C m² yr⁻¹ when sweet potato was planted in 2022 and C neutral with annual NEP of 7 g C m² yr⁻¹ when tobacco was planted in 2023. The grain yields (GY) were 537, 491, 118 and 124 g C m⁻² in 2020, 2021. 2022 and 2023 resulting in annual net ecosystem carbon balance (NECB) of -52 (corn), -242

(corn), -238 (Sweet potato) and -117 (tobacco) g C m⁻² year⁻¹. Air temperature (Ta), and soil temperature (Ts) were the dominant controls on NEP, followed by Photosynthetically active radiation (PAR). This study helps to enhance our understanding of C, water and energy flux dynamics in agricultural fields in the Great Lakes region and provides valuable data for flux up-scaling, remote sensing applications, and ecosystem modeling. It will help in evaluating the potential of agricultural fields for C sequestration to provide nature-based climate solutions.

2.2 Introduction

Atmospheric carbon dioxide (CO₂) is a major contributor to human-induced climate warming (Myhre et al., 2017; Lynch et al., 2021; Jones et al., 2023). The concentration of CO₂ in the atmosphere has increased by approximately 40% compared to pre-industrial levels (Lüthi et al., 2008; Solomon et al., 2009; IPCC, 2013; Friedlingstein et al., 2022). The agricultural sector is responsible for emitting 9.3 billion tonnes of CO₂ equivalent (CO₂eq), making up roughly 11% of the total annual global CO₂ emissions (Gilbert, 2012; Mbow et al., 2017; Lamb et al., 2021; Lynch et al., 2021). In Canada also, the agriculture sector contributes about 10% of the national greenhouse gas (GHG) emissions of 729 Mt CO2eq (Fouli et al., 2021; ECCC, 2023; Lu et al., 2023). If managed adequately, the Canadian agricultural sector can play an important role in reducing national CO₂ emissions (Gregorich et al., 2005; ECCC, 2016; Yildirim et al., 2019; Laamrani et al., 2021).

In recent years, numerous eddy covariance (EC) flux observation sites have been established in agricultural fields in Canada and across the world to study biogeochemical and hydrological processes and to determine their carbon (C) sink or source strength and potential contributions in mitigating climate change (Pattey et al., 2006; Glenn et al, 2010; Smith et al., 2010; Moravek et al., 2019; Liebig et al., 2022). These studies have investigated the relationship between

photosynthetic CO₂ uptake (crop growth) and environmental controls in agricultural systems (Hernandez-Ramirez et al., 2011; Menefee et al., 2022). However, the influence of environmental factors on crop growth and C exchanges in an area may significantly vary among different crop types due to differences in plant species, plant phenology, canopy structure, spatial distribution and management practices (Hernandez-Ramirez et al., 2011; Quan et al., 2023). Many EC flux studies have reported agricultural fields as a net source of C to the atmosphere (Baker and Griffis, 2005; Liebig et al., 2022; Anthony et al., 2023; Quan et al., 2023), often attributing this to intensive cropping practices that compromise soil organic matter stability. Some research suggests that changing land use intensity and implementing crop rotations could enhance C sequestration and reduce soil organic matter depletion (Smith et al., 2015; Land et al., 2017; Lessmann et al., 2022; Thapa et al., 2023).

The EC flux system is instrumental in measuring C flux between ecosystems and the atmosphere, significantly enhancing our understanding of how land management and environmental factors control agricultural C emissions and sequestration (Menefee et al., 2022). Climatic factors and land management practices collectively determine whether agricultural systems contribute as C sources or sinks (Fan et al., 2019). Consequently, investigating cropland C dynamics across various climates and management strategies is essential (Browning et al., 2021). Adopting best practices such as high-yield crop varieties, optimized irrigation techniques, improved soil protection, increased resilience to climate impacts, and enhanced soil C sequestration (Pellerin et al., 2017). Higher crop productivity generally affects in enhanced C uptake, leading to increased C inputs in the soil from crop residues and root biomass (Burney et al., 2010; Smith et al., 2012; Frank et al., 2017; Fan et al., 2019). However, annual climate variability can obscure treatment effects in short-term studies (Pittelkow et al., 2015; Austin et al., 2017; Büchi et al., 2017), emphasizing the

necessity for long-term research across diverse climates, soils, crop rotations, and extreme events to better understand how climatic factors and soil residues influence ecosystems and C balance.

For the agricultural fields which has been reported as a net C sink, there may be uncertainties surrounding the strength and resilience of this C sink under future climate change (Curtis and Gough, 2018; Laforge et al., 2021; O'sullivan et al., 2022). In the literature there is lack of long-term EC flux studies focusing on to evaluate the C source or sink strength of different crops and how they maybe impacted by changes in climate and extreme weather conditions. These long-term EC flux studies are very important to develop well-tested agricultural ecosystem models and to determine regional C budgets by integrating site-level knowledge with remote sensing data in major croplands such as Midwest in the USA (Wiesner et al., 2022) and Southern Ontario in Canada (Ashton et al., 2023).

In Canada, the province of Ontario is a major contributor to Canadian agricultural sector where almost 25% of Canadian farms covering 7.7% of the total farm area are located (Chen, 2022). Soybean (31.8%), Corn (24.9), winter wheat (13%) and Alfalfa (11.2%) are major crops in Ontario, Canada (Statistics Canada, 2021). Other major crops include barley, tobacco, grapes and various vegetables such as potato, tomato, cauliflower etc. Southern Ontario, where 70% of the land area is utilized for agriculture contributes 15% of Canada's net farm income (Statistics Canada, 2018). In addition, almost one-third of the Canadian population also lives in this area (Stats Canada, 2023). This region has a very conducive environment for crops due to the proximity of the Great Lakes (McKeown et al., 2005). Despite its significance, this area has only one long-term EC flux observation site at Elora focusing on productivity and C sink and source strength of crops (Wagner-Riddle, 2021; Wagner-Riddle et al., 2007). Continuous

measurements of energy, water, and C fluxes, along with climatic variables in various crops in the region are essential to provide valuable data for plot level and regional C balance studies and to develop strategies for mitigating climate change through C sequestration in agricultural fields.

This study reports the continuous eddy covariance flux measurements in a newly established agricultural flux tower site in Southern Ontario, Canada from 20020 to 2023. The field was planted with corn in 2020 and 2021, sweet potato in 2022 and tobacco in 2023. The main objectives of the study are to (i) continuously measure energy, water and C fluxes in different agricultural crops, (ii) determine the C sink and source strength of these crops and (iii) investigate major environmental controls and their impact on C dynamics and water use of difference crops. The method and findings of this research will enhance understanding to improve C sequestration in agricultural ecosystems and assess the impacts of extreme weather events on crop productivity.

2.3 Methods

2.3.1 Site description

The study site is located about 15 km southwest of Simcoe in southern Ontario, Canada (42°41'46.05"N and 80°20'55.61"W). It was planted with corn (*Zea mays*) in 2020 and 2021, sweet potato (*Ipomoea batatas*) in 2022 and tobacco (*Nicotiana tabacum*) in 2023. Site was planted with winter grass after the harvesting of sweet potato in 2022 and which was mowed back into soil in April 2023 prior to plantation of tobacco to increase soil fertility. The site is part of Turkey Point Environmental Observatory (TPEO), where EC flux, meteorological and ecological variables are being continuously made in three different ages (84-, 49- and 21-yr old as of 2023 known as CA-TP1, CA-TP3 and CA-TP4) of conifer forests since 2002 and a

deciduous (>90-yr old known as CA-TPD) forest since 2012 (Arain et al., 2022; Latifovic et al., 2024). TPEO is associated with the Global Water Futures Program, Ameriflux and Global Fluxnet. TPEO is among a handful of sites in Ameriflux and global Fluxnet with long-term (>20 years) flux data availability. The 84-year-old conifer forest site (CA-TP4) site is located in the north at 1.7 km, while 49-year-old conifer forest site (CA-TP3 is located in the northeast at 1.2 km from the CA-TPAg site. The establishment of the agricultural site has allowed TPEO to become representative of the major biomes in the Great Lakes region, encompassing coniferous and deciduous forests, as well as agricultural crops. The soil at this agricultural site is well-drained fine sandy loam. The area has a humid continental climate and has one of the longest-growing seasons in Canada with at least 150–160 frost-free days in a year. The mean annual temperature is 8.4°C and the mean annual precipitation (P) is approximately 965 mm based on the Meteorological Services of Canada climate normal data record (1991-2020) at Delhi Weather Station, Ontario.

2.3.2. Flux and meteorological data measurements, quality control and gap filling

Half-hourly fluxes of momentum, latent heat (LE), sensible heat (H), and CO₂ (Fc) were measured continuously from June 2020 to December 2023 using an open-path eddy covariance (EC) system. Flux measurements have been continuous until the writing of this paper. The EC system consisted of a sonic anemometer (model CSAT3, Campbell Scientific Inc. (CSI)) and an infrared gas analyzer, IRGA (model LI-7500; LI-COR Inc.). The IRGA and CSAT3 were installed at 5 m height on top of an aluminum boom. A footprint model (Kljun et al. 2004), was used to estimate flux footprint, determine the height of EC sensors and ensure that the majority (>80%) of fluxes originated within the agricultural field being measured. The CSAT3 was oriented facing westward (270°). Fluxes were measured at 20 Hz frequency and then half-hourly values were calculates on the site computer using a software developed by the

Biometeorology & Soil Physics Group of the University of British Columbia using Matlab (The MathWorks Inc.). Initial data quality controls and non-stationarity checks were also perfumed by the UBC flux software. Because the gas analyzer provided high frequency CO₂ concentrations as mixing ratios, therefore no subsequent Webb-Pearman-Leuning (WPL) corrections were required (Webb et al., 1980). Flux data originating from 70-80° East and 230-255° West wind directions were discarded because of the existence of a surface flood-water drainage ditch. Any large shrubs such as Sumac (*Rhus typhina*) growing along this drain were removed prior to flux measurements. The site is equipped with A/C power and internet connection for daily data checks. The high-frequency data were saved on the field minicomputer and manually transferred and backed up on the Lab data computer on biweekly or monthly basis using a data disk.

Meteorological measurements were made simultaneously with EC flux measurements. These included the downward and upward photosynthetically active radiation (PAR; Kipp & Zonen Quantum Sensor, model PQS1, CSI), as well as incoming and outgoing, longwave and shortwave solar radiation and net radiation measured with a net radiometer (SN500, net radiometer, Apogee Instruments), air temperature (Ta) and relative humidity (RH) (HC2S3, CSI) and soil heat flux (G) at 3 cm depth (HFT3, CSI). Soil temperature was measured at 2, 5, 10, and 50 cm depths using soil temperature probes (model 107b, CSI). Soil volumetric water content (VWC) was monitored using water content reflectometers (model 616, CSI), which were buried at depths of 5 and 50 cm from the soil surface. The precipitation (P) was measured using an all-weather accumulation rain gauge (model T–200B, Geonor Inc.) in the south of the agricultural site at an adjacent property of the Long Point Ecoadventure Centre. All meteorological and soil data were recorded at half-hourly intervals using a data logger (model

CR5000, CSI). Automated data downloads were conducted every half hour using the field minicomputer housed in the data logger box.

Half-hourly EC fluxes and meteorological data were quality controlled in the Lab using the Biometeorological Analysis, Collection, and Organizational Node (BACON) software developed by our group (Brodeur, 2014). All half-hourly flux and meteorological data were automatically filtered for spikes and then manually checked to identify and remove any outliers. Small gaps in meteorological variables, not exceeding a few hours were filled using linear interpolation (6.3 % of the total observations). Large gaps in meteorological variables, including January to June 2020 period were filled using data from weather stations installed at adjacent forest sites (i.e. CA-TP3 and CA-TP4) after applying linear regression analysis where needed.

Net ecosystem exchange (NEE) was calculated as NEE = $F_c + S_c$, where S_c is the rate of change in CO₂ storage within the air column below the EC sensor, estimated from the change in the present and previous half-hourly CO₂ response (Chan et al., 2018). Net ecosystem productivity (NEP) is equal to -NEE, where a positive NEP represents C fixed by the ecosystem C sink and a negative NEP represents C source or emission to the atmosphere. Half-hourly flux gap-filling and partitioning of NEP into GEP and RE was conducted using REddyProc package in R (Reichstein et al., 2005; Lasslop et al., 2010; Wutzler et al. 2018). For the gap-filling of fluxes the marginal distribution sampling (MDS) method of the REddyProc was adopted, while the partitioning of NEP into GEP and Re was conducted by using u* thresholds constrained nighttime NEP values to estimate day-time RE (Wutzler et al., 2018). After data quality control of measured NEP fluxes in total 61.83%, 56.33%, 68.62%, and 67.20% of data was retained for 2020 (Jun-Dec), 2021, 2022 to 2023, respectively. Uncertainty in annual NEP (\pm STD,

standard deviation) was derived from the aggregated values estimated using the distribution of u* thresholds of 5, 50, and 95% quantiles. For ET uncertainty values u* thresholds of 50 and 95% were used. Uncertainty associated with energy balance closure was not included in these uncertainty estimates and annual C fluxes were not corrected for the energy balance closure. Gross ecosystem productivity (GEP) was estimated as the sum of daytime NEP and RE.

Net ecosystem carbon balance (NECB) was calculated as NEP minus C removed as grain. For NECB accounting C input through seeding was not accounted, while no organic fertilizer was applied. Multivariable linear regression (MLR) and principal component analysis (PCA) were conducted to explore relationships between climatic variables and carbon and water fluxes. In both analyses, PAR, Ta, Ts, VPD, and VWC were considered as independent variables, while GEP, NEP, RE, and ET were considered as the dependent variables.

2.4 Results:

2.4.1 Meteorological conditions

Weather conditions during the study period were representative of typical humid continental climates in the Great Lake region, which has large seasonal differences in air temperature and well-distributed precipitation throughout the year (Figure 2.1 and Table 2.1). The maximum daily PAR was observed in June, while the maximum daily T_a and T_s values were observed in July. The growing season (June to September) daily mean PAR values were 402 μ mol m⁻² s⁻¹ in 2020, 429 μ mol m⁻² s⁻¹ in 2021, 455 μ mol m⁻² s⁻¹ in 2022 and 516 μ mol m⁻² s⁻¹ in 2023. The growing season daily mean T_a was 19.91±3.7 °C, 20.17±2.6 °C, 20.3±2.4 °C and 18.77±2.8°C, respectively in 2020, 2021, 2022 and 2023 whereas the respective growing season daily mean T_s at 5cm depth was 19.1±3.2°C, 20.7±1.9°C, 24.2±2.4°C and 21±2.5°C.

Similarly, the growing season daily mean VPD values were 0.37, 0.33, 0.33 and 0.31 kPa in 2020, 2021, 2022 and 2023 respectively.

Annual total precipitation (P) values were 1127, 1009, 947 and 979 mm yr⁻¹ in 2020, 2021, 2022 and 2023, respectively. Overall, the observed P followed typical seasonal patterns characteristic of a continental climate, except for May and August 2021 (38 and 46 mm) and May and September 2023 (25 and 42 mm), when the site experienced a significant reduction in monthly total P as compared to 30-year normal P (1991-2020) collected from Delhi weather station Ontario (Environment and natural resources, Canada) (Table 2.1). Moreover, the highest annual P was observed in 2020 (1127 mm), which contributed to higher soil volumetric water content (VWC) compared to other years. The growing season daily mean VWC was 0.19, 0.15, 0.13 and 0.15 m³ m⁻³ in 2020, 2021, 2022 and 2023, respectively.

2.4.2 Energy flux dynamics

There was a good agreement between radiative (Rn + G) and turbulent (H + LE) fluxes (Figure 2.2). Regression of daily mean radiative and turbulent fluxes for corn in 2020 (2021) had slope of 0.81 (0.87), intercept of 2.5 (4.9) W m⁻² and R² of 0.82 (0.81). Similarly, the regression of daily mean radiative and turbulent fluxes for sweet potato and tobacco in 2022 and 2023 had slope of 0.87 and 0.91, intercept of 17.1 and 9.9 W m⁻² and R² of 0.82 and 0.87, respectively. The energy balance ratio (EBR), calculated as (Rn-G)/(H+LE) was 0.82 and 0.90 for two consecutive corn crops in 2020 and 2021, respectively, while, EBR for sweet potato and tobacco was 0.93 and 0.94 in 2022 and 2023, respectively. This indicates that approximately 82%, 90%, 93% and 94% of the available energy was transferred from the surface to the atmosphere through turbulent fluxes in 2020, 2021, 2022 and 2023, respectively.

The time series of monthly mean Rn, LE, H, and G is shown in Figure 2.3. All energy balance components (Rn, LE, H, and G) peaked in June and July each year. Rn values declined from September when the fall season started and reached about 10-20 W m⁻² by the end of October (Figure 2.3a). A significant proportion of Rn was transferred to the atmosphere as LE during the peak growing season months (June-August), with (LE/Rn) ratios of 0.85 and 0.74 for corn in 2020 and 2021 and 0.79 for sweet potato. A slightly higher LE/Rn ratio of 0.88 was observed for tobacco. The variability in LE/Rn ratios is influenced by crop type and climatic conditions. Overall, the growing season (June to September) monthly mean Rn was 132, 127, 125 and 113 W m⁻² in 2020, 2021, 2021 and 2023, respectively, while corresponding monthly mean LE values were 91, 102, 95 and 84 W m⁻² in 2020, 2021, 2022 and 2023, respectively. The corn and tobacco crops exhibited maximum LE in July, while sweet potato had its maximum LE in August (Figure 2.3b). A notable reduction in LE was observed in May 2021, September 2020 and June and September 2023. Low values of H were also observed in July 2020 and June, July and August in 2021 (Figure 2.3c). Overall, the growing season monthly mean H values were 20, 18, 32 and 29 W m⁻² in 2020, 2021, 2022 and 2023, respectively.

Compared to the other three major components of the energy balance, monthly mean G values remained low throughout the year, with maximum G observed in June coinciding with maximum radiation value (Figure 2.3d). The growing season monthly mean G values were 3.6, 3.7, 2.4 and 4.9 Wm⁻² in 2020, 2021, 2022 and 2023, respectively.

2.4.3 Carbon flux dynamics

C flux dynamics showed a distinct seasonal pattern with NEP reflecting periods of dormancy, rapid vegetative growth, and senescence, as shown in Figure 2.4 (a-d). The specific timing of maximum C uptake and loss varied from year to year. For corn in 2020, the growing season spanned from May 23 to September 29, lasting 130 days (Figure 2.4 and 2.5). During this period, the mean daily NEP was 4.45 g C m⁻² d⁻¹, with the maximum NEP of 12.57 g C m⁻² d⁻¹ observed in July. In contrast, the corn growing season in 2021 began a half-month later on June 9 due to delayed planting and ended on September 21, spanning over 105 days. Hence, the growing season length in 2021 was 25 days less than 2020. In 2021, the mean daily NEP was 5.57 g C m⁻² d⁻¹, with the maximum NEP of 10.97 g C m⁻² d⁻¹ observed in August. The growing season for sweet potato crop in 2022 started on July 6th and ended on September 19th with only 76 days of active growth. It shows that in 2022 crop photosynthetic uptake started 43 days later than in 2020 and 27 days later than in 2021, while it ended at almost similar time as other years. For sweet potato crop the mean daily NEP was 4 g C m⁻² d⁻¹, with the peak NEP of 7.2 g C m⁻² d⁻¹ occurring in August. The duration of the growing season for tobacco planted in 2023 was 125 days (1st July to 3rd October) when crop was harvested with the mean NEP values of 0.9 g C m⁻² d⁻¹. Prior to planting tobacco, the site was planted with winter grass, which caused an early start of photosynthesis in the spring in 2023, where daily NEP values became positive from mid-March to April with a total NEP of 22 g C m⁻² (Figure 2.4d and 2.5b). This winter grass was moved back into the soil at the end of April prior to the planting of tobacco. After mowing daily NEP values became negative and reached up to -4 g C m⁻² day⁻¹. Planting of winter grass caused the site to become a net C sink over the January to April 2023 period with a total NEP of 22 g C m⁻² (Figure 2.5). Overall, the total growing season NEP values were 579, 543, 304 and 113 g C m⁻² in 2020, 2021, 2022 and 2023, respectively (Table 2.2).

On the annual basis, the site was a strong C sink, with annual NEP values of 485 g C m⁻² y⁻¹ and 249 g C m⁻² y⁻¹, respectively when corn was planted in 2020 and 2021 (Figure 2.5, Table 2.2). It was a C source with an annual NEP of -120 g C m⁻² y⁻¹ when sweet potato was planted in 2022. The site was C neutral in 2023 for tobacco with an annual NEP of 7 g C m⁻² y⁻¹. The annual GEP values were 1289, 1359, 705 and 885 g C m⁻² y⁻¹ in 2020, 2021, 2022 and 2023, respectively, while corresponding annual RE values were 804, 1110, 825, and 878 g C m⁻² y⁻¹ (Figure 2.5, Table 2.2).

Additionally, the annual NECB was -52 (corn), -241 (corn), -238 (sweet potato) and -117 (tobacco) g C m⁻² year⁻¹ and respective grain yields (GY) was 537, 491, 118 and 124 g C m⁻² in 2020, 2021, 2022 and 2023 (Table 2.2). The maximum NECB is associated with corn crops, consistent with the year of the highest recorded annual NEP of 485 (2020) and 249 (2021) g C m⁻² year⁻¹. The minimum NECB was recorded in 2022 for sweet potatoes when the site was a source of C with an annual NEP value of -120 g C m⁻² year⁻¹. These findings show substantial changes in the site's C balance and are indicative of a shifting ecosystem response during the study period.

The results reveal substantial variations in NEP and NECB during the growing seasons of 2020, 2021, and 2023, reflecting their dynamic relationship with the annual C balance. In 2020, the corn crop with 130 days of growing season recorded NEP of 579 g C m⁻² and a positive NECB of 42 g C m⁻². However, the annual NEP decreased to 485 g C m⁻², suggesting C uptake losses from respiration during the non-growing period and/or from harvested residues. In 2021, the growing season NEP was 543 g C m⁻² with a positive NECB of 52 g C m⁻². However, annual NEP declined to 249 g C m⁻², resulting in a negative NECB of -242 g C m⁻². This decline

indicates that external factors, particularly drought conditions experienced in May and August, 2021 had a significant impact on carbon dynamics.

In 2022, despite a reduced growing season of 76 days for potatoes, the growing season NEP reached 304 g C m⁻² with a noteworthy NECB of 186 g C m⁻². However, the annual NEP remained negative at -120 g C m⁻², revealing that the advantages gained during the growing season were inadequate to offset annual losses. During the tobacco growing season, drought stress was observed in May and September, resulting in the growing season NEP of 113 g C m⁻² and an annual NEP of 7 g C m⁻², with a NECB of -117 g C m⁻². This analysis provides the critical interplay between growing season conditions and annual carbon dynamics, emphasizing how drought stress can adversely affect both immediate productivity and long-term carbon retention in agricultural systems.

2.4.3 Water flux dynamics

ET is a major component of the water cycle in crops. Dynamics of daily ET values is shown in Figure 4e-h. During the initial period of the growing season, daily ET values were about 1-2 mm d⁻¹, while during the peak growing season in July-August daily ET values exceeded 6 mm d⁻¹. In contrast to NEP, there were very small differences in peak ET values among different crops types. (Figure 4c-h). Overall, the growing season mean daily ET was 3.1, 3.7, 3.8 and 2.9 mm d⁻¹ for 2020, 2021, 2022 and 2023, respectively.

On the annual basis, total ET for 2020, 2021, 2022 and 2023 was to 680, 727, 732 and 715 mm y⁻¹, respectively, accounting for approximately 60%, 72%, 77% and 73% of the annual total precipitation (Table 2.2). Furthermore, through monthly ET and precipitation

assessments, it was evident that the site faced water scarcity in August 2021 and September 2023 when ET exceeded precipitation by 276% (August 2021) and 170% (September 2023).

2.4.5 Water and light use efficiency

The analysis of growing seaosn water use efficiency (WUE) in various crop types showed a strong to moderate correlation between ET and GEP with R² of 0.80 for corn (2020), 0.65 for corn (2021), 0.70 for sweet potato (2021), and 0.57 for tobacco (2023) (Figure 6). In 2020, the mean daily WUE was at 3.85 g C kg⁻¹ H₂O⁻¹ reflecting relatively efficient water utilization in biomass production. In 2021, the daily WUE decreased slightly to 3.34 g C kg⁻¹ H₂O⁻¹ as compared to the previous year's corn crops. Transitioning to sweet potato in 2022, caused a remarkable decrease in WUE with mean daily value of 2.18 g C kg⁻¹ H₂O⁻¹, indicating a less efficient utilization of water for biomass production in sweet potato compared to corn. Lastly, in 2023, during tobacco cultivation, the daily WUE further declined to 1.94 g C kg⁻¹ H₂O⁻¹, indicating the lowest efficiency in water utilization observed across this period.

In addition, the analysis of the efficiency of light (PAR) utilization for photosynthesis (GEP) across different crops by applying Michaelis-Menten hyperbolic curve over the growing season from 2020 to 2023 showed significant variations in photosynthetic C uptake efficiency among the different crops (Figure 2.7). Corn had the highest C uptake or GEP under similar light conditions, followed by sweet potato in 2022, and tobacco in 2023 (Figure 2.7). At PAR level of about 1000 μmol m⁻² s⁻¹, GEP of corn was 20 to 22 μmol m⁻² s⁻¹, whereas sweet potato and tobacco absorbed only about 10 μmol m⁻² s⁻¹, respectively (Figure 2.7). While sweet potato and tobacco showed a plateau in GEP when PAR exceeded 1000 μmol m⁻² s⁻¹, GEP in corn continued to increase with increasing light levels. The highest GEP values in corn reached

about 28 to 31 µmol m⁻² s⁻¹. These findings indicate that corn is more efficient in utilizing available light for photosynthesis, leading to higher C uptake and growth.

2.4.6 Environmental controls on carbon and water fluxes

The multivariable linear regression (MLR) and principal component analysis (PCA) revealed significant relationships between climatic factors with C and water fluxes across all crop types (Table 2.3, Figure 2.8). Table 2.3 presents the correlation coefficients of key climatic variables (PAR, Ta, Ts, VPD, VWC) with GEP, NEP, RE, and ET, spanning the years 2020 to 2023. MLR results indicated that GEP, RE, ET, and NEP were significantly influenced by climate factors (P < 0.0001), with R² values of 0.48, 0.17, 0.79, and 0.60, respectively, emphasizing the overall impact of climatic variables. Similarly, PCA results showed that temperature variables (Ta and Ts) primarily influenced C and water balances (Figure 2.8).

The results from regression analysis further demonstrated that GEP was significantly affected by both Ta and Ts. Ta presents a strong positive effect on GEP, with an estimate of 0.047, an R^2 value of 0.66, and high statistical significance (P < 0.0001), while Ts had an estimate of 0.339 and an R^2 value of 0.69, also highly significant (P < 0.0001). Although PAR positively affected GEP, its impact was substantial (P < 0.0001, $P^2 = 0.45$). VPD had a moderate effect on GEP (P = 0.007, $P^2 = 0.42$), while VWC had a weak effect (P = 0.009, $P^2 = 0.17$), suggesting that temperature and radiative energy were more influential in driving GEP.

NEP showed moderate positive correlations with strong significance (P < 0.0001). Similar to GEP, NEP was correlated with PAR, Ta, Ts, VPD, and VWC, with respective R^2 values of 0.20, 0.38, 0.40, 0.25, and 0.13. Ta and Ts had the most pronounced effects on NEP. Both

temperature variables also strongly influenced RE, with estimates of 0.064 for Ta and 0.185 for Ts, and high significance (P < 0.0001). The correlation of Ta and Ts with RE had R^2 values of 0.86 and 0.88, respectively. PAR also had a significant positive impact on RE (P < 0.0001, $R^2 = 0.52$), indicating its key role in respiration. VPD showed a marginally significant effect on RE (P = 0.54), while VWC had a weak to moderate impact (P = 0.0067), suggesting soil moisture was less influential than temperature and light for RE.

ET was significantly driven by Ta, Ts, and PAR. Ta and Ts had significant positive effects on ET, with estimates of 0.022 and 0.071, and R^2 values of 0.72 and 0.75, respectively (P < 0.0001). PAR also significantly influenced on ET (estimate = 0.001, P = 0.0001), explaining 60% of the variance. VPD had a significant influence (P < 0.0001), while VWC exhibited a nonsignificant negative effect (estimate = -0.473, P = 0.1345, $R^2 = 0.04$). The negative relationship between VWC and ET contrasted with its positive effects on GEP and NEP, highlighting the complex interactions between soil moisture and ecosystem processes.

2.5 Discussion

2.5.1 Energy and Water Flux Dynamics

The energy balance of agricultural fields is affected by crop type and canopy attributes (Duveiller et al., 2018; Dare-Idowu et al., 2021). There are usually large differences in the partitioning of available energy among different crop types or during various stages of crop development (Stöckle et al., 2009; Murchie et al., 2012). Radiation or available energy plays a significant role to determine the intensity of turbulent fluxes (Hernandez-Ramirez et al., 2010; Flores-Velazquez, 2022). In agriculture fields, a significant portion of Rn is partitioned into LE, which is the primary process through which water is transferred from the land surface to

the atmosphere, involving soil evaporation and plant transpiration (Shuttleworth, 2007; Kool et al., 2014). Hence, LE (or ET) is the composite flux that links both energy and water cycles, and its magnitude is governed by meteorological conditions, canopy structure and seasonal characteristics (Jasechko et al., 2013; Wang et al., 2014). Our study showed a discernible pattern in LE that represented the growth cycle of crops. Maximum LE or ET was observed in July or early August coinciding with peak growth periods and maximum temperatures. However, in August 2021, the site experienced drought conditions when a significant reduction in precipitation was observed which impacted the corn productivity in 2021. Overall, at our site 85%, 74%, 79% and 88% of Rn was utilized as LE in 2020, 2021, 2022 and 2023, respectively, corroborating to findings from other studies in the literature (e.g. Suyker and Verma, 2008; Hernandez-Ramirez et al., 2010; Yan et al., 2019; Dare-Idowu et al., 2021). Our turbulent flux observations (LE+H) were also consistent with earlier studies, including Hernandez-Ramirez et al. (2010), who reported that 89% of the available energy (Rn-G) was partitioned as LE+H fluxes in their corn field in the Midwestern USA, and Hatfield et al. (2007), who suggested that 80% of available energy was transferred to atmosphere as LE+H fluxes in their corn sites in Central Iowa, USA. In our study, we observed that 82%, 90%, 93% and 94% of available energy was partitioned as LE+H fluxes in 2020, 2021, 2022 and 2023, respectively.

Our study showed annual ET values of 680 (corn), 727 (corn), 732 (sweet potato) and 715 (tobacco) mm y⁻¹ for 2020, 2021, 2022 and 2023, respectively. These annual ET values were similar to the long-term ET values reported for the US Midwest corn belt in southwest Michigan, USA by Abraha et al. (2020). Abraha et al. (2020) estimated mean annual ET of 584 mm y⁻¹ from 2010 to 2018. Furthermore, Abraha et al. (2015) reported annual ET ranging from 480 mm y⁻¹ to 639 mm y⁻¹ in the same region in Michigan, USA.

Our findings regarding WUE in various crop types also aligned well with prior research demonstrating similar trends. For instance, in a study focusing on corn cultivation in Southern Ontario, Canada, De Haan et al. (2022) reported WUE of 3.5 g C kg⁻¹ H₂O⁻¹. Similar WUE values ranging from 3.5 to 4.5 were reported in Michigan, USA by Abraha et al. (2016) as well. These WUE values are consistent our observations of 3.85 and 3.34 g C kg⁻¹ H₂O⁻¹ for corn crops in 2020 and 2021. Additionally, Jiang et al. (2021) found WUE values from 1.4 to 4.3 g C kg⁻¹ H₂O⁻¹ in the sweet potatoes in Atlantic Canada, which compared well with our value of 2.18 g C kg⁻¹ H₂O⁻¹ in 2022. These prior studies provide valuable context and support for the trends observed in our research, indicating the importance of considering crop-specific WUE in agricultural management practices.

2.5.2 Carbon flux dynamics

Our observed annual NEP values were 485 (corn), 249 (corn), -120 (sweet potato) and 7 (tobacco) g C m⁻² y⁻¹ for 2020, 2021, 2022 and 2023, respectively (Table 2.2). The two-year mean annual NEP value of 367 g C m⁻² y⁻¹ for our corn crops for 2020 and 2021 agreed well with carbon uptake observations made at other corn sites in North America as shown in Table 4 (Hollinger et al., 2005; Hernandez-Ramirez et al., 2011). Hernandez-Ramirez et al. (2011) reported that the annual NEP for a corn field in Iowa, USA ranged from 534 to 360 g C m⁻² y⁻¹ from 2004 to 2007. Additionally, Hollinger et al. (2005) observed annual NEP value of 576 g C m⁻² y⁻¹ for a corn field in Champaign, IL, USA, which is also similar to our results. The similarity in annual NEP values between our study site and other sites can be attributed to their geographic location and similar environmental conditions in the Great Lakes. In contrast, Glenn et al. (2010) reported annual NEP of 72 g C m⁻² y⁻¹ in Winnipeg, Manitoba, Canada,

indicating substantial deviation in annual NEP when compared to our site. It can be attributable to distinct environmental conditions in the boreal region and remarkably lower temperatures in Manitoba (Table 2.4).

Furthermore, our observed annual RE values were 804, 1110, 825 and 878 g C m⁻² y⁻¹, for corn in 2020 and 2021, sweet potato in 2022 and tobacco in 2023, respectively, while corresponding GEP values were 1289, 1359, 705 and 885 g C m⁻² y⁻¹. Similar annual GEP and RE values have been reported by Suyker & Verma (2012) for a corn field in Nebraska, USA. Mean RE/GEP ratio of 0.72 for our corn crops was also similar to RE/GEP ratio of 0.63 reported by Suyker & Verma (2012).

Our study revealed a shift in carbon dynamics in 2022, as our site became a source of carbon with an annual NEP value of -120 g C m⁻² y⁻¹. This change was attributed to the cultivation of sweet potatoes, which had a shorter growing season of only 76 days as compared to corn crops (i.e. 130 and 105 days). The differential response of C balance budgets based on the choice of crop type at the same agricultural field has also been noted by Liebig et al. (2022).

The GPP for tobacco indicated a moderate capacity for C assimilation, with growing season values of 661 g C m-2. Tobacco was effective at capturing C but at a lower rate compared to corn. The NEP for tobacco was notably lower, with a growing season NEP of 113 g C m-2. This disparity between GPP and NEP underscores that, despite tobacco's effective carbon capture, the net carbon gain remains modest due to significant respiratory losses (Domiciano et al., 2020; Zhang et al., 2021).

The C balance in the study area is significantly influenced by crop type, climatic conditions, and the duration and length of the growing season. Corn, a C4 plant, was cultivated in 2020 and 2021, with its growing season typically extending from early May to early October. During these periods, the dynamics of NEP, GEP, and RE were closely observed. In 2020, the maximum C uptake was recorded throughout the growing season, reflecting strong carbon sink potential, with an annual NEP of 485 g C m⁻² y⁻¹. However, in 2021, a significant reduction in C uptake occurred, particularly in May and August, due to drought conditions characterized by reduced precipitation resulting in an annual NEP of 249 g C m⁻² y⁻¹. These drought periods shortened the optimal growth phases, thereby reducing the effective length of the growing season and impacting the overall C balance. In 2023, similar drought conditions were observed in May and September, coinciding with critical phases of crop development. That year, tobacco, a C3 plant, was cultivated with a growing season from early May to mid-September. Under comparable reductions in precipitation, the tobacco crops experienced a more substantial decline in C uptake than corn did under similar conditions in 2021. The annual NEP for tobacco was only 7 g C m⁻² y⁻¹, indicating a low net carbon gain. This difference highlights the sensitivity of C3 crops like tobacco, which require more consistent water supply, to reductions in precipitation during key growth periods.

The GPP for tobacco demonstrated a moderate capacity for carbon assimilation, with growing season values reaching 661 g C m⁻². Although tobacco was relatively effective at capturing C, its NEP was considerably lower, at 113 g C m⁻² for the growing season. This disparity between GPP and NEP underscores that, despite tobacco's capacity for carbon capture, the net carbon gain remains modest due to significant respiratory losses, as supported by findings from Domiciano et al. (2020) and Zhang et al. (2021).

These findings suggest that the C balance feedback in agricultural ecosystems is shaped not only by climatic conditions, such as the occurrence and timing of droughts, but also by crop type, its physiological characteristics (C3 vs. C4), and the length of the growing season. C4 crops like corn generally exhibit greater resilience to water stress and can maintain photosynthetic activity over longer periods under high light and temperature conditions. In contrast, C3 crops like tobacco are more susceptible to drought, which can shorten their growing season and reduce carbon uptake. Therefore, understanding these interactions is essential for evaluating carbon dynamics and developing strategies to enhance carbon sequestration in agricultural systems.

Furthermore, the NECB was calculated to evaluate the net carbon loss from both corn and sweet potato, employing NEP and grain yield. Our findings reveal the dominant influence of corn crops on the carbon balance throughout the study period, demonstrated by their robust carbon sequestration capacity compared to sweet potato. Corn crops exhibited significantly higher grain yield than sweet potato, recording respective values of 537 and 491 g C m⁻² for 2020 and 2021, while sweet potato yielded merely 118 g C m⁻² in 2022 and tobacco yielded 124 g C m⁻². The findings in grain yield align with results from various studies in North American sites; including Cates and Jackson (2019) reported a range of grain yields for corn crops ranging from 398 to 676 g C m⁻², Verma et al. (2005) observed nearly 520 g C m⁻² and Evans (2022) found 485 g C m⁻². The substantially higher grain yield of corn significantly increased the NECB compared to sweet potato and tobacco crops. Annual NECB values were determined to be -52, -242, -238 and -117 g C m⁻² y⁻¹ for the respective year. Similar observations regarding NECB were recorded in North American studies; Quan et al. (2023) reported -271 g C m⁻² for potatoes in British Columbia. The differences between annual and growing seasons NECB represent the site's role as a carbon source during non-growing seasons.

The results focus on the intricate relationship between growing season length, crop type, and annual C dynamics. The corn crops of 2020 and 2021 present strong C retention during their respective growing seasons; however, the negative annual NECB indicates that external factors, such as increased respiration and extreme weather events, significantly influence the overall C balance. This study revealed the dynamic effects of different crops on C balance and water use efficiency. It showed that selecting the right crop is crucial for managing C storage and enhancing agricultural sustainability. It will help to develop better strategies to address climate change and promote sustainable farming, particularly in the Great Lakes region.

2.6 Conclusion

An analysis of seasonal and annual energy, water, and C fluxes in different crops was conducted from 2020 to 2023 in a newly established agricultural flow tower site in Southern Ontario, Canada. The site was planted with corn in 2020 and 2021, sweet potato in 2022 and tobacco in 2023. Overall, the site was a C sink with annual NEP values of 485 and 249 g C m² yr⁻¹, respectively for corn in 2020 and 2021. The site was a C source with annual NEP value of –120 g C m² yr⁻¹ for sweet potato in 2022 and it was C neutral with annual NEP of 7 g C m² yr⁻¹ for tobacco in 2023. The grain yields (GY) were 537, 491, 118 and 124 g C m⁻² in 2020, 2021, 2022 and 2023 resulting in annual net ecosystem carbon balance (NECB) of -52 (corn), –242 (corn), –238 (Sweet potato) and –117 (tobacco) g C m⁻² year⁻¹. Annual ET values were 680, 727, 732 mm yr⁻¹ and 715, in 2020, 2021, 2022 and 2023, respectively, accounting for 60%, 72%, 77% and 73% of the annual total precipitation. This study emphasizes the significant influence of agricultural crop choices on the C dynamics within the ecosystem.

Study further highlights the profound impact of environmental variables, including PAR, temperature, soil moisture on energy, water, and C fluxes.

This research contributes to enhance our understanding of energy, water, and C fluxes within the Great Lakes region, offering valuable insights for the development of more sustainable and effective agricultural practices and policies across eastern North America. Furthermore, our findings contribute to the broader knowledge base in this research field, facilitating a better understanding of climate change's impacts on agricultural ecosystems and the formulation of adaptation and mitigation strategies.

2.7 Acknowledgement

This study was funded by the Natural Sciences and Engineering Research Council (NSERC) grants, including Discovery and Alliance Mission grants, Global Water Futures Program (GWF) - Southern Forests Water Future and GWF Observatory grants and the US National Science Foundation (NSF) - Social Science and Humanities Research Council (SSHRC) of Canada funded Global Centre for Climate Change Impacts on Transboundary Waters project. In kind support from the Natural Resources Canada (NRCan), Ontario Ministry of Natural Resources and Forestry (OMNRF), Ontario Ministry of Environment, Conservation and Parks, and the St. Williams Conservation Reserve Community Council (SWCRCC) to the Turkey Point Environmental Observatory is gratefully acknowledged. We specially thank Frank de Leebeck to providing access to his farm to conduct this research and Dave Pond of the Long Point Ecoadventure Centre for allowing to install our accumulation rain gauge on their property. Lab group members including Noah Stegman are acknowledged for their contributions to flux data collection and downloads. We acknowledge Dr. Shusen Wang from NRCan-CCRS and Audrey Heagy from SWCRCC for their support to this project. We acknowledge Sarah Knox, Paul Moore and Rosie Howard at McGill University for gap filling our EC fluxes using REddyProc software that is being established as a common program for Canadian flux tower sites.

2.8 References

- Abraha, M., Chen, J., Chu, H., Zenone, T., John, R., Su, Y. J., ... & Robertson, G. P. (2015). Evapotranspiration of annual and perennial biofuel crops in a variable climate. *Gcb Bioenergy*, 7(6), 1344-1356.
- Abraha, M., Chen, J., Hamilton, S. K., & Robertson, G. P. (2020). Long-term evapotranspiration rates for rainfed corn versus perennial bioenergy crops in a mesic landscape. *Hydrological Processes*, *34*(3), 810-822.
- Abraha, M., Gelfand, I., Hamilton, S. K., Shao, C., Su, Y. J., Robertson, G. P., & Chen, J. (2016). Ecosystem water-use efficiency of annual corn and perennial grasslands: contributions from land-use history and species composition. *Ecosystems*, 19, 1001-1012.
- Anthony, T. L., Szutu, D. J., Verfaillie, J. G., Baldocchi, D. D., & Silver, W. L. (2023). Carbon-sink potential of continuous alfalfa agriculture lowered by short-term nitrous oxide emission events. *Nature communications*, *14*(1), 1926.
- Ashton, L., Lieberman, H. P., Morrison, C., & Samson, M. É. (2023). Carbon sequestration in Canada's croplands: a review of multiple disciplines influencing the science–policy interface. *Environmental Reviews*, *31*(4), 652-668.
- Austin, E. E., Wickings, K., McDaniel, M. D., Robertson, G. P., & Grandy, A. S. (2017). Cover crop root contributions to soil carbon in a no-till corn bioenergy cropping system. Gcb Bioenergy, 9(7), 1252-1263.
- Baker, J. M., & Griffis, T. J. (2005). Examining strategies to improve the carbon balance of corn/soybean agriculture using eddy covariance and mass balance techniques. *Agricultural and Forest Meteorology*, 128(3-4), 163-177.

- Beamesderfer, E. R., Arain, M. A., Khomik, M., & Brodeur, J. J. (2020). The impact of seasonal and annual climate variations on the carbon uptake capacity of a deciduous forest within the Great Lakes Region of Canada. *Journal of Geophysical Research: Biogeosciences*, 125(9), e2019JG005389.
- Brodeur, J. (2014). *Data-driven approaches for sustainable operation and defensible results*in a long-term, multi-site ecosystem flux measurement program (Doctoral dissertation).

 McMaster University, Hamilton, ON-Canada.
- Browning, D. M., Russell, E. S., Ponce-Campos, G. E., Kaplan, N., Richardson, A. D., Seyednasrollah, B., ... & Taylor, S. D. (2021). Monitoring agroecosystem productivity and phenology at a national scale: A metric assessment framework. Ecological Indicators, 131, 108147.
- Büchi, L., Wendling, M., Amossé, C., Jeangros, B., Sinaj, S., & Charles, R. (2017). Long and short term changes in crop yield and soil properties induced by the reduction of soil tillage in a long term experiment in Switzerland. Soil and Tillage Research, 174, 120-129.
- Burney, J. A., Davis, S. J., & Lobell, D. B. (2010). Greenhouse gas mitigation by agricultural intensification. Proceedings of the national Academy of Sciences, 107(26), 12052-12057.
- Cates, A. M., & Jackson, R. D. (2019). Cover crop effects on net ecosystem carbon balance in grain and silage maize. *Agronomy Journal*, 111(1), 30-38.
- Chan, F. C., Arain, M. A., Khomik, M., Brodeur, J. J., Peichl, M., Restrepo-Coupe, N., ... & Skubel, R. (2018). Carbon, water and energy exchange dynamics of a young pine plantation forest during the initial fourteen years of growth. *Forest Ecology and Management*, 410, 12-26.

- Chen, Z. J. (2022). Canadian Agriculture at a Glance, *Ontario is an agricultural powerhouse* that leads in many farming categories. Statistics Canada. Accessed on 13 Feb 2024, available at https://www150.statcan.gc.ca/n1/pub/96-325-x/2021001/article/00006-eng.htm
- Curtis, P. S., & Gough, C. M. (2018). Forest aging, disturbance and the carbon cycle. *New Phytologist*, 219(4), 1188-1193.
- Dare-Idowu, O., Brut, A., Cuxart, J., Tallec, T., Rivalland, V., Zawilski, B., ... & Jarlan, L. (2021). Surface energy balance and flux partitioning of annual crops in southwestern France. *Agricultural and Forest Meteorology*, *308*, 108529.
- De Haan, K., Khomik, M., Kessel, E., Green, A., Kompanizare, M., Helgason, W., ... & Petrone, R. M. (2022). Vegetation-related influences on carbon and water dynamics of two temperate forage crops. Agronomy Journal, 114(3), 1782-1799.
- Domiciano, D., Nery, F. C., de Carvalho, P. A., Prudente, D. O., de Souza, L. B., Chalfun-Júnior, A., ... & Marchiori, P. E. R. (2020). Nitrogen sources and CO2 concentration synergistically affect the growth and metabolism of tobacco plants. *Photosynthesis research*, 144(3), 327-339.
- Duveiller, G., Hooker, J., & Cescatti, A. (2018). The mark of vegetation change on Earth's surface energy balance. *Nature communications*, *9*(1), 679.
- ECCC (2016). Working Group on Carbon Pricing Mechanisms Final Report, Environment and Climate Change Canada (ECCC). Accessed on 13 Feb 2024, available on https://publications.gc.ca/collections/collection_2016/eccc/En4-287-2016-eng.pdf.
- ECCC (2023). National Inventory Report 1990 –2021: Greenhouse Gas Sources and Sinks in Canada Canada's Submission to The United Nations Framework Convention on Climate Change. Part 3. Public Inquiries Centre, Environment and Climate Change

- Canada (ECCC). https://publications.gc.ca/collections/collection_2023/eccc/En81-4-2021-3-eng.pdf
- Environment and natural resources, Canada. Data access on May 2024, access from https://climate.weather.gc.ca/climate_normals/results_1991_2020_e.html?searchType =stnProv&lstProvince=ON&txtCentralLatMin=0&txtCentralLatSec=0&txtCentralLo ngMin=0&txtCentralLongSec=0&stnID=162000000&dispBack=0
- Evans, J. F. (2022). Carbon dioxide Net Ecosystem Exchange Altered by Crop Rotation Diversification and Use of Cover Crops (Doctoral dissertation, University of Guelph). https://atrium.lib.uoguelph.ca/items/3b504ddd-d0f3-43c7-95ec-58f94c967f72
- Fan, J., McConkey, B. G., Liang, B. C., Angers, D. A., Janzen, H. H., Kröbel, R., ... & Smith,W. N. (2019). Increasing crop yields and root input make Canadian farmland a large carbon sink. Geoderma, 336, 49-58.
- Frank, S., Havlík, P., Soussana, J. F., Levesque, A., Valin, H., Wollenberg, E., ... & Obersteiner, M. (2017). Reducing greenhouse gas emissions in agriculture without compromising food security?. Environmental Research Letters, 12(10), 105004.
- Frantz M.L., Muller R.L., Schaeffer V.P., Köhler A.K., Schneider R.C.S., Pezzini C. (2022).

 Determination Of Carbon Sequestration in Tobacco Plants. *Coresta Congress, Online,*2022, Agronomy/Phytopathology Groups, Ap 45. Available On:

 Https://Www.Coresta.Org/Sites/Default/Files/Abstracts/2022 Ap45 Frantz.Pdf
- Friedlingstein, P., O'sullivan, M., Jones, M. W., Andrew, R. M., Gregor, L., Hauck, J., ... & Zheng, B. (2022). Global carbon budget 2022. *Earth System Science Data Discussions*, 2022, 1-159.
- Fouli, Y., Hurlbert, M., & Kröbel, R. (2021). Greenhouse Gas Emissions from Canadian Agriculture: Estimates and Measurements. *SPP Briefing Paper*, 14, 35.

- Flores-Velazquez, J., Akrami, M., & Villagrán, E. (2022). The Role of Radiation in the Modelling of Crop Evapotranspiration from Open Field to Indoor Crops. *Agronomy*, 12(11), 2593.
- Gilbert, N. (2012). One-third of our greenhouse gas emissions come from agriculture. *Nature*, 31, 10-12.
- Glenn, A. J., Amiro, B. D., Tenuta, M., Stewart, S. E., & Wagner-Riddle, C. (2010). Carbon dioxide exchange in a northern Prairie cropping system over three years. *Agricultural and forest meteorology*, 150(7-8), 908-918.
- Gregorich, E. G., Rochette, P., VandenBygaart, A. J., & Angers, D. A. (2005). Greenhouse gas contributions of agricultural soils and potential mitigation practices in Eastern Canada. *Soil and Tillage Research*, 83(1), 53-72.
- Hagenimana, V., Karuri, E. G., & Oyunga, M. A. (1998). Oil content in fried processed sweetpotato products. *Journal of food processing and preservation*, 22(2), 123-137.
- Hatfield, J. L., Prueger, J. H., & Kustas, W. P. (2007). Spatial and temporal variation of energy and carbon fluxes in Central Iowa. *Agronomy Journal*, 99(1), 285-296.
- Hernandez-Ramirez, G., Hatfield, J. L., Prueger, J. H., & Sauer, T. J. (2010). Energy balance and turbulent flux partitioning in a corn–soybean rotation in the Midwestern US. *Theoretical and Applied Climatology*, 100, 79-92.
- Hernandez-Ramirez, G., Hatfield, J. L., Parkin, T. B., Sauer, T. J., & Prueger, J. H. (2011). Carbon dioxide fluxes in corn—soybean rotation in the midwestern US: Inter-and intra-annual variations, and biophysical controls. *Agricultural and Forest Meteorology*, 151(12), 1831-1842.

- Hollinger, S. E., Bernacchi, C. J., & Meyers, T. P. (2005). Carbon budget of mature no-till ecosystem in North Central Region of the United States. *Agricultural and Forest Meteorology*, 130(1-2), 59-69.
- Holou, R. A. Y., & Kindomihou, V. M. (2017). The biofuel crops in global warming challenge: Carbon capture by corn, sweet sorghum and switchgrass biomass grown for biofuel production in the USA. *Frontiers in Bioenergy and Biofuels. IntechOpen*, 139-151.
- IPCC, (2013). Summary for Policymakers. In: Climate Change 2013: The Physical Science Basis. Contribution of Working Group I to the Fifth Assessment Report of the Intergovernmental Panel on Climate Change [Stocker, T.F., D. Qin, G.-K. Plattner, M. Tignor, S.K. Allen, J. Boschung, A. Nauels, Y. Xia, V. Bex and P.M. Midgley (eds.)]. Cambridge University Press, Cambridge, United Kingdom and New York, NY, USA.
- Jasechko, S., Sharp, Z. D., Gibson, J. J., Birks, S. J., Yi, Y., & Fawcett, P. J. (2013). Terrestrial water fluxes dominated by transpiration. *Nature*, 496(7445), 347-350.
- Jiang, Y., Ramsay, M., Meng, F., & Stetson, T. (2021). Characterizing potato yield responses to water supply in Atlantic Canada's humid climate using historical yield and weather data: Implications for supplemental irrigation. *Agricultural Water Management*, 255, 107047
- Jones, M. W., Peters, G. P., Gasser, T., Andrew, R. M., Schwingshackl, C., Gütschow, J., ... & Le Quéré, C. (2023). National contributions to climate change due to historical emissions of carbon dioxide, methane, and nitrous oxide since 1850. *Scientific Data*, 10(1), 155.
- Kool, D., Agam, N., Lazarovitch, N., Heitman, J. L., Sauer, T. J., & Ben-Gal, A. (2014). A review of approaches for evapotranspiration partitioning. *Agricultural and forest meteorology*, 184, 56-70.

Laamrani, A., Voroney, P. R., Gillespie, A. W., & Chehbouni, A. (2021). Development of a land use carbon inventory for agricultural soils in the Canadian province of Ontario. *Land*, 10(7), 765.

Latifovic et al., 2024

- Liebig, M. A., Saliendra, N. Z., & Archer, D. W. (2022). Carbon fluxes from a spring wheat—corn—soybean crop rotation under no-tillage management. *Agrosystems, Geosciences & Environment*, 5(3), e20291.
- Lu, H., Xu, Z. D., Cheng, Y. F., Peng, H., Xi, D., Jiang, X., ... & Shan, Y. (2023). An inventory of greenhouse gas emissions due to natural gas pipeline incidents in the United States and Canada from 1980s to 2021. *Scientific Data*, 10(1), 282.
- Lamb, W. F., Wiedmann, T., Pongratz, J., Andrew, R., Crippa, M., Olivier, J. G., ... & Minx, J. (2021). A review of trends and drivers of greenhouse gas emissions by sector from 1990 to 2018. *Environmental research letters*, 16(7), 073005.
- Land, M., Haddaway, N. R., Hedlund, K., Jørgensen, H. B., Kätterer, T., & Isberg, P. E. (2017).

 How do selected crop rotations affect soil organic carbon in boreo-temperate systems?

 A systematic review protocol. *Environmental Evidence*, 6(1), 1-8.
- Laforge, J., Corkal, V., & Cosbey, A. (2021). Farming the future: Agriculture and climate change on the Canadian Prairies. International Institute for Sustainable Development.

 Accessed February, 14, 2024. Available at https://www.iisd.org/system/files/2021-11/farming-future-agriculture-climate-change-canadian-prairies.pdf
- Lasslop, G., Reichstein, M., Papale, D., Richardson, A. D., Arneth, A., Barr, A., ... & Wohlfahrt, G. (2010). Separation of net ecosystem exchange into assimilation and

- respiration using a light response curve approach: critical issues and global evaluation. *Global change biology*, *16*(1), 187-208.
- Lessmann, M., Ros, G. H., Young, M. D., & de Vries, W. (2022). Global variation in soil carbon sequestration potential through improved cropland management. *Global Change Biology*, 28(3), 1162-1177.
- Lüthi, D., Le Floch, M., Bereiter, B., Blunier, T., Barnola, J. M., Siegenthaler, U., ... & Stocker, T. F. (2008). High-resolution carbon dioxide concentration record 650,000–800,000 years before present. *nature*, 453(7193), 379-382.
- Lynch, J., Cain, M., Frame, D., & Pierrehumbert, R. (2021). Agriculture's contribution to climate change and role in mitigation is distinct from predominantly fossil CO2-emitting sectors. *Frontiers in sustainable food systems*, 4, 518039.
- Mbow, H. O. P., Reisinger, A., Canadell, J., & O'Brien, P. (2017). Special Report on climate change, desertification, land degradation, sustainable land management, food security, and greenhouse gas fluxes in terrestrial ecosystems (SR2). *Ginevra*, *IPCC*, 650.
- Menefee, D., Scott, R. L., Abraha, M., Alfieri, J. G., Baker, J., Browning, D. M., ... & Smith,
 D. (2022). Unraveling the effects of management and climate on carbon fluxes of US
 croplands using the USDA Long-Term Agroecosystem (LTAR) network. *Agricultural* and Forest Meteorology, 326, 109154
- Moravek, A., Singh, S., Pattey, E., Pelletier, L., & Murphy, J. G. (2019). Measurements and quality control of ammonia eddy covariance fluxes: a new strategy for high-frequency attenuation correction. *Atmospheric Measurement Techniques*, *12*(11), 6059-6078.

- Murchie, E. H., Reynolds, M., & Meyers, R. A. (2012). Crop radiation capture and use efficiency. *Encyclopaedia of sustainability science and technology. New York:*Springer, New York, 2615-2638.
- Myhre, G., Aas, W., Cherian, R., Collins, W., Faluvegi, G., Flanner, M., ... & Tsyro, S. (2017).

 Multi-model simulations of aerosol and ozone radiative forcing due to anthropogenic emission changes during the period 1990–2015. *Atmospheric Chemistry and Physics*, 17(4), 2709-2720.
- O'sullivan, M., Friedlingstein, P., Sitch, S., Anthoni, P., Arneth, A., Arora, V. K., ... & Zaehle, S. (2022). Process-oriented analysis of dominant sources of uncertainty in the land carbon sink. *Nature communications*, *13*(1), 4781.
- Pattey, E., Edwards, G., Strachan, I. B., Desjardins, R. L., Kaharabata, S., & Wagner Riddle, C. (2006). Towards standards for measuring greenhouse gas fluxes from agricultural fields using instrumented towers. *Canadian journal of soil science*, 86(3), 373-400.
- Peichl, M., Arain, M. A., & Brodeur, J. J. (2010). Age effects on carbon fluxes in temperate pine forests. Agricultural and Forest Meteorology, 150(7-8), 1090-1101.
- Pellerin, S., Bamière, L., Angers, D., Béline, F., Benoit, M., Butault, J. P., ... & Chemineau, P. (2017). Identifying cost-competitive greenhouse gas mitigation potential of French agriculture. Environmental Science & Policy, 77, 130-139.
- Pittelkow, C. M., Linquist, B. A., Lundy, M. E., Liang, X., Van Groenigen, K. J., Lee, J., ... & Van Kessel, C. (2015). When does no-till yield more? A global meta-analysis. Field crops research, 183, 156-168.
- Quan, N., Lee, S. C., Chopra, C., Nesic, Z., Porto, P., Pow, P., ... & Black, T. A. (2023). Estimating net carbon and greenhouse gas balances of potato and pea crops on a

- conventional farm in western Canada. *Journal of Geophysical Research: Biogeosciences*, 128(3), e2022JG007113.
- Reichstein, M., Falge, E., Baldocchi, D., Papale, D., Aubinet, M., Berbigier, P., ... & Valentini, R. (2005). On the separation of net ecosystem exchange into assimilation and ecosystem respiration: review and improved algorithm. *Global change biology*, 11(9), 1424-1439.
- Shuttleworth, W. J. (2007). Putting the" vap" into evaporation. *Hydrology and Earth System Sciences*, 11(1), 210-244.
- Smith, P., Lanigan, G., Kutsch, W. L., Buchmann, N., Eugster, W., Aubinet, M., ... & Jones,
 M. (2010). Measurements necessary for assessing the net ecosystem carbon budget of croplands. *Agriculture, Ecosystems & Environment*, 139(3), 302-315.
- Smith, P. G. (2015). Long-term temporal trends in agri-environment and agricultural land use in Ontario, Canada: transformation, transition and significance. *Journal of Geography and Geology*, 7(2), 32.
- Smith, W. N., Grant, B. B., Campbell, C. A., McConkey, B. G., Desjardins, R. L., Kröbel, R., & Malhi, S. S. (2012). Crop residue removal effects on soil carbon: Measured and intermodel comparisons. Agriculture, ecosystems & environment, 161, 27-38.
- Solomon, S., Plattner, G. K., Knutti, R., & Friedlingstein, P. (2009). Irreversible climate change due to carbon dioxide emissions. *Proceedings of the national academy of sciences*, 106(6), 1704-1709.
- Statistics Canada (2017). Norfolk County by the Numbers: Census of Agriculture 2016.

 Norfolk County Tourism & Economic Development Division, Norfolk, Ontario.

 https://www.norfolkbusiness.ca/wp-content/uploads/2018/02/Norfolk-Ag-By-the-Numbers.pdf

- Statistics Canada (2018). Net Farm Income, CANSIM (Database), Table 002 0009.
- Suyker, A. E., & Verma, S. B. (2008). Interannual water vapor and energy exchange in an irrigated maize-based agroecosystem. *Agricultural and Forest Meteorology*, 148(3), 417-427.
- Statistics Canada (2021). Census of Agriculture 2021 (3438). https://www150.statcan.gc.ca/n1/pub/96-325-x/2021001/article/00006-eng.htm
- Statistics Canada. 2023. (table). *Census Profile*. 2021 Census of Population. Statistics Canada Catalogue no. 98-316-X2021001. Ottawa. Released November 15, 2023. https://www12.statcan.gc.ca/census-recensement/2021/dp-pd/prof/index.cfm?Lang=E (accessed February 13, 2024).
- Stockle, C. O., & Kemanian, A. R. (2009). Crop radiation capture and use efficiency: a framework for crop growth analysis In 'Crop physiology: applications for genetic improvement and agronomy'. (Eds VO Sadras, DF Calderini) pp. 145–170.
- Suyker, A. E., & Verma, S. B. (2012). Gross primary production and ecosystem respiration of irrigated and rainfed maize—soybean cropping systems over 8 years. *Agricultural and Forest Meteorology*, 165, 12-24.
- Thapa, V. R., Ghimire, R., Adhikari, K. P., & Lamichhane, S. (2023). Soil organic carbon sequestration potential of conservation agriculture in arid and semi-arid regions: A review. *Journal of Arid Environments*, 217, 105028.
- Verma, S. B., Dobermann, A., Cassman, K. G., Walters, D. T., Knops, J. M., Arkebauer, T. J.,
 ... & Walter-Shea, E. A. (2005). Annual carbon dioxide exchange in irrigated and rainfed maize-based agroecosystems. *Agricultural and Forest Meteorology*, 131(1-2), 77-96.

- Wang, L., Good, S. P., & Caylor, K. K. (2014). Global synthesis of vegetation control on evapotranspiration partitioning. *Geophysical Research Letters*, 41(19), 6753-6757.
- Wagner-Riddle C. (2021). AmeriFlux FLUXNET-1F CA-ER1 Elora Research Station, Ver. 3-5, AmeriFlux AMP, (Dataset). https://doi.org/10.17190/AMF/1832154.
- Wagner-Riddle, C., A. Furon, N.L. Mclaughlin, I. Lee, J. Barbeau, S. Jayasundara, J. Warland (2007). Intensive measurement of nitrous oxide emissions from a corn—soybean—wheat rotation under two contrasting management systems over 5 years. Global Change Biol., 13, 1722-1736.
- Webb, E. K., Pearman, G. I., & Leuning, R. (1980). Correction of flux measurements for density effects due to heat and water vapour transfer. *Quarterly Journal of the Royal Meteorological Society*, 106(447), 85-100.
- Wiesner, S., Desai, A. R., Duff, A. J., Metzger, S., & Stoy, P. C. (2022). Quantifying the natural climate solution potential of agricultural systems by combining eddy covariance and remote sensing. Journal of Geophysical Research: Biogeosciences, 127(9), e2022JG006895.
- Wutzler, T., Lucas-Moffat, A., Migliavacca, M., Knauer, J., Sickel, K., Šigut, L., ... & Reichstein, M. (2018). Basic and extensible post-processing of eddy covariance flux data with REddyProc. *Biogeosciences*, 15(16), 5015-5030.
- Yan, H., Acquah, S. J., Zhang, C., Wang, G., Huang, S., Zhang, H., ... & Wu, H. (2019). Energy partitioning of greenhouse cucumber based on the application of Penman-Monteith and Bulk Transfer models. *Agricultural Water Management*, 217, 201-211.
- Yildirim, T., Bilyea, T., Buckingham, D., Bigley, E., & de Vynck, L. (2019). Clean growth in agriculture. White paper, Clean Economy Fund, Canadian Agri-food Policy Institute,

Ottawa. Accessed on 13 Feb 2024, available on https://capi-icpa.ca/wp-content/uploads/2019/03/2019-05-15-CAPI-CEF-FINAL-Report-WEB.pdf

Zhang, L., Zhou, X., Li, G., & Liu, F. (2021). Elevated CO2 modulates carbon assimilation and leaf water use efficiency of Nicotiana tabacum L.(tobacco) under patchy soil nutrient deficiency. *Industrial Crops and Products*, *166*, 113500.

Table 2.1. Monthly and annual total precipitation (P) values and Temperature (T) in 2020, 2021, 2022 and 2023. Normal precipitation over 30-year period (1991-2020) is also given.

Marath	2020		2021		2022		2023		1991-2020	
Month	P	T	P	T	P	T	P	T	P	T
January	109	-0.71	44	-2.71	7	-8.43	91	-0.77	81	-5.0
February	52	-2.92	61	-6.73	28	-4.62	76	-1.18	58	-4.5
March	109	3.56	54	3.28	91	1.15	135	0.46	71	0.3
April	121	5.62	80	7.98	54	6.57	104	8.43	87	6.8
May	82	12.32	38	12.51	95	15.13	25	12.77	88	13.6
June	75	20.00	92	21.21	89	19.01	76	18.34	82	19.0
July	121	23.19	184	20.47	108	20.85	123	20.79	89	21.2
August	115	20.25	46	21.76	105	20.69	97	18.74	80	20.1
September	88	17.35	112	16.91	138	16.33	42	17.19	86	16.4
October	83	9.12	210	13.53	91	9.55	72	11.49	86	10.0
November	88	6.31	67	3.42	53	4.86	56	3.18	83	3.9
December	84	-0.12	23	1.50	87	-0.49	82	2.69	76	-1.7
Annual	1127	9.5	1009	9.43	947	8.38	979	9.34	965	8.4

Table 2.2. Annual and growing season (GS) total GEP, NEP, RE and ET. GEP, NEP, RE, Grain yield (GY) and net ecosystem carbon balance (NECB) values in g C m^{-2} and ET values in mm. The uncertainty is represented as \pm standard deviation, derived from daily measurements.

	2020 (Corn)		2021 (Corn)		2022 (Potato)		2022 (Tobacco)	
Year		GS		GS	Annual	GS	Annual	GS
	Annual	DOY	Annual	DOY		DOY		DOY
	Aimuai	144-273		160-264		187-262		152-276
		(130 days)		(105 days)		(76 days)		(125 days)
GEP	1289 ±6.1	1275 ±7.1	1359 (5.7)	1255±4.1	705±3.3	589 ±2.7	885±2.8	661±2.8
NEP	485 ±3.7	579 ±4.6	249 ±3.5	543 ±3.5	-120±2.1	304 ±2.5	7±1.6	113±2.1
RE	804 ±2.1	696 ±2.5	1110 ±2.7	712 ±1.2	825±1.9	385 ±0.9	878±1.9	536±1.3
ET	680 ±1.3	406 ±1.3	727 ±1.4	393 ±1.1	732 ±1.4	287 ±1.3	715±1.2	370±1.2
GY^*		537		491		118		124
NECB**	-52	42	-242	52	-238	186	-117	-11

^{*} The carbon content of grain yield (GY) was 43.0% of corn (Holou & Kindomihou, 2017), 32.9% of sweet potato (Hagenimana et al., 1998), and 36.9% of tobacco plants (Frantz et al., 2022), respectively.

^{**}Net ecosystem C balance (NECB) was calculated as NECB = (NEP – GY). Negative NECB indicates C loss from the ecosystem.

Table 2.3. The relationship of climatic variables (PAR, Ta, Ts, VPD, VWC) with biomass production (GEP), carbon uptake (NEP), respiration (RE), and water balance (ET) accumulated with different crops from 2020 to 2023. The significance level is indicated based on the P value, where * represents non-significance, ** shows weak to moderate significance, and *** indicates very strong significance.

GEP									
Multivariable linear regression					Simple linear regression				
	Estimate	Standard Error	$R^{2}(P)$	\mathbb{R}^2	pValue	Significance			
Intercept	-1.892	0.300		-	-	-			
PAR	-0.001	0.001	0.48	0.39	0.0001	***			
Ta	0.047	0.032	0.46	0.66	0.0001	***			
Ts	0.339	0.035	(0.0001)	0.69	0.0001	***			
VPD	0.664	0.514		0.42	0.007	**			
VWC	5.234	1.458		0.17	0.009	*			
			NEP						
Intercept	-1.471	0.232		-	-	-			
PAR	-0.001	0.001		0.20	0.0001	***			
Ta	-0.016	0.024	0.17	0.38	0.0001	***			
Ts	0.154	0.027	(0.0001)	0.40	0.0001	***			
VPD	0.69	0.397	(0.0001)	0.25	0.0001	***			
VWC	3.247	1.127		0.13	0.0001	***			
			RE						
Intercept	-0.420	0.096		-	-	-			
PAR	-0.001	0.001	0.70	0.52	0.0001	***			
Ta	0.064	0.010	0.79	0.86	0.0001	***			
Ts	0.185	0.011	(0.0001)	0.88	0.0001	***			
VPD	-0.034	0.165	()	0.54	0.0001	***			
VWC	1.986	0.468		0.19	0.0067	**			
	ET								
Intercept	0.552	0.074		-	-	-			
PAR	0.001	0.001	0.60	0.60	0.0001	***			
Ta	0.022	0.007	0.60	0.72	0.0001	***			
Ts	0.071	0.009	(0.0001	0.75	0.0001	***			
VPD	0.340	0.128	(0.56	0.0001	***			
VWC	-0.473	0.362		0.04	0.1345	*			

Table 2.4. Annual NEP of the corn crop in different study sites of North America.

Site location	NEP (g C m ⁻² y ⁻¹)	Mean annual Precipitation (mm)	Mean annual Temperature (°C)	Site- year	Reference
Turkey Point, ON, CA	367	1024	9.7	2	Study Site
Mandan, ND, USA	120	420	6	2	Liebig et al. (2022)
Westham Island, BC, CA	70	967	10.8	2	Quan et al. (2023)
Ames, IA, USA	466	942	9.7	4	Hernandez-Ramirez et al. (2011)
Champaign, IL, USA	576	-	-	3	Hollinger et al. (2005)
Mead, NE, USA	441	570	11.0	3	Verma et al. (2005)
Rosemount, MN, USA	294	956	-	2	Baker & Griffis, (2005)
Ames, Iowa, USA	327	740	-	10	Dold et al. (2017)
Winnipeg, MB, CA	72	292	4.7	1	Glenn et al. (2010)

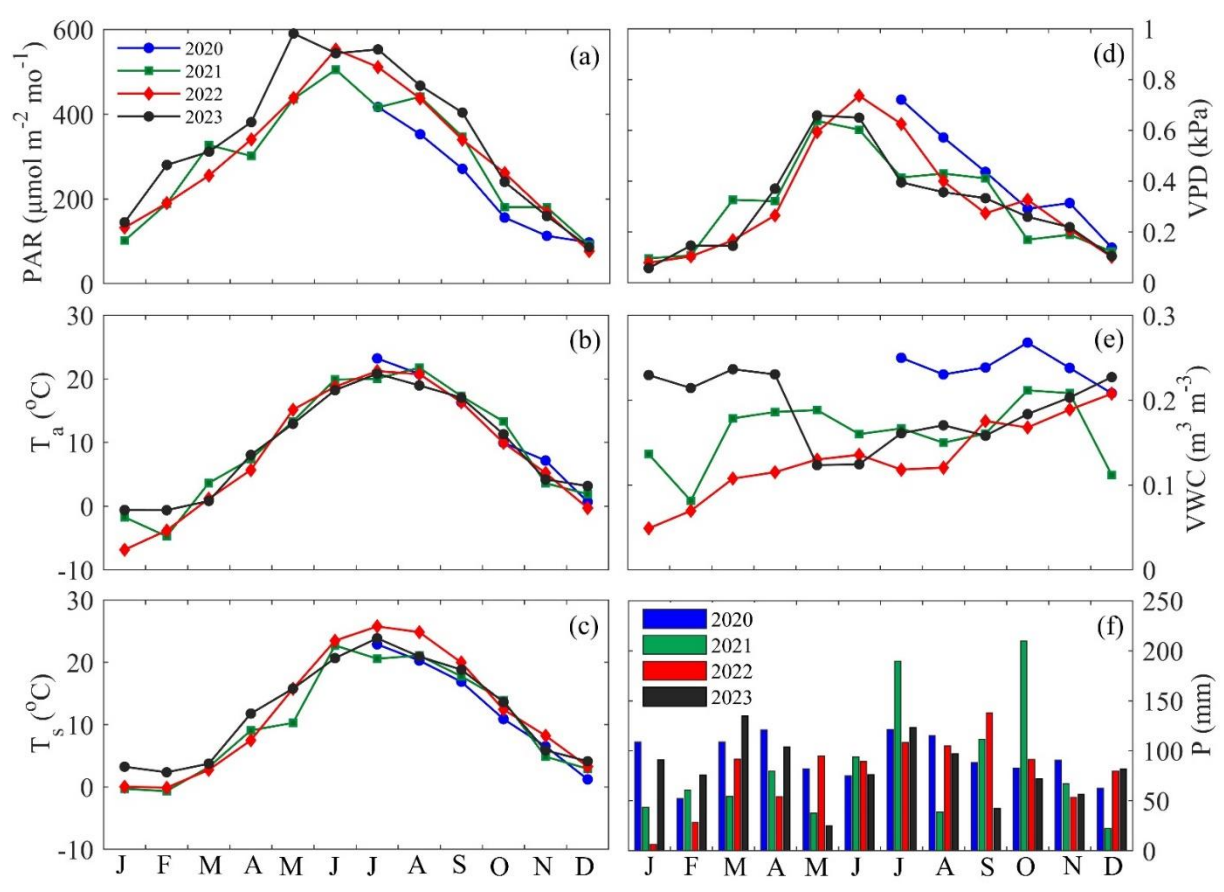


Figure 2.1. The annual course of the meteorological conditions at Turkey Point Agricultural site for 2020 to 2023: (a) monthly mean Photosynthetically Active Radiation (PAR), (b) monthly mean air temperature (Ta), (c) monthly mean soil temperature (Ts) at 5-cm depth, (d) monthly mean vapor pressure deficit (VPD), (e) monthly mean volumetric water content (VWC) in upper 5-cm and 10-40 cm soil layers, and (f) monthly total precipitation (P).

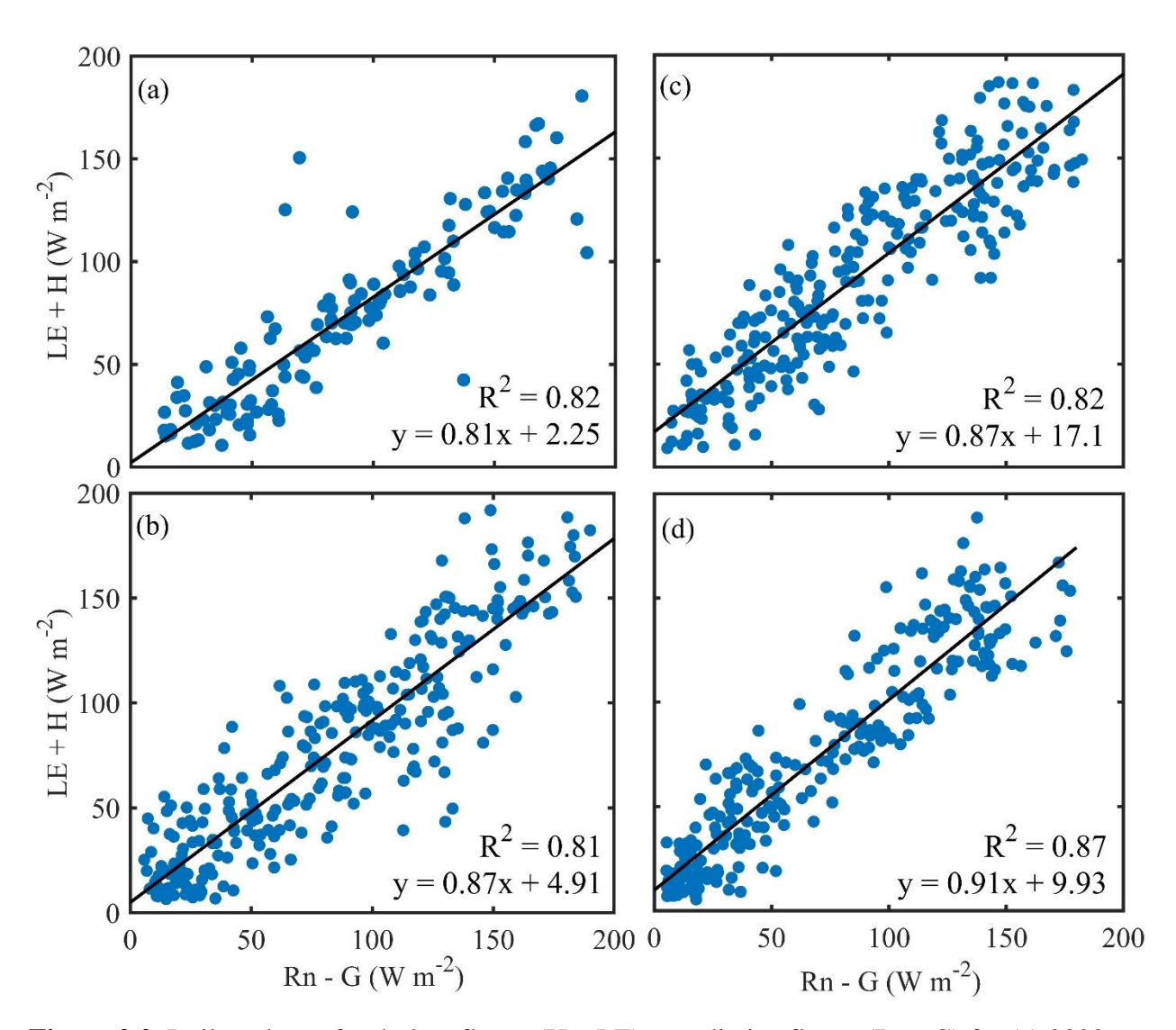


Figure 2.2. Daily values of turbulent fluxes (H + LE) vs radiative fluxes (Rn - G) for (a) 2020, (b) 2021, (c) 2022 and (d) 2023, respectively. Data were obtained from non-gap-filled daily observations excluding abnormal values.

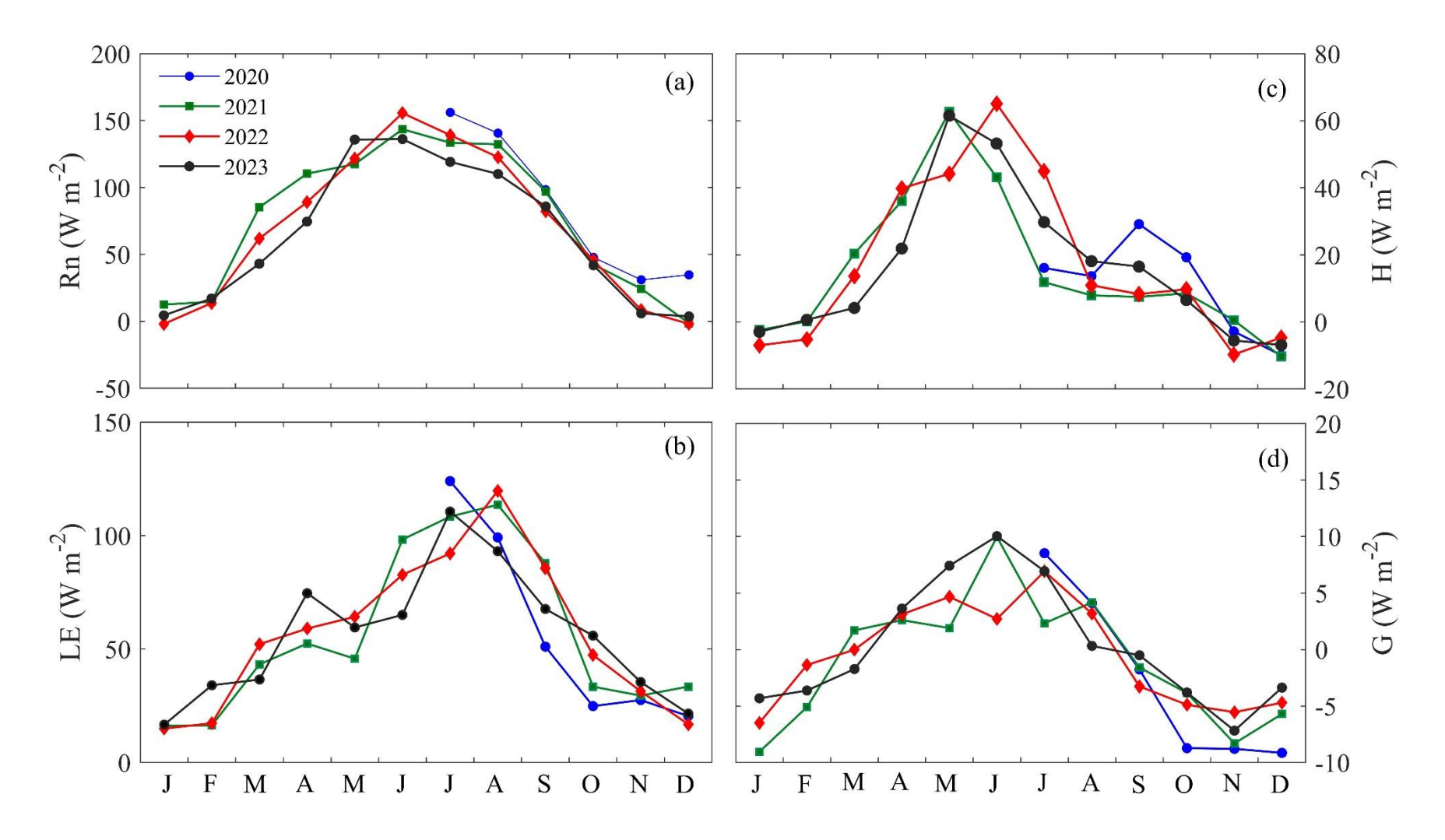


Figure 2.3. The monthly mean energy fluxes for 2020, 2021, 2022 and 2023. Monthly mean values of (a) net radiation (Rn), (b) latent heat flux (LE), (c) sensible heat flux (H), and (d) soil heat flux (G).

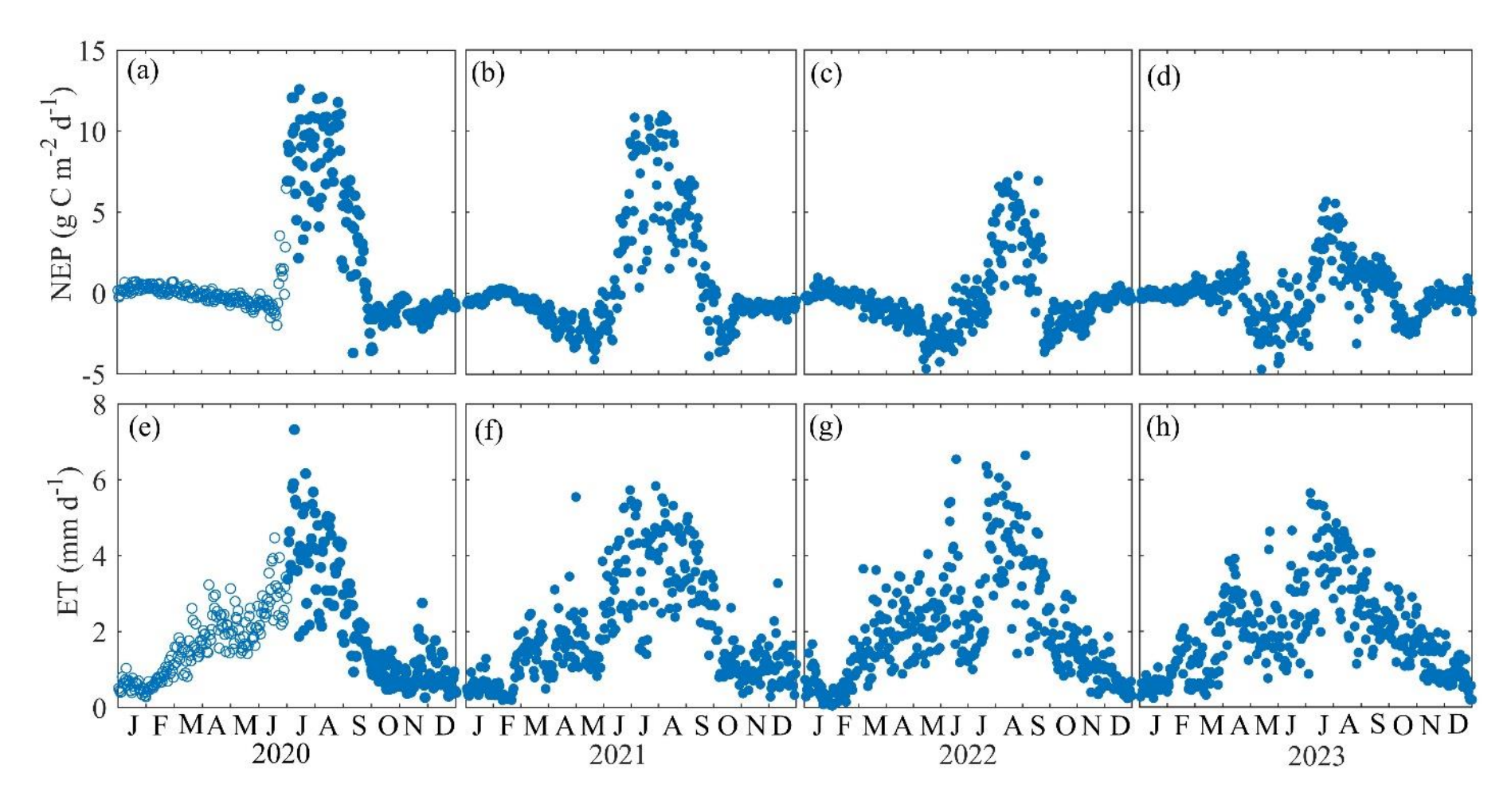


Figure 2.4. Daily values of net ecosystem productivity, NEP (a-d) and evapotranspiration, ET (e-h) values for 2020, 2021, 2022 and 2023. The open circle from the NEP and ET values of the figure (a) and (e) represents the gap-fill NEP and ET.

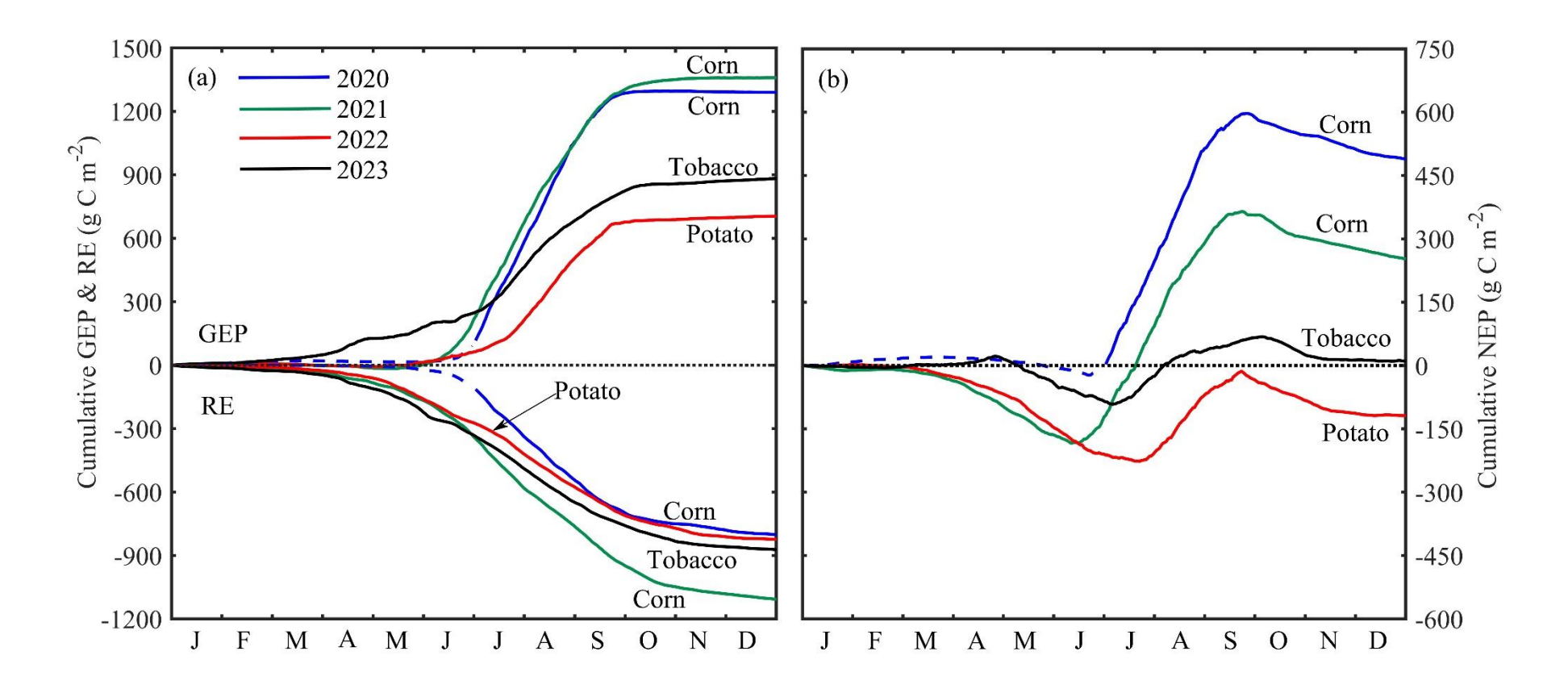


Figure 2.5. The cumulative values of (a) GEP and RE and (b) NEP for 2020, 2021, 2022 and 2023. The dashed lines in the cumulative lines indicate gap-filled data while solid lines are measured values.

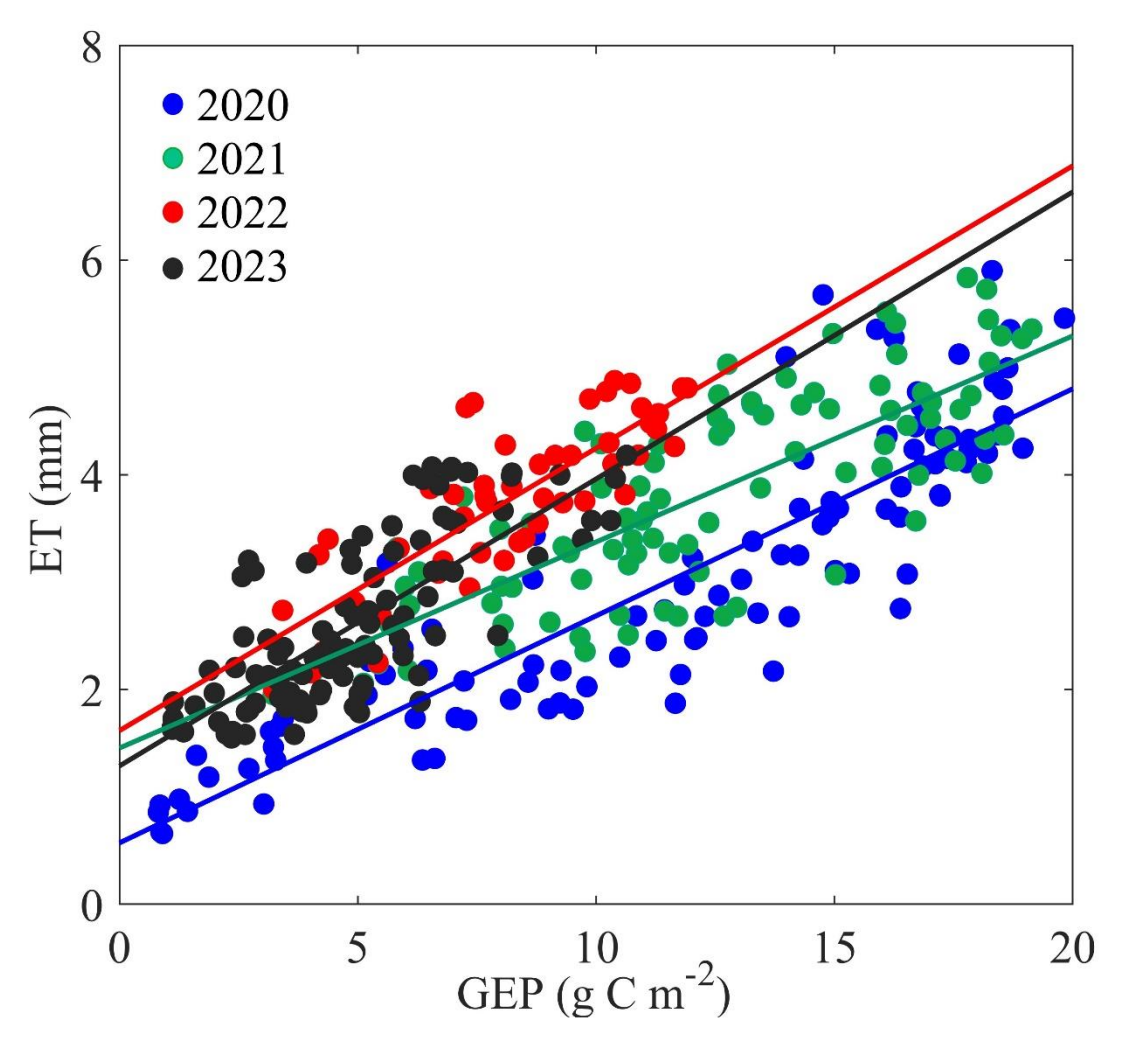


Figure 2.6. Water use efficiency (WUE) from 2020 to 2023. The GEP and ET represent the growing season daily values from different crop systems.

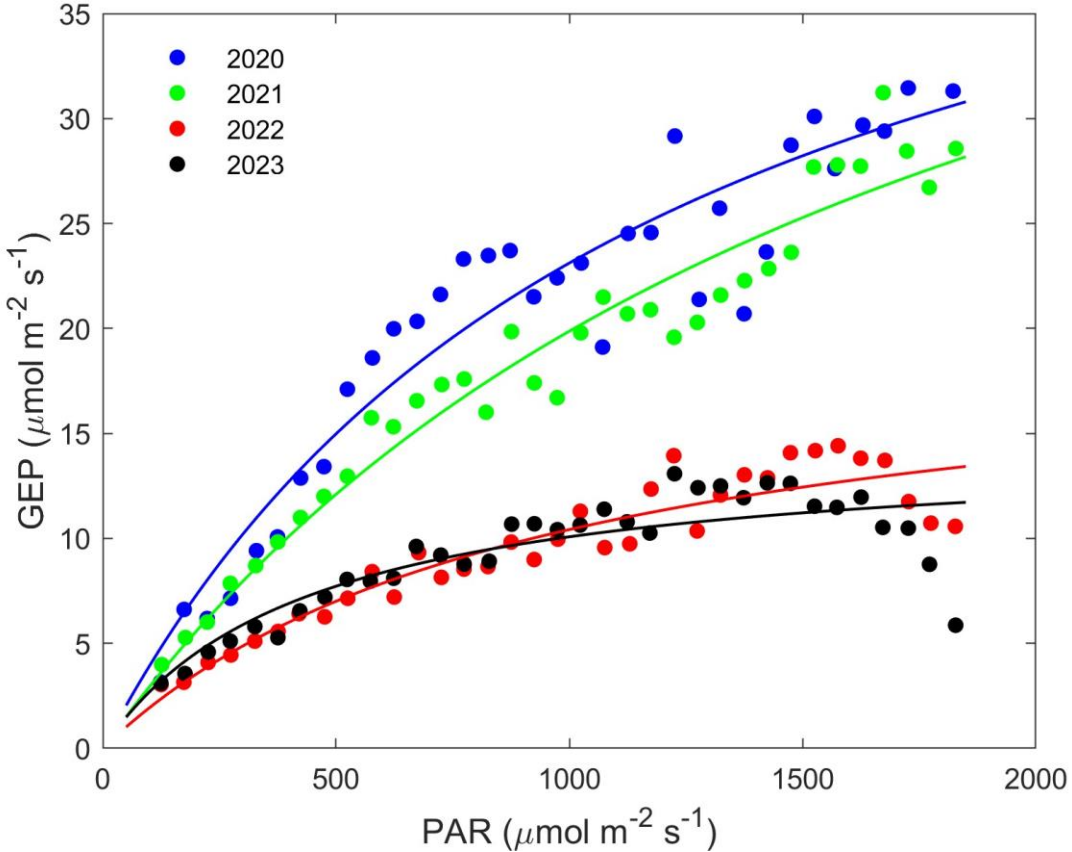


Figure 2.7. The relationship between Gross Primary Production (GEP) and Photosynthesis Active Radiation (PAR) across different crops. Non-gap-filled daytime measurements were conducted during the growing seasons of 2020 (corn), 2021 (corn), 2022 (sweet potato), and 2023 (tobacco). The figure presents the bin-averaged half-hourly GEP and PAR levels from 2020 to 2023, with a bin size for averaging set at 50 μmol m⁻² s⁻¹. The curves represent the relationship between GEP and PAR, fitted using by the hyperbolic model where the quantum yield (α) value was 0.0426, 0.0310, 0.0214 and 0.0330 mol CO2 mol-1 photons, respectively for 2020, 2021, 2022 and 2023 with the maximum photosynthetic capacity (Vmax) value of 50.57, 55.47, 20.33 and 14.49 μmol m-2 s-1. R2 was 0.90. 0.95, 0.88 an0.74 for 2020, 2021, 2022 and 2023, respectively, while corresponding σ values were 14.65, 9.48, 6.79 and 8.33.

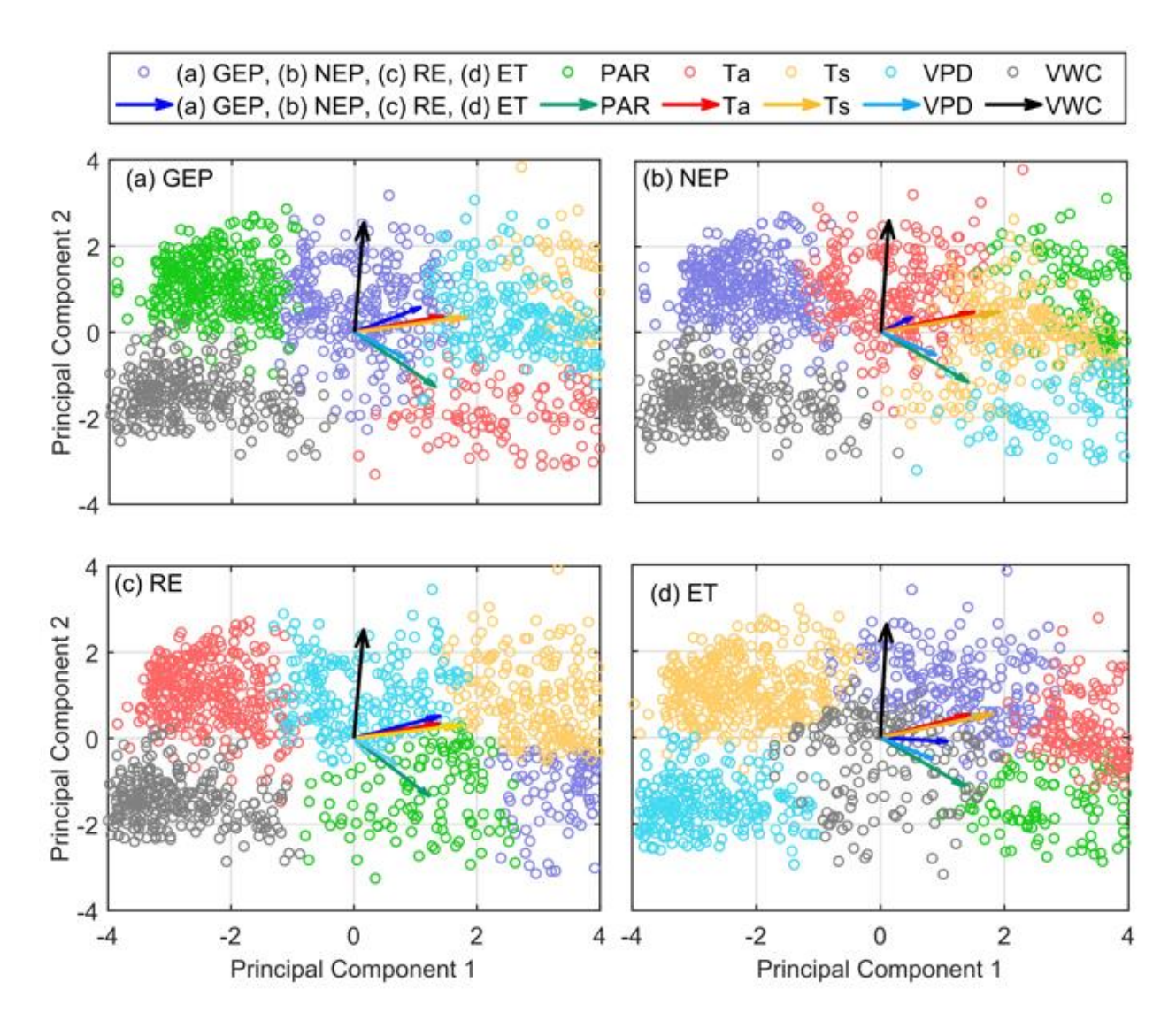


Figure 2.8. Principal component analysis (PCA) of environmental controls with panels: (a) for GEP, (b) for NEP, (c) for RE, and (d) for ET.

CHAPTER 3

EVALUATING THE EFFECTIVENESS OF DIFFERENT VARIABLE RETENTION HARVESTING TREATMENTS ON FOREST CARBON UPTAKE USING REMOTE SENSING

3.1 Abstract

Variable retention harvesting (VRH) is an ecologically based forest management practice applied to emulate natural post-disturbance residual canopy structure and increase the biodiversity and resilience of a regenerating stand. The pattern and density of canopy retention also influences the productivity, mortality, and carbon (C) sequestration rates of residual trees. In this study, we used high-resolution satellite and drone remote sensing data to evaluate the effect of five different VRH treatments on growth and C uptake of a 90-year-old red pine (Pinus resinosa Ait.) plantation forest in southern Ontario, Canada. The treatments included four different combinations of harvesting intensity residual tree distribution including 33% aggregate retention (33A), 55% aggregate retention (55A), 33% dispersed retention (33D), and 55% dispersed retention (55D) and an unharvested control (CN) each replicated four times in 1 ha plots. Satellite- and drone-derived normal difference vegetation index (NDVI) and gross primary productivity (GPP) were estimated for each treatment during the growing seasons from 2010 to 2020. Over this period, observed mean daily NDVI values ranged from 0.25 to 0.86 among treatments, where the 55D treatment consistently showed the highest NDVI values. Overall, the highest mean daily GPP values were observed in the CN treatment, followed by the 55D, 55A, 33D, and 33A treatments. Remote sensing-derived mean annual GPP for the entire 20 ha study site was 1651 ± 89 g C m $^{-2}$ year $^{-1}$, with a range of 1407 to 1864 g C m $^{-2}$ year⁻¹ from 2010 to 2020. Satellite-derived annual GPP values were linearly related with observed annual GPP ($R^2 = 0.88$, p = 0.032) measured using the eddy covariance technique in an adjacent white pine plantation of similar age and height over the study period. Study results

suggested that VRH treatments that create a uniformly dispersed residual canopy retaining more than half of the initial basal area (e.g. 55D) is a viable forest management practice where optimizing forest growth and C uptake is a primary management objective. Our study will help forest managers and researchers to develop methodologies to evaluate the effectiveness of forest management practices, tailor them to achieve climate mitigation and adaptation goals and to develop forest management pathways for nature-based climate solutions.

3.2 Introduction

Forest ecosystems cover 30% of Earth's land surface area (Heino et al., 2015) and play a major role in the global carbon (C) cycle (Ontl et al., 2016; Reichstein and Carvalhais, 2019). At the stand level, growth and C uptake of managed forests is strongly influenced by tree density, age, species composition, and anthropogenic disturbances such as harvesting and thinning (Mayer et al., 2020; Ameray et al., 2021; Park et al., 2018; Simard et al., 2020). Forest growth and C uptake can be monitored using remote sensing techniques. Sentinel-2A and Sentinel-2B satellites of the COPERNICUS system of the European Union's Earth observation program (Drusch et al., 2012; Binet et al., 2022), provide new capabilities for high-resolution multispectral sensor-based forest ecosystem monitoring (Löw and Koukal, 2020). These sensors provide up to 10 m spatial resolution with an approximate five-day temporal resolution (Drusch et al., 2012) and are capable of continuous, long-term monitoring of forest characteristics and growth. Continuous forest monitoring using a single satellite can be complicated due to data outliers, atmospheric noise, abnormal weather, and scarcity of accessible data (Kogan, 1990; Lastovicka et al., 2020). Landsat-8 and Landsat-7 satellites of the National Aeronautics and Space Administration (NASA) and the United States Geological Survey (USGS) provide multispectral data sources for long-term forest monitoring (Masek et al., 2013). Landsat satellite data has 30 m spatial resolution and 16-day temporal resolution with global coverage in visible (VIS), near-infrared (NIR), short wave infrared (SWIR), and thermal infrared (TIR) wavelengths (Landsat, 2011, 2019). In addition, the use of unmanned aerial vehicles (UAV) or drones mounted with remote sensing sensors are also rapidly becoming mainstream platforms for forest monitoring (Dainelli et al., 2021).

The most commonly used remote sensing-derived indicators for monitoring forest growth and productivity are leaf area index (LAI) (Sebastiani et al., 2023; Kaplan et al., 2023; Ali et al., 2022), the normalized difference vegetation index (NDVI) (Chen et al., 2006; Lausch et al., 2018; Matsushita et al., 2007; Shen et al., 2018; Tucker & Sellers, 1986; Vescovo et al., 2011; Zhao and Chen, 2005) and gross primary productivity (GPP) (Gao et al., 2015; Mao et al., 2012; Zhang et al., 2016, 2017). The Sentinel (10 m resolution) and Landsat-based NDVI (30 m resolution) have shown a good correlation with forest growth and productivity (Frampton et al., 2013; Han et al., 2021). The MODIS-derived moderate resolution estimate of GPP (250 to 500 m resolution) is the most widely used productivity indicator in the terrestrial ecosystem literature (Guo et al., 2006; Heinsch et al., 2006; Running and Zhao, 2015; Zhao et al., 2006; Grabska-Szwagrzyk & Tymińska-Czabańska, 2023). Some researchers have also estimated plot-level GPP using Sentinel (10 m resolution) and Landsat (15 to 30 m resolution) data (Morell-Monzó et al., 2020). Additionally, GPP can be measured at the plot-level using the eddy covariance (EC) technique (Arain et al., 2022; Baldocchi, 2019, 2020; Beamesderfer et al., 2020; Wohlfahrt and Gu, 2015).

In order to reduce greenhouse gas emissions and mitigate climate change, nature-based climate solutions have been suggested as cost-effective strategies to increase C sequestration in terrestrial ecosystems (Kaarakka et al., 2021; Creutzig et al., 2022; Marvin et al., 2023).

Improved forest management, conservation and restoration have been identified as key pathways to achieve this goal. In Canada, a large portion (~66%) of forests receive some form of active management to maintain economic and ecological sustainability (Natural Resources Canada (NRC), 2016). Among these forest management practices, variable retention harvesting (VRH) is an ecologically based approach that was originally developed to reduce reliance on clearcutting to harvest timber and to promote stand regeneration (Franklin et al., 1997). This silvicultural approach retains a portion of living and dead trees that vary in density and spatial arrangement to create a post-harvest residual canopy structure that emulates that created by the natural disturbance regime of a given area (Franklin et al., 1997, 2007; Palik and D'Amato, 2019). The effects of VRH on biodiversity, growth, mortality, and other biophysical and ecosystem processes have been widely studied in North America over the past few decades (Aubry et al., 2009; Beese et al., 2019; Palik et al., 2002; Puettmann et al., 2016; Roberts and Harrington, 2008; Xing et al., 2018). Structural changes to the residual canopy due to VRH and other partial harvesting practices enhance the photosynthetic energy supply to remaining trees, reduce competition for water and nutrients, and consequently increase growth and C uptake (Philpott et al., 2018; Zugic et al., 2021). However, VRH impacts on residual tree growth vary depending upon the intensity and pattern of canopy retention and their effects on stand microclimate and energy balance and and land type (Aussenac, 2000; Roberts and Harrington, 2008; Xing et al., 2018; Makipaa et al., 2023). In this regard, remote sensing techniques can help to quantify changes in forest structure, environmental conditions, growth and C uptake to determine the effectiveness of various practices to meet specific management objectives (Löw and Koukal, 2020; McRoberts and Tomppo, 2007; Pause et al., 2016; Fassnacht et al., 2023).

In 2014, an 83-year-old red pine (Pinus resinosa Ait.) plantation was subjected to five different VRH treatments with the objective of restoring the forest stand to its native forest composition

(Zugic et al., 2021; Bodo and Arain, 2022; Bodo et al., 2023). The treatments combined two levels of basal area retention with uniformly dispersed or aggregate, "patch" retention: 33% aggregate retention (33A), 55% aggregate retention (55A), 33% dispersed retention (33D), 55% dispersed retention (55D) and an unharvested control (CN). This completely randomized experimental design provided an opportunity to examine the effects of these five VRH treatments on growth and C uptake of the residual canopy utilizing multi-sensor remote sensing data. It also provided opportunities to explore how VRH treatments can contribute to develop forest management pathways for nature-based climate solutions. The specific objectives of our study are to (i) quantify the annual differences in NDVI among VRH treatments over the pre-harvest (2010-2013) and post-harvest (2014-2020) periods, (ii) determine the rate of acclimation of growth of residual trees to the post-harvest treatment environment and (iii) evaluate which treatment(s) might be most effective in enhancing future residual forest canopy growth and C sequestration.

3.3 Methods

3.3.1 Site description

The study site is located within the St. Williams Conservation Reserve (42.705134° N and 80.354219°W), about 12 km southwest of the town of Simcoe in Norfolk County in southern Ontario, Canada (Figure 3.1). The site is part of the Turkey Point Environmental Observatory (TPEO) and has been associated with the Global Water Futures program and AmeriFlux and global Fluxnet networks (Arain et al., 2022).

The plantation was established in 1931 by planting seedlings at 2 m \times 2 m spacing (2500 trees ha⁻¹). It was thinned in 1959–1960 when every fourth row of trees was harvested, perhaps along

with light selective thinning of remaining rows. It was selectively thinned in the mid-1980s to remove a maximum of one-third of the remaining canopy trees (McKenzie et al., 2023). In February 2014, the stand was thinned a third time when five VRH treatments were randomly assigned to four replicate plots (20 plots, ~1 ha each). At the time of VRH treatment, the plantation was almost pure red pine with an average basal area of $38.4 \pm 5.5 \text{ m}^2 \text{ ha}^{-1}$ and tree density of 641.3 ± 103.2 trees ha⁻¹. Tree diameter at 1.3 m height was 28.6 ± 4.3 m, ranging from 17.2 to 47.2 m, with an average height of 23.8 ± 2.8 m (Bodo and Arain 2022; Zugic et al., 2021). The primary understory vegetation species consist of yellow mandarin (Disporum lanuginosum), bracken fern (Pteridium), red trillium (Trillium erectum), poison ivy (*Toxicodendron radicans*), Canada mayflower (*Maianthemum canadense*), Allegheny raspberry (*Rubus allegheniensis*), black cherry (*Prunus serotina*), red maple (*Acer rubrum*), black oak (*Quercus velutina*), eastern white pine (*Pinus strobus*), wood violet (*Viola palmata*), and several moss species (*Bryophyta*).

The climate in the region is warm humid continental with a 30-year (1980–2010) mean annual air temperature (Tair) of 8.0 °C and mean annual precipitation (P) of 1036 mm, based on data from the Environment and Climate Change Canada weather station at Delhi, Ontario, Canada. Snowfall accounts for about 13% of annual P.

3.3.2 Data Set

4.3.2.1 Satellite data

The Sentinel-2 multispectral instrument captures 13 spectral bands, including 10 m spatial resolution of VIS and NIR, and 20 m spatial resolution of SWIR spectrum every five days (Drusch et al., 2012; Sun et al., 2022). Landsat-7 and Landsat-8 satellites provide earth surface

imagery at 30 m resolution with 16-day temporal resolution and were used to fill the gap in Sentinel-2 dataset (Landsat, 2011, 2019). Both satellite datasets were obtained from https://earthexplorer.usgs.gov/ and used to estimate NDVI and GPP of each treatment plot. Agreement between these two data sets was assessed for a day (11 June 2018) when both satellites passed over our site at the same time (\sim 15 minutes). A significant (p = 0.039), positive linear relationship (R² = 0.62) was observed between NDVI provided by Sentinel-2 and Landsat-8.

3.3.2.2 Drone instrumentation and data retrieval

We used a drone-sensor system developed by the Natural Resources Canada - Canada Center for Remote Sensing (Canisius et al., 2019) to estimate NDVI of VRH plots for 2019 and 2020 and compared the drone and satellite-measured plot-level NDVI values. The drone system consisted of a digital camera (Zenmuse Z3), one pyranometer, one quantum sensor, one VIS spectrometer, and one NIR spectrometer. A ground sub-system included a similar establishment of sensors. Drone flight missions were conducted on 25 June 2019 and 17 July 2020 using the Litchi-DJI (drone mission controlling app). Drone cameras, ground and UAV data loggers, and ground and UAV microcomputers generated the VIS and NIR spectrometer's response at millisecond intervals, including the real-time response. Retrieved data were temporally adjusted through mission record and sensor response time was reviewed with recorded video time, which was spatially adjusted using ArcMap (Esri) GIS interface coordinates.

3.3.2.3 Eddy covariance flux and meteorological measurements

Energy, water and CO₂ fluxes have been continuously measured at an adjacent eastern white pine plantation of similar age and height using the EC technique since 2003 (Arain et al., 2022). This plantation is also part of TPEO and known as CA-TP4 in global Fluxnet and TP39 (Arain and Restrepo-Coupe, 2005; Arain et al., 2022). Because of close proximity, both red and white pine plantations share similar landforms and meteorological characteristics. Meteorological variables, including downward and upward photosynthetically active radiation (PAR), net radiation, Tair, relative humidity, wind speed and direction, precipitation, and soil temperature and soil moisture at several (2, 5, 10, 20. 50 and 100 cm) depths at two locations were also continuously measured. All flux, meteorological and soil data were verified, gap-filled and averaged to half-hour intervals. Further details are provided in Arain et al. (2022). GPP measured by EC (GPPEC) was used as a reference for comparison with satellite derived GPP as described in section 3.3.3.

3.3.3 Satellite GPP estimates

Satellite data and observed PAR and Tair from the CA-TP4 site were used to calculate GPP following Zhang et al. (2016, 2017) as shown in Figure 4.2. Sentinel-2 SWIR 20 m band and Landsat data available at 30 m resolution were resampled to 10 m resolution without any statistical transformation for spatial adjustment. Further details are described in Supplementary section (3.9).

3.3.4 Statistical analysis

The weighted double logistic (WDL) function described in Yang et al., (2019) was used to fit the time series data for mean daily NDVI and GPP values. WDL uses two logistic functions

according to vegetation growth activity namely, the growing part (f1) and the declining part (f2) to set the model parameters which can provide the daily time series as shown in the following equation (Yang et al., 2019).

$$y = f_1 + f_2 + e (3.1)$$

$$f_1 = \frac{c_1}{1 + e^{a_1 + b_1 t}} + d_1 \tag{3.2}$$

$$f_2 = \frac{c_2}{1 + e^{a_2 + b_2 t}} + d_2 \tag{3.3}$$

$$e = max (c_1 + d_1, c_2 + d_2)$$
(3.4)

where y is the time series of NDVI and GPP, d and c+d denote the minimum value (min(f)) and maximum value $(\max(f)),$ respectively; c indicates the local amplitude; and a and b determine the shape and slope of the logistic function, respectively. The subscripts 1 and 2 identify the parameters of the growing and declining parts, respectively. In the retrieval of these unknown parameters, the initial d and c are assigned as min(f) and max(f)-min(f), respectively. Thus, the principal challenge is to derive parameters a and b. Considering the different weights of each data point, we transformed the non-linear fitted regression into a linear one by a function transformation as a1+b1 t=In(c1f1-d1-1). Furthermore, the weighted Least Squares (WLS) method was applied to solve the analytic expression of the logistic function for each part (f1 and f2).

Two-dimensional principal component analysis (PCA) was used to determine shifts in comparative monthly mean NDVI among VRH treatments that occurred seven years post-harvest using data from seven composite images for each VRH plot for 2014 and 2020 (Jollife

and Cadima, 2016). We also graphically displayed the PCA results for NDVI in a biplot using MATLAB (Jollife and Cadima, 2016).

3.4 Results

3.4.1 Climate

Time series of meteorological variables measured at the adjacent white pine plantation (CA-TP4) from 2010 to 2020 are shown in Figure 3.3. Growing season and annual values of meteorological variables are presented in Table 3.1. Maximum mean daily PAR reached 750 μmol m⁻² s⁻¹. Maximum (minimum) mean annual PAR of 357 (314) μmol m⁻² s⁻¹ was observed in 2016 (2019). The highest mean annual Tair of 11.2 °C was observed in 2012, whereas the lowest value of 8.1 °C was recorded in 2014. The highest (lowest) mean daily vapor pressure deficit (VPD) of 0.5 (0.34) kPa was recorded in 2020 (2010). Similarly, the highest annual total P of 1649 mm occurred in 2018, whereas the lowest annual P of 778 mm was recorded in 2016 (Figure 3.4). In 2014, 2016 and 2017, comparatively dry growing season conditions had a significant impact on forest growth. This is evident from the lower NDVI observed in 2014, 2016, and 2017, indicating reduced photosynthetic activity during these years (Table 3.1). Conversely, the years 2010, 2018, 2019, and 2020 experienced comparatively higher P during the growing season, coinciding with maximum NDVI values.

In the study region, the local climate during the winter season is significantly influenced by both eastern and western oscillations (Shah, et al., 2022; Thorne and Arain, 2015). Specifically, winter temperatures are intricately linked to the North Atlantic Oscillation (NAO), Arctic Oscillation (AO), and Eastern Pacific Oscillation (EPO), while the total snowfall is correlated with the Pacific-North American (PNA) and El Niño-Southern Oscillation (ENSO) (Thorne

and Arain, 2015). These oscillations play a key role in C dynamics of the forest ecosystem during the winter and spring seasons (Zhang eta al., 2011). However, our study is focused on investigating the dynamics of the forest C sequestration and growth during the summer-dominated growing season.

3.4.2 Effects of variable retention harvesting on forest growth

The VRH treatments caused changes in stand structure and growth that are reflected in spatial patterns of monthly mean NDVI (Figure 3.5). These differences in NDVI are most prominent or clearly shown in variations from pre-harvest and post-harvest (Figure 3.5). Plot-level mean daily NDVI values over the growing season (April to October) were 0.57, 0.56, 0.56, 0.57, and 0.56 in 33A, 55A, 33D, 55D, and CN plots, respectively, during the pre-harvest period from 2010 to 2013 (Table 3.2). The mean daily NDVI values for the first growing season after harvest in 2014 were 0.42, 0.43, 0.45, 0.50, and 0.51 in 33A, 55A, 33D, 55D, and CN treatments, respectively. Similarly, mean daily NDVI values for the growing season over the entire post-harvesting period from 2014 to 2020 were 0.51, 0.53, 0.54, 0.60, and 0.58 in the 33A, 55A, 33D, 55D, and CN treatments, respectively. In the post-harvesting period, 55D treatment had the highest NDVI value, followed by CN, 55A, 33D and 33A treatments as shown in time series of mean daily NDVI values for each VRH treatment in Figure 3.6a.

Overall, mean daily NDVI values ranged from 0.25 to 0.86 among treatments from 2010 to 2020 (Figure 3.6a). The lowest seasonal NDVI values for all treatments were observed in 2016, while the highest NDVI values were observed in 2020 (Table 3.2). Differences among treatments were comparatively small from 2014 to 2016. Thereafter, treatment differences became more prominent from 2017 to 2020. Again, the mean daily NDVI was consistently

highest in the 55D treatment and the lowest in the 33A treatment. These treatment differences were most strongly expressed in the peak growing season (July-August), with the highest NDVI values observed in the 55D treatment, followed by the CN, 55A, 33D and 33A treatments (Figure 3.6a). The seasonal trend lines fitted to mean daily NDVI values also showed the highest growth in the 55D treatment, followed by the CN, 55A, 33D and 33A treatments (Figure 3.6a).

We performed two-dimensional PCA to better understand the NDVI contribution of each treatment for the post-harvest period from 2014 to 2020. PCA1 represents 80%, and PCA2 includes 9% of the total monthly NDVI data from 2014 to 2020. Results of PCA analysis showed a positive relationship among 55D, 55A and CN treatments and negative relationships between 33D and 33A treatments (Figure 3.7). This analysis showed that 55D and CN treatments had a closer relationship and maximum forest biomass and growth followed by 55A. This relationship was weak between CN and 33D and 33A treatments.

The box plots of NDVI values measured on 25 June 2019 and 17 July 2020 using drone also showed the maximum NDVI in the 55D treatment, followed by CN, 55A, 33D and 33A treatments (Figure 3.8a,b). We found a significant, linear relationship ($p \le 0.005$, $R2 \ge 0.90$) between satellite-based GPP and drone-measured NDVI (Figure 3.8c-g). We also found a significant, linear relationship ($p \le 0.005$, $R2 \ge 0.80$) between drone- and satellite-based NDVI measurements (Figure 3.8h).

3.4.3 Effect of variable retention harvesting treatments on forest C uptake

We estimated forest C uptake for each treatment using satellite-derived GPP. Seasonal cycle of mean daily GPP values is shown in Figure 3.6b. Similarly, cumulative daily GPP values over the growing season are shown in Figure 3.9. These plots indicated that forest C uptake varied with year and treatment (Figure 3.6b, Figure 3.9). The highest growing season cumulative GPP occurred prior to harvest in 2010 for most treatments except for CN. The lowest GPP was observed in 2016 for all treatments except CN. Growing season cumulative GPPEC values are also shown in Figure 9f for reference, where cumulative GEPEC was the highest in 2014 and the lowest in 2012. Overall, the fitted trend lines to daily GPP suggested that C uptake in CN and 55D plots was higher than the other treatments (Figure 3.6b).

Comparison of growing season mean daily GPP for all VRH treatments with EC observed daily GPPEC showed that C uptake was quite similar among treatment plots during the pre-harvest period (2010-2013) (Figure 3.10). Mean daily GPP ranged from 9.37 to 9.65 g C m⁻² d⁻¹, while mean daily GPPEC was 8.62 g C m⁻² d⁻¹, which was similar to the CN treatment. Large differences in mean daily GPP occurred among VRH treatments during the post-harvest period, with these differences among treatment plots becoming more stronger over time. In the post-harvest period, the mean daily GPP values were 8.71, 8.75, 8.74, 9.31, and 9.65 g C m⁻² d⁻¹ for 33A, 55A, 33D, 55D, and CN treatments, respectively. Pooled over all 7-growing seasons, daily GPP was highest in the CN treatment, followed by 55D, 55A, 33D, and 33A treatments (Figure 3.10, Table 3.2).

From the annual basis, the highest annual GPP of the pre-harvest period was observed in 2010 and in the post-harvesting period, the highest GPP was observed in 2020 in the CN and 55D

treatments (Table 3.2). Mean annual GPP was 1700, 1695, 1687, 1703, and 1692 g C m⁻² y⁻¹ in the 33A, 55A, 33D, 55D, and CN treatments, respectively over the pre-harvest period from 2010 to 2013 (Table 3.2). The mean annual GPP values in the first year after harvest in 2014 were 1492, 1473, 1489, 1506, and 1591 g C m⁻² y⁻¹ in 33A, 55A, 33D, 55D, and the CN treatment, respectively. Similarly, mean annual GPP values in the seventh year after harvest in 2020 were 1569, 1575, 1574, 1675, and 1736 g C m⁻² y⁻¹ in 33A, 55A, 33D, 55D, and CN treatment, respectively. CN plot showed the highest annual GPP, followed by the 55D, 55A, 33D and 33A treatments. The annual GPPEC values had a significant, positive linear relationship (p=0.032, R² = 0.88) with GPP values derived from remote sensing. The highest annual GPPEC of 1705 g C m⁻² y⁻¹ was recorded in 2014 and the lowest annual GPPEC of 1511 g C m⁻² y⁻¹ was observed in 2012 (Table 3.2).

3.5 Discussion

3.5.1 Effect of variable retention harvesting on forest growth and C uptake

Partial harvesting or thinning is a well-established forest management approach applied to enhance forest growth and development (Ashton and Kelty, 2018). The effect of different spatial patterns and intensity of partial harvesting or thinning on growth in red pine (Looney et al., 2018; Powers et al., 2009) and other forest types (Bose et al., 2014; Palik et al., 2002; Roberts and Harrington 2008; Xing et al., 2018) have previously been investigated. However, most studies have focused on enhancing fibre or timber growth with less attention given to C sequestration (Zugic et al., 2021). With recent climatic warming due to increasing greenhouse gas emissions and land use changes, there has been a renewed focus on tree planting, forest management, forest ecosystem conservation to enhance biological carbon sinks and identify potential nature-based climate solutions. Some studies have highlighted the need to adapt forest

management techniques to changing climatic conditions to ensure sustained forest growth and resilience (D'Amato et al., 2013; Drever et al., 2006; Keenan, 2015; Magruder et al., 2013; Sohn et al., 2016; Wagner et al., 2014). Recent advances in high-resolution remote sensing and drone technologies can help to evaluate the stand level impacts of different harvesting treatments on forest growth and C uptake. Despite these advances, it is still challenging to evaluate the effectiveness of forest management practices to achieve both wood production and C sequestration objectives.

Our study used high-resolution remote sensing data from Sentinel-2 and Landsat-8 satellites to explore the impact of VRH on temporal variation in forest growth and C uptake. Our results have shown that Sentinel-2 data is a valid approach to estimate forest biophysical properties and biomass productivity because of its high spatial resolution (Lima et al., 2019). Our NDVI results indicate that forest photosynthetic capacity and GPP was quite similar among all plots prior to harvesting and the establishment of VRH treatments. Any difference in GPP among plots were mainly driven by climate variability (Arain et al, 2022). However, after the harvesting and establishment of treatments in the winter of 2014, there was a consistent trend of increasing NDVI, specifically from 2017 to 2020, with the 55D treatment showing the highest NDVI values. Low NDVI values immediately after the harvesting in in 2014 and 2016 were probably due to both acclimation of trees to new microclimate and drier summer of 2016.

Forest structure has a strong influence on the exchange of energy, water and C with the atmosphere (Aussenac, 2000; Collalti et al., 2018; Luyssaert et al., 2007). Different partial harvesting intensity and pattern applied in our study created heterogeneity in the spatial distribution of residual forest cover and stand microclimate. These forest structural changes

can also affect light, nutrient and soil moisture availability (Aussenac, 2000; Boyden et al., 2012; Palik et al., 1997; Siebers and Kruse, 2019; Zhang et al., 2021). Changes in light, soil moisture and other resources can impact photosynthesis and evapotranspiration, thus impacting forest productivity (Collalti et al., 2018; Li et al., 2020; Bodo and Arain, 2022). Our study results suggest that the 55D treatment had the highest growth rate based on NDVI and GPP. This can be attributed to the comparatively higher tree density combined with uniformly spaced residual trees in the 55D treatment that provides individual trees with greater light and soil moisture availability and a more favorable microenvironment for growth compared to the 55A treatment. Our study results are consistent with previous research at this site using tree ring growth and sapflow measurements that found the 55D treatment exhibited the highest post-harvest tree-level growth and C sequestration rates (Zugic et al. 2021) and water use (Bodo and Arain, 2022).

Red pine and other plantation forests are an important part of the landscape in the western Great Lakes region of North America, providing numerous ecosystem services and economic benefits (Buckman et al., 2006; Gilmore and Palik, 2006; Palik and D'Amato, 2019). Therefore, the results of our study have broader significance and applicability for forest managers and policy makers in the Great Lakes region and eastern North America. Several studies have indicated that partial harvesting or thinning can reduce the vulnerability of red pine plantations and natural stands to climatic stresses (D'Amato et al., 2013; Jones et al., 2019; Magruder et al., 2013; Powers et al., 2010). However, our remote sensing study results have clearly indicated that the application of the uniformly dispersed residual canopy retaining more than half of the initial basal area (such as 55D) is a viable forest management option that can enhance rates of both timber production and C sequestration. Application of this VRH may also help forests to better adapt to climate change (Zugic et al., 2021; Bodo and Arain, 2022). Our study results

will help in developing new forest management approaches which are tailored to enhance both timber production and C sequestration. It will also help in developing forest management pathways for nature-based climate solutions.

3.5.2 Study limitations

Our study focused on estimating forest growth and C uptake in VRH treatments using multidimensional remote sensing data such as from Sentinel and Landsat sources. However, there are several challenges when using remote sensing techniques for forest inventories, such as scarcity of data, atmospheric noise, cloudy sky conditions, measurement interval differences among satellite data sources, and the accessibility of data processing tools. In this regards, more frequent drone missions may help to supplement these satellite data. Drone data can also help in site-level validation studies. Integration of satellite and drone data with forest C cycle models can help to obtain reliable forest biomass estimates.

In forest ecosystems, remote sensing data mainly captures information from the canopy level, overlooking the contribution of understory vegetation. It is challenging to accurately quantify the contribution of the understory to total forest C uptake (Thrippleton et al., 2016; Landuyt et al., 2018). Understory tree regeneration and ground vegetation may play a significant role in the rapid recovery of C stocks following stand-replacing forest disturbances because the trees present in the understory can capitalize on increased resource availability that enhances photosynthetic activity and growth (Brown et al., 2010; Edburg et al., 2012; Williams et al., 2014). We recognize the importance of understory in estimation of total forest growth and C uptake estimates and recommend exploring its relative contribution in future research to provide a more accurate evaluation of VRH impacts on forest growth and C sequestration.

3.6 Conclusions

Our study examined the effect of five VRH treatments on forest growth and C sequestration in a red pine plantation in the Great Lakes region of southern Ontario, Canada. It presented quantitative estimates of GPP for all five VRH treatments and found that retention of more than half of the initial basal area in uniform dispersal form (e.g. 55D treatment) exhibited higher productivity and C uptake than lower retention levels or an aggregate spatial distribution of residual canopy trees. Our study will help researchers and forest managers to develop forest management practices tailored to enhance both wood production and C sequestration and to achieve climate mitigation and adaptation goals. The data capture and analytical methods developed in our study can also be applied to quantify the forest growth and C sequestration at larger spatial scales in forested regions.

3.7 Acknowledgment

This study was funded by the Global Water Futures Program (GWF) and Natural Sciences and Engineering Research Council (NSERC) grants awarded to M.A Arain. In kind support from the Ontario Ministry of Natural Resources and Forestry (OMNRF), Ontario Ministry of Environment, Conservation and Parks, the St. Williams Conservation Reserve Community Council (SWCRCC) is gratefully acknowledged. We thank Steve Williams from OMNRF for his help and contributions in designing and establishing the VRH experiment. Additional thanks to the Natural Resources Canada – Canada Centre for Remote sensing drone team (Francis Canisius and Sylvain G. Leblanc) for their help with the fieldwork and data collection. We thank our Lab group members for their contributions on flux data measurements. We acknowledge Dr. Alemu Gonsamo for his advice and Audrey Heagy from SWCRCC for her

continued support for our research project. We also acknowledge to GWF Program – Southern Forests Water Futures Project and NSERC grants for providing research funding.

3.8 References

- Ali, A., Imran, M., Ali, A., & Khan, M. A. (2022). Evaluating Sentinel-2 red edge through hyperspectral profiles for monitoring LAI & chlorophyll content of Kinnow Mandarin orchards. *Remote Sensing Applications: Society and Environment*, 26, 100719.
- Allen, R. G., Tasumi, M., Morse, A., Trezza, R., Wright, J. L., Bastiaanssen, W., Kramber, W., Lorite, I., & Robison, C. W. (2007). Satellite-based energy balance for mapping evapotranspiration with internalized calibration (METRIC)—Applications. *Journal of Irrigation and Drainage Engineering*, 133, 395–406.
- Ameray, A., Bergeron, Y., Valeria, O., Montoro Girona, M., & Cavard, X. (2021). Forest carbon management: A review of silvicultural practices and management strategies across boreal, temperate, and tropical forests. *Current Forestry Reports*, 7, 245–266.
- Arain, M. A., & Restrepo-Coupe, N. (2005). Net ecosystem production in a temperate pine plantation in southeastern Canada. *Agricultural and Forest Meteorology*, 128, 223–241.
- Arain, M. A., Xu, B., Brodeur, J. J., Khomik, M., Peichl, M., Beamesderfer, E., Restrepo-Coupe, N., & Thorne, R. (2022). Heat and drought impact on carbon exchange in an age-sequence of temperate pine forests. *Ecological Processes*, 11(7).
- Ashton, M. S., & Kelty, M. J. (2018). The practice of silviculture: Applied forest ecology. John Wiley & Sons, Inc.
- Aubry, K. B., Halpern, C. B., & Peterson, C. E. (2009). Variable-retention harvests in the Pacific Northwest: A review of short-term findings from the DEMO study. *Forest Ecology and Management*, 258, 398–408.
- Aussenac, G. (2000). Interactions between forest stands and microclimate: Ecophysiological aspects and consequences for silviculture. *Annals of Forest Science*, 57, 287–301.
- Baldocchi, D. D. (2020). How eddy covariance flux measurements have contributed to our understanding of global change biology. *Global Change Biology*, 26(1), 242–260.
- Baldocchi, D., & Penuelas, J. (2019). The physics and ecology of mining carbon dioxide from the atmosphere by ecosystems. *Global Change Biology*, 25, 1191–1197.
- Beamesderfer, E. R., Arain, M. A., & Khomik, M. (2020). The impact of seasonal and annual climate variations on the carbon uptake capacity of a deciduous forest within the Great

- Lakes region of Canada. *Journal of Geophysical Research: Biogeosciences*, 125, e2019JG005389.
- Beese, W. J., Deal, J., Dunsworth, B. G., Mitchell, S. J., & Philpott, T. J. (2019). Two decades of variable retention in British Columbia: A review of its implementation and effectiveness for biodiversity conservation. *Ecological Processes*, 8, 33.
- Binet, R., Bergsma, E., & Poulain, V. (2022). Accurate sentinel-2 inter-band time delays. ISPRS Annals of the Photogrammetry, *Remote Sensing and Spatial Information Sciences*, 1, 57-66.
- Bodo, A. V., & Arain, M. A. (2022). Effects of variable retention harvesting on canopy transpiration in a red pine plantation forest. *Ecological Processes*, 11, 1.
- Bodo, A. V., Parker, W. C., Elliott, K. A., & Arain, M. A. (2023). Below canopy evapotranspiration in four different variable retention harvesting treatments in a red pine plantation forest. *Hydrological Processes*, 37, e14789.
- Bose, A. K., Harvey, B. D., Brais, S., Beaudet, M., & Leduc, A. (2014). Constraints to partial cutting in the boreal forest of Canada in the context of natural disturbance-based management: A review. *Forestry*, 87, 11–28.
- Boyden, S., Montgomery, R., Reich, P. B., & Palik, B. (2012). Seeing the forest for the heterogeneous trees: Stand-scale resource distributions emerge from tree-scale structure. *Ecological Applications*, 22, 1578–1588.
- Brown, M., Black, T. A., Nesic, Z., Foord, V. N., Spittlehouse, D. L., Fredeen, A. L., ... & Trofymow, J. A. (2010). Impact of mountain pine beetle on the net ecosystem production of lodgepole pine stands in British Columbia. *Agricultural and Forest Meteorology*, 150, 254-264.
- Buckman, R. E., Bishaw, B., Hanson, T. J., & Benford, F. A. (2006). Growth and yield of red pine in the Lake States. US Department of Agriculture, Forest Service, General Technical Report, NC-271.
- Canisius, F., Wang, S., Croft, H., Leblanc, S. G., Russell, H. A. J., Chen, J., & Wang, R. (2019). A UAV-based sensor system for measuring land surface albedo: Tested over a boreal peatland ecosystem. *Drones*, 3, 27.

- Chen, X. L., Zhao, H. M., Li, P. X., & Yin, Z. Y. (2006). Remote sensing image-based analysis of the relationship between urban heat island and land use/cover changes. *Remote Sensing of Environment*, 104, 133-146.
- Collalti, A., Trotta, C., Keenan, T. F., Ibrom, A., Bond-Lamberty, B., Grote, R., ... & Matteucci, G. (2018). Thinning can reduce losses in carbon use efficiency and carbon stocks in managed forests under warmer climate. *Journal of Advances in Modeling Earth Systems*, 10, 2427–2452.
- Creutzig, F., Niamir, L., Bai, X., Callaghan, M., Cullen, J., Díaz-José, J., ... & Ürge-Vorsatz, D. (2022). Demand-side solutions to climate change mitigation consistent with high levels of well-being. *Nature Climate Change*, 12(1), 36-46.
- D'Amato, A. W., Bradford, J. B., Fraver, S., & Palik, B. J. (2013). Effects of thinning on drought vulnerability and climate response in north temperate forest ecosystems. *Ecological Applications*, 23, 1735–1742.
- Dainelli, R., Toscano, P., Di Gennaro, S. F., & Matese, A. (2021). Recent advances in unmanned aerial vehicles forest remote sensing—a systematic review. Part II: Research applications. *Forests*, 2, 397.
- Drever, C. R., Peterson, G., Messier, C., Bergeron, Y., & Flannigan, M. (2006). Can forest management based on natural disturbances maintain ecological resilience? *Canadian Journal of Forest Research*, 36, 2285-2299.
- Drusch, M., del Bello, U., Carlier, S., Colin, O., Fernandez, V., Gascon, F., Hoersch, B., Isola, C., Laberinti, P., Martimort, P., Meygret, A., & Spoto, F. (2012). Sentinel-2: ESA's optical high-resolution mission for GMES operational services. *Remote Sensing of Environment*, 120, 25–36.
- Edburg, S. L., Hicke, J. A., Lawrence, D. M., & Thornton, P. E. (2011). Simulating coupled carbon and nitrogen dynamics following mountain pine beetle outbreaks in the western United States. *Journal of Geophysical Research: Biogeosciences*, 116, G04033.
- Fassnacht, F. E., White, J. C., Wulder, M. A., & Næsset, E. (2023). Remote sensing in forestry: Current challenges, considerations and directions. *Forestry: An International Journal of Forest Research*.

- Frampton, W. J., Dash, J., Watmough, G., & Milton, E. J. (2013). Evaluating the capabilities of Sentinel-2 for quantitative estimation of biophysical variables in vegetation. *ISPRS Journal of Photogrammetry and Remote Sensing*, 82, 83–92.
- Franklin, J. F., Berg, D. R., Thornburgh, D. A., & Tappeiner, J. C. (1997). Alternative silvicultural approaches to timber harvesting: Variable retention harvest systems. In K. A. Kohm & J. F. Franklin (Eds.), Creating a forest for the 21st century: The science of ecosystem management (pp. 11-139). Island Press.
- Franklin, J. F., Mitchell, R. J., & Palik, B. J. (2007). Natural disturbance and stand development principles for ecological forestry. US Department of Agriculture, Forest Service, General Technical Report, NRS-19.
- Gilmore, D. W., & Palik, B. J. (2006). A revised manager's handbook for red pine in the North Central region. US Department of Agriculture, Forest Service, General Technical Report NC-264.
- Grabska-Szwagrzyk, E., & Tymińska-Czabańska, L. (2023). Sentinel-2 time series: A promising tool in monitoring temperate species spring phenology. *Forestry: An International Journal of Forest Research*.
- Guo, Y. P., Zhou, H. F., & Zhang, L. C. (2006). Photosynthetic characteristics and protective mechanisms against photooxidation during high temperature stress in two citrus species. *Scientia Horticulturae*, 108, 260–267.
- Han, A., Qing, S., Bao, Y., Na, L., Bao, Y., Liu, X., Zhang, J., & Wang, C. (2021). Short-term effects of fire severity on vegetation based on Sentinel-2 satellite data. *Sustainability*, 13, 432.
- Heino, M., Kummu, M., Makkonen, M., Mulligan, M., Verburg, P. H., Jalava, M., & Räsänen, T. A. (2015). Forest loss in protected areas and intact forest landscapes: A global analysis. *PLOS ONE*, 10, e0138918.
- Heinsch, F. A., Zhao, M., Running, S. W., Kimball, J. S., Nemani, R. R., Davis, K. J., Bolstad,
 P. V., Cook, B. D., Desai, A. R., Ricciuto, D. M., Law, B. E., Oechel, W. C., Kwon,
 H., Luo, H., Wofsy, S. C., Dunn, A. L., Munger, J. W., Baldocchi, D. D., Xu, L., &
 Flanagan, L. B. (2006). Evaluation of remote sensing based terrestrial productivity from
 MODIS using regional tower eddy flux network observations. *IEEE Transactions on Geoscience and Remote Sensing*, 44, 1908–1925.

- Jollife, I. T., & Cadima, J. (2016). Principal component analysis: A review and recent developments. *Philosophical Transactions of the Royal Society A: Mathematical, Physical and Engineering Sciences*, 374(2065), 20150202.
- Jones, S. M., Botttero, A., Kastendick, D. N., & Palik, B. J. (2019). Managing red pine stand structure to mitigate drought impacts. *Dendrochronologia*, 57, 125623.
- Kaarakka, L., Cornett, M., Domke, G., Ontl, T., & Dee, L. E. (2021). Improved forest management as a natural climate solution: A review. *Ecological Solutions and Evidence*, 2(1), e12090.
- Kaplan, G., Fine, L., Lukyanov, V., Malachy, N., Tanny, J., & Rozenstein, O. (2023). Using Sentinel-1 and Sentinel-2 imagery for estimating cotton crop coefficient, height, and leaf area index. *Agricultural Water Management*, 276, 108056.
- Keenan, R. J. (2015). Climate change impacts and adaptation in forest management: A review. *Annals of Forest Science*, 72(2), 145–167.
- Kogan, F. N. (1990). Remote sensing of weather impacts on vegetation in non-homogeneous areas. *International Journal of Remote Sensing*, 11(8), 1405–1419.
- Landsat Science Team. (2011, March 11). Landsat 7 Science Data Users Handbook. NASA. http://landsathandbook.gsfc.nasa.gov/inst_cal/prog_sect8_2.html (Accessed: 18 October 2015).
- Landuyt, D., Perring, M. P., Seidl, R., Taubert, F., Verbeeck, H., & Verheyen, K. (2018).
 Modelling understorey dynamics in temperate forests under global change Challenges and perspectives. *Perspectives in Plant Ecology, Evolution and Systematics*, 31, 44–54.
- Lastovicka, J., Svec, P., Paluba, D., Kobliuk, N., Svoboda, J., & Hladky, R. (2020). Sentinel-2 data in an evaluation of the impact of disturbances on forest vegetation. *Remote Sensing*, 12(12), 1914.
- Lausch, A., Borg, E., Bumberger, J., Dietrich, P., Heurich, M., Huth, A., Jung, A., Klenke, R., Knapp, S., Mollenhauer, H., Paasche, H., Paulheim, H., & Schröder, B. (2018).
 Understanding forest health with remote sensing, Part III: Requirements for a scalable multi-source forest health monitoring network based on data science approaches.
 Remote Sensing, 10(7), 1120.
- Li, C., Barclay, H., Roitberg, B., & Lalonde, R. (2020). Forest productivity enhancement and compensatory growth: A review and synthesis. *Frontiers in Plant Science*, 11, 575211.

- Lima, T. A., Beuchle, R., Langner, A., Grecchi, R. C., Griess, V. C., & Achard, F. (2019).
 Comparing Sentinel-2 MSI and Landsat 8 OLI imagery for monitoring selective logging in the Brazilian Amazon. *Remote Sensing*, 11(8), 961.
- Looney, C. E., D'Amato, A. W., Palik, B. J., Fraver, S. W., & Kastendick, D. N. (2018). Size-growth relationship, tree spatial patterns, and tree-tree competition influence tree growth and stand complexity in a 160-year red pine chronosequence. *Forest Ecology and Management*, 424, 85–94.
- Löw, M., & Koukal, T. (2020). Phenology modelling and forest disturbance mapping with Sentinel-2 time series in Austria. *Remote Sensing*, 12(24), 4191.
- Luyssaert, S., Inglima, I., Jung, M., Richardson, A. D., Reichstein, M., Papale, D., Piao, S. L.,
 Schulze, E. D., Wingate, L., Matteucci, G., Aragao, L., Aubinet, M., Beer, C.,
 Bernhofer, C., Black, K. G., Bonal, D., Bonnefond, J. M., Chambers, J., Ciais, P., &
 Janssens, I. A. (2007). CO2 balance of boreal, temperate, and tropical forests derived from a global database. *Global Change Biology*, 13(12), 2509–2537.
- Magruder, M., Chhin, S., Palik, B., & Bradford, J. B. (2013). Thinning increases climatic resilience of red pine. Canadian Journal of Forest Research, 43(10), 878–889.
- Makipaa, R., Abramoff, R., Adamczyk, B., Baldy, V., Biryol, C., Bosela, M., ... & Lehtonen, A. (2023). How does management affect soil C sequestration and greenhouse gas fluxes in boreal and temperate forests?: A review. *Forest Ecology and Management*.
- Mao, J., Thornton, P. E., Shi, X., Zhao, M., & Post, W. M. (2012). Remote sensing evaluation of CLM4 GPP for the period 2000-09. *Journal of Climate*, 25(15), 5327–5342.
- Marvin, D. C., Sleeter, B. M., Cameron, D. R., Nelson, E., & Plantinga, A. J. (2023). Natural climate solutions provide robust carbon mitigation capacity under future climate change scenarios. *Scientific Reports*, 13(1), 19008.
- Masek, J. G., Goward, S. N., Kennedy, R. E., Cohen, W. B., Moisen, G. G., Schleeweis, K., & Huang, C. (2013). United States forest disturbance trends observed using Landsat time series. *Ecosystems*, 16(6), 1087–1104.
- Matsushita, B., Yang, W., Chen, J., Onda, Y., & Qiu, G. (2007). Sensitivity of the enhanced vegetation index (EVI) and normalized difference vegetation index (NDVI) to topographic effects: A case study in high-density cypress forest. *Sensors*, 7(11), 2636–2651.

- Mayer, M., Prescott, C. E., Abaker, W. E., Augusto, L., Cécillon, L., Ferreira, G. W., ... & Viscarra Rossel, R. A. (2020). Tamm review: Influence of forest management activities on soil organic carbon stocks: A knowledge synthesis. *Forest Ecology and Management*, 466, 118127.
- McKenzie, S. M., Parker, W. C., & Pisaric, M. J. F. (2023). Tree-ring growth varies with climate and stand density in a red pine plantation forest in the Great Lakes region of North America. *Dendrochronologia*, 79, 126091.
- McRoberts, R. E., & Tomppo, E. O. (2007). Remote sensing support for national forest inventories. *Remote Sensing of Environment*, 110(4), 412–419.
- Morell-Monzó, S., Estornell, J., & Sebastiá-Frasquet, M.-T. (2020). Comparison of Sentinel-2 and high-resolution imagery for mapping land abandonment in fragmented areas. *Remote Sensing*, 12(12), 2062.
- Natural Resources Canada. (2016). The state of Canada's forests. Annual report 2016. Government of Canada. https://cfs.nrcan.gc.ca/pubwarehouse/pdfs/37265.pdf
- Olmedo, G. F., Ortega-Farías, S., de la Fuente-Sáiz, D., Fonseca-Luego, D., & Fuentes-Peñailillo, F. (2016). Water: Tools and functions to estimate actual evapotranspiration using land surface energy balance models in R. *The R Journal*, 8(2), 352–369.
- Ontl, T. A., Janowiak, M. K., Swanston, C. W., Daley, J., Handler, S., Cornett, M., Hagenbuch, S., Handrick, C., McCarthy, L., & Patch, N. (2020). Forest management for carbon sequestration and climate adaptation. *Journal of Forestry*, 118(1), 86–101.
- Palik, B. J., & D'Amato, A. W. (2019). Variable retention harvesting in Great Lakes mixed-pine forests: Emulating a natural model in managed ecosystems. *Ecological Processes*, 8(1), 16.
- Palik, B. J., Mitchell, R. J., Houseal, G., & Pederson, N. (1997). Effects of canopy structure on resource availability and seedling responses in a longleaf pine ecosystem. *Canadian Journal of Forest Research*, 27(9), 1458–1464.
- Peng, C., Zhou, X., Zhao, S., Wang, X., Zhu, Q., Piao, S., & Fang, J. (2009). Quantifying the response of forest carbon balance to future climate change in northeastern China: Model validation and prediction. *Global and Planetary Change*, 66(3–4), 179–194.

- Poovey, J. (2021). Evaluating environmental impacts of red pine plantation management on plant and soil properties in northern Minnesota (Doctoral dissertation). Retrieved from ProQuest Dissertations Publishing. (28001464)
- Pugh, T. A. M., Lindeskog, M., Smith, B., Poulter, B., Arneth, A., Haverd, V., & Calle, L. (2019). Role of forest regrowth in global carbon sink dynamics. *Proceedings of the National Academy of Sciences*, 116(10), 4382–4387.
- Ramachandra, T. V., Bharath, H. A., & Sowmyashree, M. V. (2019). Monitoring forest landscape dynamics using geoinformatics in Shimoga district, India. *Journal of Environmental Management*, 232, 1177–1193.
- Ratcliffe, S., Holzwarth, F., Nadrowski, K., Levick, S., Wirth, C., & Scherer-Lorenzen, M. (2015). Tree neighbourhood matters Tree species composition drives diversity–productivity patterns in a near-natural beech forest. *Forest Ecology and Management*, 335, 225–234.
- Reyes, J. D., Acosta, J., Gallego, M., & Manjarrez, J. R. (2021). Land surface temperature and normalized difference vegetation index assessment using Sentinel-2 and Landsat 8 OLI data. *International Journal of Remote Sensing*, 42(7), 2535–2555.
- Reyer, C. P. O., Silveyra Gonzalez, R., Dolos, K., Hartig, F., Hauf, Y., Noack, M., Rammig, A., Rammig, A., & Lasch-Born, P. (2020). The PROFOUND database for evaluating vegetation models and simulating climate impacts on European forests. *Earth System Science Data*, 12(1), 41–64.
- Royer, A., & Poirier, S. (2010). Satellite data in situ measurements for studying snow cover and climate change impacts in Canada. *Climate Change*, 98, 151–173.
- Saatchi, S. S., Harris, N. L., Brown, S., Lefsky, M., Mitchard, E. T. A., Salas, W., ... & Morel,
 A. (2011). Benchmark map of forest carbon stocks in tropical regions across three continents. *Proceedings of the National Academy of Sciences*, 108(24), 9899–9904.
- Sader, S. A., Bertrand, M., & Wilson, E. H. (2003). Satellite change detection of forest harvest patterns on an industrial forest landscape. *Forest Science*, 49(3), 341–353.
- Sáez-de-Cámara, E., González-Aparicio, I., Hidalgo, J., Monteiro, A., Alonso, L., Knap, W. H., & Lozano, J. A. (2015). Assessment of future forest fire risk in the Pyrenees based on ENSEMBLES regional climate projections. *Forest Ecology and Management*, 321, 18–29.

- Sharma, R., Maraseni, T., Cockfield, G., & Lal, P. (2017). An analysis of the delays in REDD+ project approval in Indonesia. *Forest Policy and Economics*, 83, 56–65.
- Skakun, R. S., Franklin, S. E., & Wulder, M. A. (2003). Sensitivity of the thematic mapper enhanced wetness difference index to detect mountain pine beetle red attack damage. *Remote Sensing of Environment*, 86(4), 433–443.
- Song, X.P., Tan, P. Y., Edwards, P., & Richards, D. (2022). Global patterns of the contributions of urban greenspaces to public health and environmental quality. *Environmental Research Letters*, 17(5), 053001.
- Spring, D. A., Kennedy, M. J., Chomitz, K. M., Mourato, S., Fraser, A. S., & Cacho, O. J. (2008). Optimal forest rotation with carbon sequestration and carbon markets: A new policy for RIL logging? *Ecological Economics*, 65(3), 572–579.
- Stanley, T. R., Nelson, J. P., & Newmark, W. D. (2021). Effects of roads on the distribution of forest mammals in Tanzanian national parks. *Conservation Biology*, 35(2), 599–609.
- Swanson, M. E., Franklin, J. F., Beschta, R. L., Crisafulli, C. M., DellaSala, D. A., Hutto, R. L., Lindenmayer, D. B., & Swanson, F. J. (2011). The forgotten stage of forest succession: Early-successional ecosystems on forest sites. *Frontiers in Ecology and the Environment*, 9(2), 117–125.
- Thom, D., & Seidl, R. (2016). Natural disturbance impacts on ecosystem services and biodiversity in temperate and boreal forests. *Biological Reviews*, 91(3), 760–781.
- Tucker, C. J. (1979). Red and photographic infrared linear combinations for monitoring vegetation. *Remote Sensing of Environment*, 8(2), 127–150.
- Van der Plas, F., Manning, P., Allan, E., Scherer-Lorenzen, M., Verheyen, K., Wirth, C., Zavala, M. A., & Fischer, M. (2016). Jack-of-all-trades effects drive biodiversity-ecosystem multifunctionality relationships in European forests. *Nature Communications*, 7, 11109.
- Verkerk, P. J., Mavsar, R., Giergiczny, M., Lindner, M., Edwards, D., & Schelhaas, M.-J. (2014). Assessing impacts of intensified biomass production and biodiversity protection on ecosystem services provided by European forests. *Ecosystem Services*, 9, 155–165.

- Villamor, G. B., & van Noordwijk, M. (2016). Gender specific land use decisions and implications for ecosystem services in semi-matrilineal Sumatra. *Global Environmental Change*, 39, 69–80.
- Visser, M. D., van Breugel, M., & Bongers, F. (2020). The global importance of liana forests. *Nature Plants*, 6, 317–318.
- Vlam, M., Baker, P. J., Bunyavejchewin, S., & Zuidema, P. A. (2014). Temperature and rainfall strongly drive temporal growth variation in Asian tropical forest trees. *Oecologia*, 174(4), 1449–1461.
- Wang, W., Qiao, X., Pan, J., Qiao, Y., Yan, C., Li, Y., & Zhao, J. (2020). Advances in high-throughput phenotyping in forestry: Implications for forest breeding and genetic resource management. *Forestry*, 93(2), 263–272.
- Waring, R. H., & Running, S. W. (2007). Forest ecosystems: Analysis at multiple scales (3rd ed.). Academic Press.
- Wegner, K., & Kraft, R. (2016). How forest management strategies affect biodiversity and habitat structure in temperate forests. *Forest Ecology and Management*, 359, 206–215.
- White, J. C., Wulder, M. A., Varhola, A., Vastaranta, M., Coops, N. C., Cook, B. D., Pitt, D., & Woods, M. (2013). A best practices guide for generating forest inventory attributes from airborne laser scanning data using an area-based approach. *Forestry*, 86(5), 463–479.
- Williams, C. A., Gu, H., MacLean, R., Masek, J., & Collatz, G. J. (2016). Disturbance and the carbon balance of US forests: A quantitative review of impacts from harvests, fires, insects, and droughts. *Global and Planetary Change*, 143, 66–80.
- Wu, J., Yu, Q., Zha, D., Yan, B., & Tian, L. (2022). Mapping annual forest cover in the Asia-Pacific region from 2000 to 2020 using time-series Landsat images. *Remote Sensing*, 14(5), 1238.
- Zhu, Z., & Woodcock, C. E. (2012). Object-based cloud and cloud shadow detection in Landsat imagery. *Remote Sensing of Environment*, 118, 83–94

3.9 Supplementary

3.9.1 Remote Sensing Indices

The NDVI was calculated using Equation 3.5 (Rouse et al., 1974),

$$NDVI = (R800 - R670)/(R800 + R670)$$
(3.5)

where Ri is reflectance at the band centered at a given wavelength i.

Sentinel-2 and Landsat-8 provides a potential assessment of plant ecosystems through Soil Adjusted Vegetation Index (SAVI) measurement at a high-resolution surface cover. SAVI was calculated for GPP analysis using following equation,

$$SAVI = (1 + L) \times (RNIR - Rred) / (L + RNIR + Rred)$$
(3.6)

where RNIR is the reflectance radiance in the infrared band, and Rred is the reflectance or radiance in a red band; L is a soil correction factor that by default uses L=0.5 and suggested value of L=0.1 (Allen et al., 2007). This value varies with the amount of coverage of green vegetation, in very high coverage vegetation regions, L=0, and areas with no green vegetation, L=1 (Olmedo et al., 2016).

3.9.2 Remote Sensing GPP

Several approaches can be used to estimate GPP where the MODIS GPP data is widely applied on a global and regional scale. However, the MODIS-based GPP data are moderate to low-resolution, which makes complex for plot-level application. In this circumstance, our study focused on a combined approach to produce plot-level GPP from satellite and eddy covariance flux measurements using the Vegetation Photosynthesis Model (VPM) (Zhang et al., 2016).

The VPM GPP product provides a satisfactory level of biomass estimation for the North American region (Zhang et al., 2016). Our study utilized Sentinel S2, Landsat, EC-measured PAR, and temperature and references GEP data from Turkey Point Flux Station (TP39 or CA-TP4; Arain et al., 2022) using the following equations:

$$GPP = APARchl \times \epsilon g \tag{3.7}$$

$$APARchl = PAR \times fPARchl$$
 (3.8)

$$fPARchl = (NDVI - 0.1) \times 1.25 \tag{3.9}$$

$$\epsilon g = \epsilon 0 \times Tscalar \times Wscalar$$
 (3.10)

$$T_{scalar} = \frac{(T - T_{max}) \times (T - T_{min})}{(T - T_{max}) \times (T - T_{min}) - (T - T_{opt})^2}$$
(3.11)

$$W_{scalar} = \frac{1 + LSWI}{1 + LSWI_{max}} \tag{3.12}$$

$$LSWI = (RNIR - RSWIR)/(RNIR + RSWIR)$$
(3.13)

where, APARchl is absorbed photosynthetically active radiation (PAR); fPARchl is the fraction of PAR estimated by chlorophyll or linear function of NDVI, which is modified from Xiao et al. (2004). Here, 0.1 and 1.25 are constants to adjust for vegetated land and validated from Solar-induced Chlorophyll Fluorescence (SIF) (Zhang et al., 2017); ϵg is the light use efficiency (LUE), $\epsilon 0$ is the apparent quantum yield or maximum light use efficiency ($\mu mol CO_2/\mu mol PAR$); Tscalar, Wscalar are the downward-parameter scalars for the effects of temperature and water on LUE by C3/C4 photosynthetic pathways; T, T_{min} , T_{max} , and T_{opt} refer to the mean, maximum, minimum, and optimum temperature for photosynthesis, respectively (we useed 10 to 16 hours of local time measurement); LSWI is the land surface water index.

Table 3.1. Mean annual photosynthetically active radiation (PAR), air temperature (Tair), daily mean vapor pressure deficit (VPD) and total annual precipitation (P) and growing season (April-October) precipitation (PGS) measured at the CA-TP4 site from 2010 to 2020.

	PAR (µmol m ⁻² s ⁻¹)	Average Tair (°C)	VPD (kPa)	P (mm)	PGS (mm)	
Year	(Minimum;	(Minimum;	(Minimum;	(Minimum;	(Minimum;	
	Maximum)	Maximum)	Maximum)	Maximum)	Maximum)	
2010	334 ± 206	9.5±10	0.34 ± 0.2	896±6.0	535±6.8	
	(19; 761)	(-14.2; 27.5)	(0; 1.30)	(0; 52.8)	(0; 52.8)	
2011	317±222	9.6±10	0.36 ± 0.3	1293±7.1	589±7.1	
	(16; 749)	(-14.3; 29.6)	(0; 1.46)	(0; 39.7)	(0; 39.7)	
2012	346±221	11.2±9	0.48 ± 0.3	1001±6.4	601±8.0	
	(13; 768)	(-11.5; 28.6)	(0.02; 1.93)	(0; 50.2)	(0; 50.2)	
2013	336±215	9.1±10	0.4±0.2	1266±8.8	614±10.2	
	(16; 773)	(-13.7; 27.9)	(0.02; 1.47)	(0; 81.8)	(0; 81.8)	
2014	345±212	8.1±11	0.38 ± 0.2	1429±8.6	574±8.2	
	(9; 784)	(-18.6; 25.8)	(0.02; 1.38)	(0; 78.1)	(0; 60.2)	
2015	353±209	9.5±11	0.43 ± 0.3	811±6.5	500±8.1	
2015	(20; 773)	(-20.7; 26.7)	(0.03; 1.52)	(0; 61.4)	(0; 61.4)	
2016	357±219	10±10	0.47 ± 0.3	778±4.8	347±4.7	
	(27; 778)	(-15.8; 27.4)	(0.01; 1.74)	(0; 28.6)	(0; 28.6)	
2017	330±210	9.9±9	0.42 ± 0.3	1153±7.5	474±8.1	
	(19; 760)	(-14.6; 25.7)	(0; 1.59)	(0; 80.5)	(0; 80.5)	
2018	325 ± 217	9.4±10	0.42 ± 0.3	1649±7.3	851±7.6	
	(15; 764)	(-17.9; 27.1)	(0.03; 1.61)	(0; 60.2)	(0; 60.2)	
2019	314±198	8.9±10	0.42 ± 0.3	1122±5.6	554±5.3	
	(14; 764)	(-18.6; 27.0)	(0.03; 1.47)	(0; 35.9)	(0; 35.9)	
2020	334±225	10.2±9	0.5 ± 0.3	1127±6.8	577±8.1	
	(12; 870)	(-11.4; 27.6)	(0.03; 1.70)	(0; 93.5)	(0; 93.5)	

Table 3.2. Daily mean (a) NDVI (+ 1 SD) for the growing season and (b) annual total GPP (g C m⁻² y⁻¹) for each VRH treatment from 2010 to 2020. VRH treatments were applied in February 2014. (c) Observed annual total GPPEC (g C m⁻² y⁻¹) using eddy covariance (EC) technique in the adjacent white pine plantation is also shown.

the adjacent write pine prantation is also shown.													
Year													
VRH	2010	2011	2012	2013	2014	2015	2016	2017	2018	2019	2020		
(a) NDVI													
33A	0.58 ± 0.07	0.56 ± 0.07	0.57 ± 0.08	0.56 ± 0.1	0.42 ± 0.10	0.53 ± 0.07	0.47 ± 0.07	0.48 ± 0.07	0.51 ±0.11	0.56 ± 0.08	0.57 ±0.12		
55A	0.58 ± 0.06	0.56 ± 0.07	0.57 ± 0.07	0.54 ±0.08	0.43 ±0.11	0.52 ± 0.07	0.50 ± 0.08	0.53 ± 0.08	0.54 ± 0.08	0.57 ±0.08	0.59 ±0.10		
33D	0.58 ± 0.07	0.56 ± 0.06	0.57 ± 0.08	0.55 ± 0.10	0.45 ±0.12	0.52 ± 0.08	0.50 ± 0.06	0.54 ± 0.08	0.55 ± 0.10	0.59 ±0.09	0.61 ±0.11		
55D	0.57 ± 0.08	0.56 ± 0.07	0.57 ± 0.09	0.57 ± 0.11	0.50 ± 0.11	0.58 ± 0.08	0.55 ± 0.08	0.59 ± 0.11	0.62 ±0.11	0.67 ±0.13	0.69 ±0.11		
CN	0.58 ± 0.08	0.56 ± 0.06	0.56 ± 0.08	0.54 ± 0.12	0.51 ±0.13	0.57 ± 0.09	0.52 ±0.09	0.57 ±0.10	0.59 ± 0.09	0.67 ±0.07	0.64 ±0.11		
(b) GPP													
33A	1746	1703	1730	1622	1492	1615	1407	1642	1624	1528	1675		
55A	1742	1686	1722	1633	1473	1554	1471	1638	1773	1472	1650		
33D	1734	1690	1715	1611	1489	1570	1432	1688	1670	1529	1642		
55D	1729	1703	1721	1660	1506	1509	1554	1753	1744	1827	1834		
CN	1719	1705	1708	1636	1591	1669	1571	1864	1787	1834	1840		
Observed GPPEC													
GPPEC	1571	1521	1511	1553	1705	1663	1650	1678	1594	1603	1649		

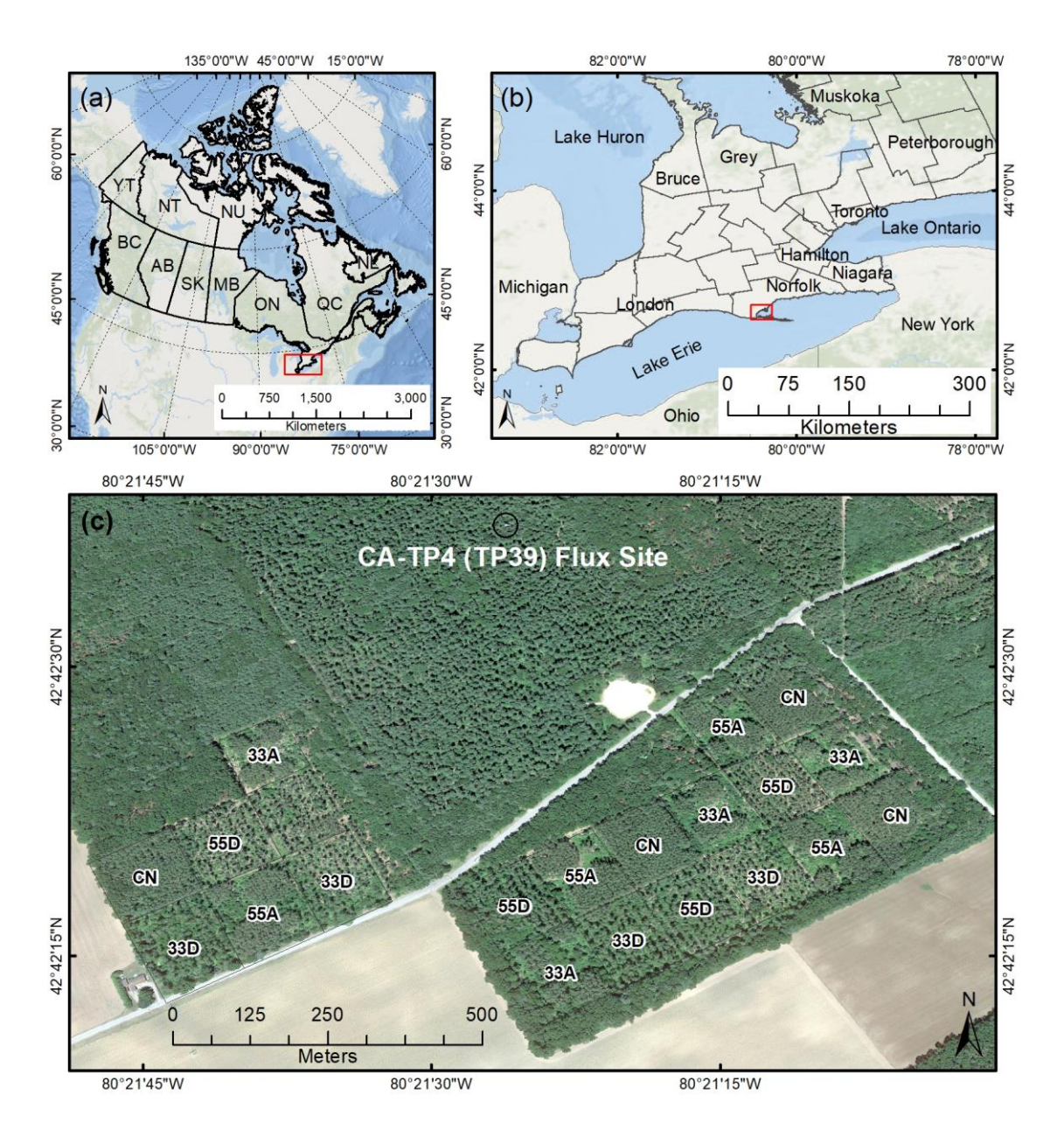


Figure 3.1. a) Location map of Canada, b) Southern Ontario regional map and c) Aerial view of location of the variable retention harvesting treatment plots of the red pine plantation (1931). Eddy covariance flux tower in the adjacent white pine plantation (1939 known as CA-TP4 in global Fluxnet) is also shown.

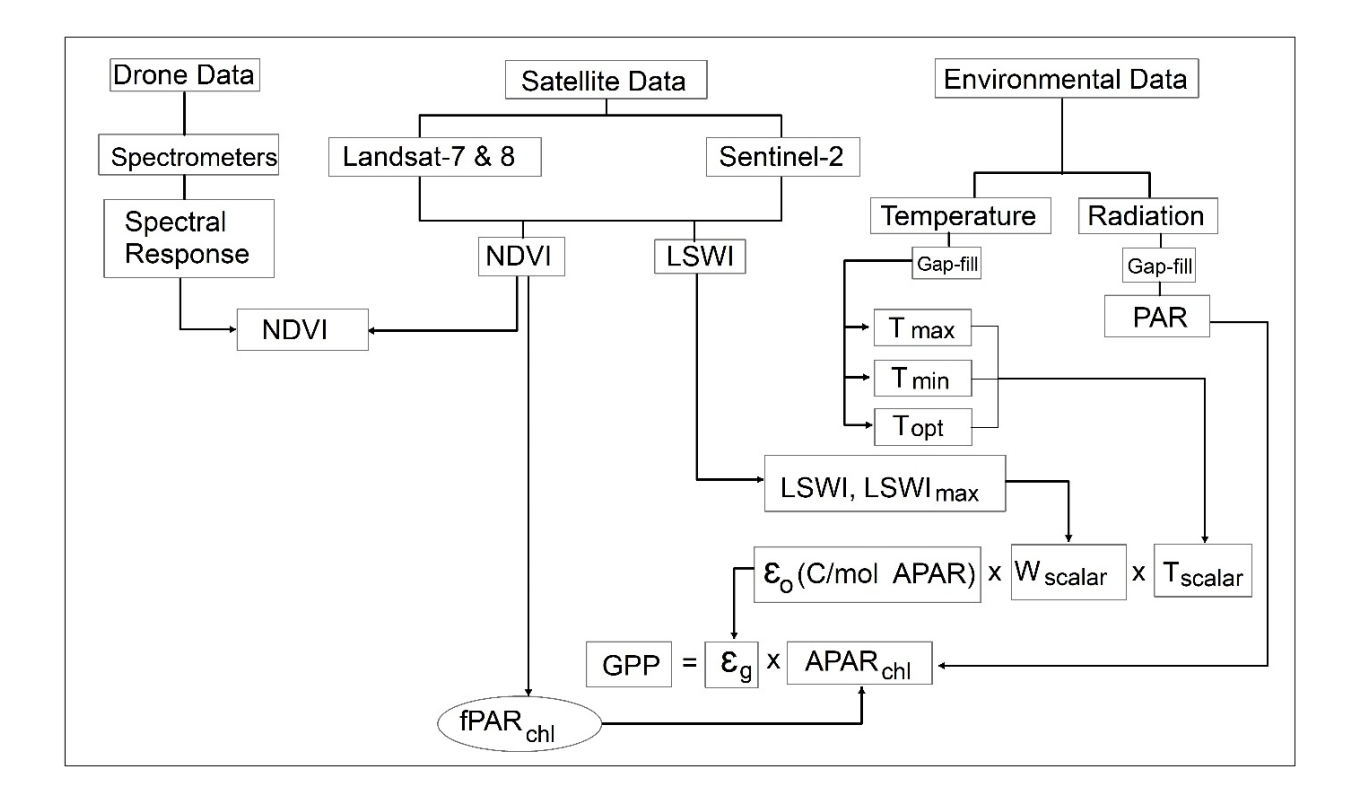


Figure 3.2. Workflow of the data analysis to estimate satellite gross primary productivity (GPP) where PAR is photosynthetically active radiation; APARchl is absorbed photosynthetically active radiation; fPARchl is the fraction of PAR estimated by chlorophyll or linear function of normalized difference vegetation index (NDVI). εg is light use efficiency (LUE), $\varepsilon 0$ is the apparent quantum yield or maximum LUE ($\mu mol\ CO_2/\mu mol\ m-2\ s-1\ PAR$); Tscalar, Wscalar are the downward-parameter scalars for the effects of temperature and water on LUE by C3/C4 photosynthetic pathways; T, T_{min} , T_{max} , and T_{opt} refer to the mean, maximum, minimum, and optimum temperature for photosynthesis, respectively; LSWI is the land surface water index. Data analysis follows Zhang et al., (2016 and 2017).

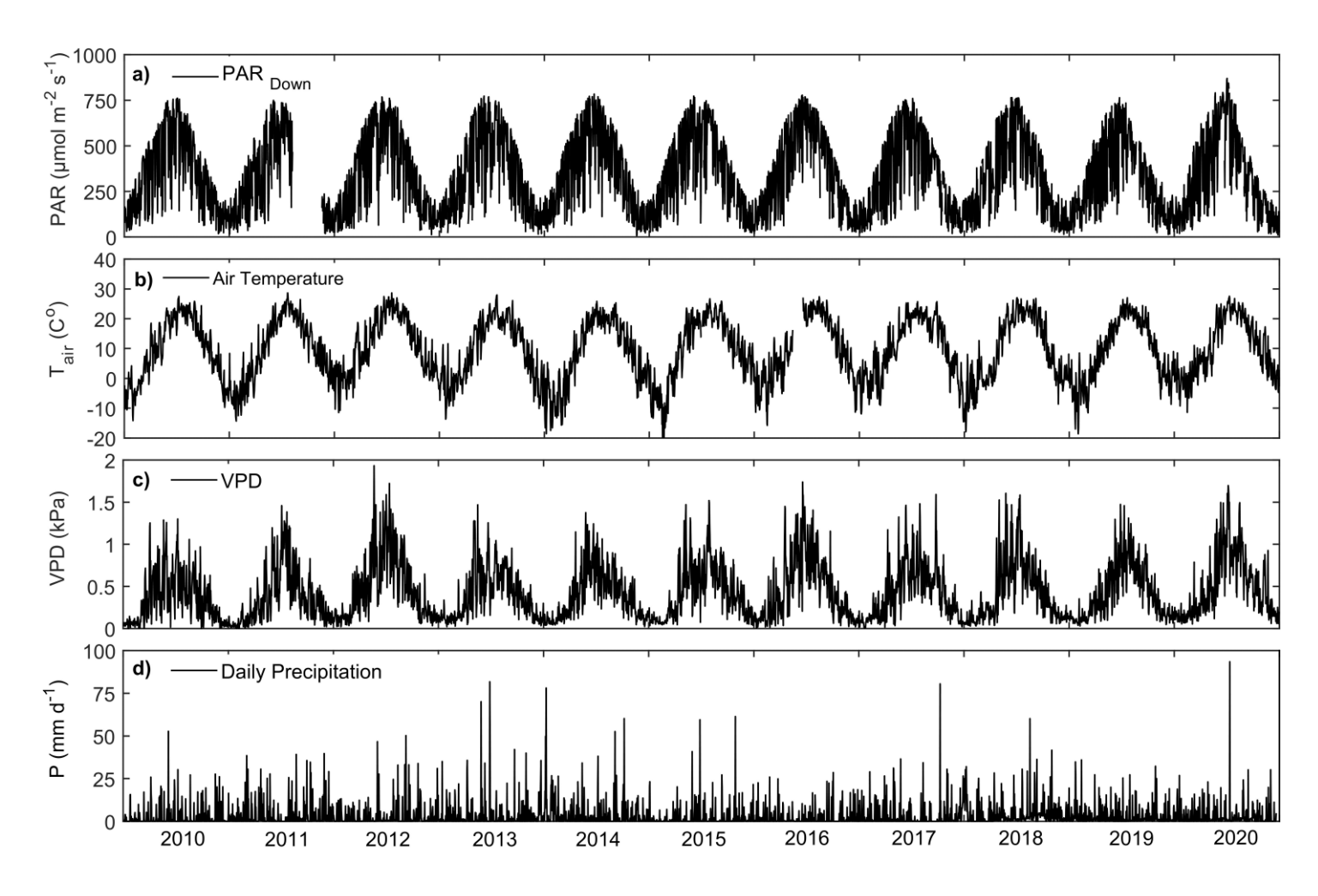


Figure 3.3. Time series of daily mean or total meteorological variables from 2010 to 2020. (a) downward photosynthesis active radiation (PAR), (b) air temperature above canopy at 28 m height, (c) vapor pressure deficit (VPD) and (d) daily total precipitation (P).

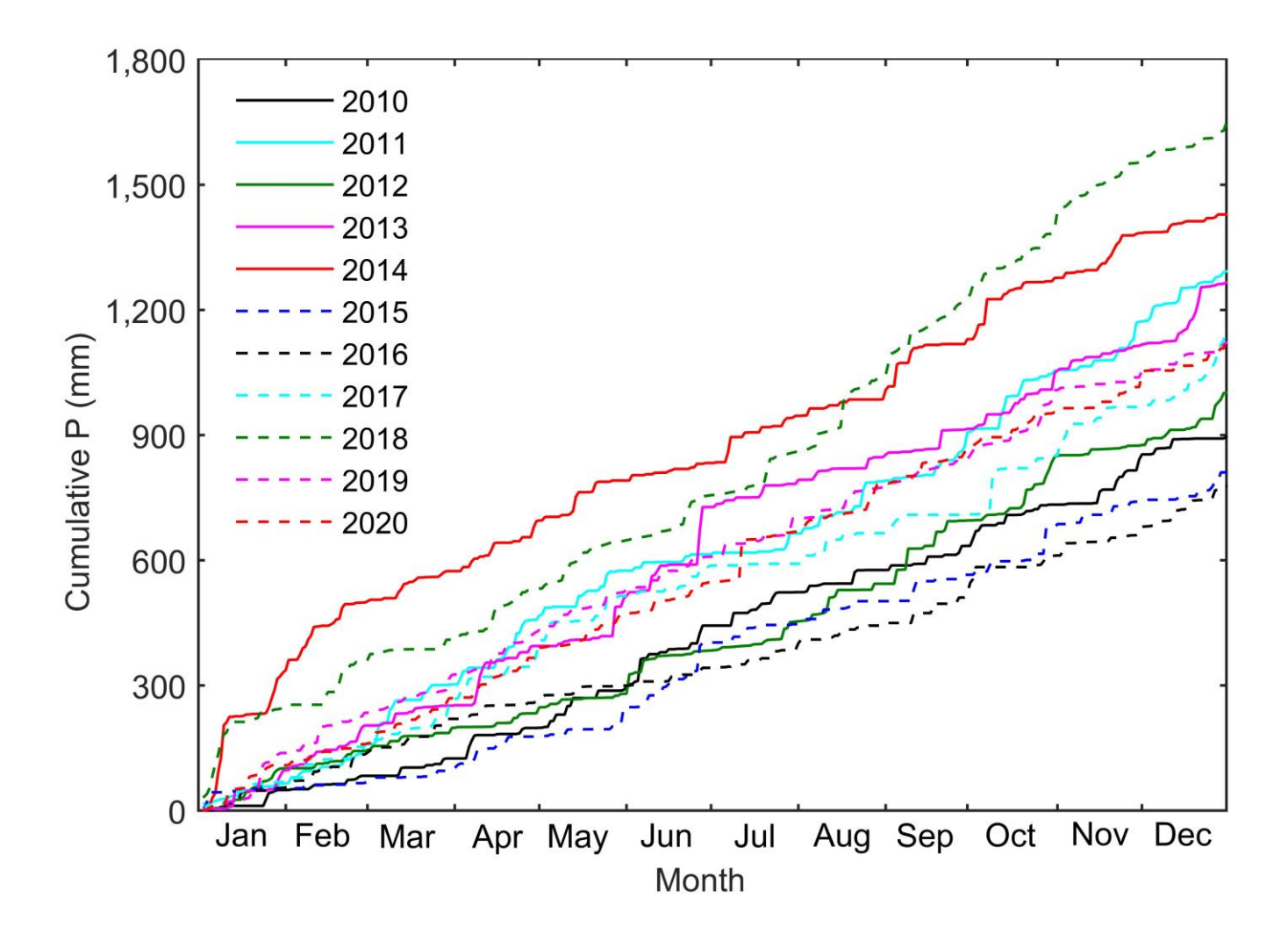


Figure 3.4. Yearly cumulative total precipitation (P) from 2010 to 2020.

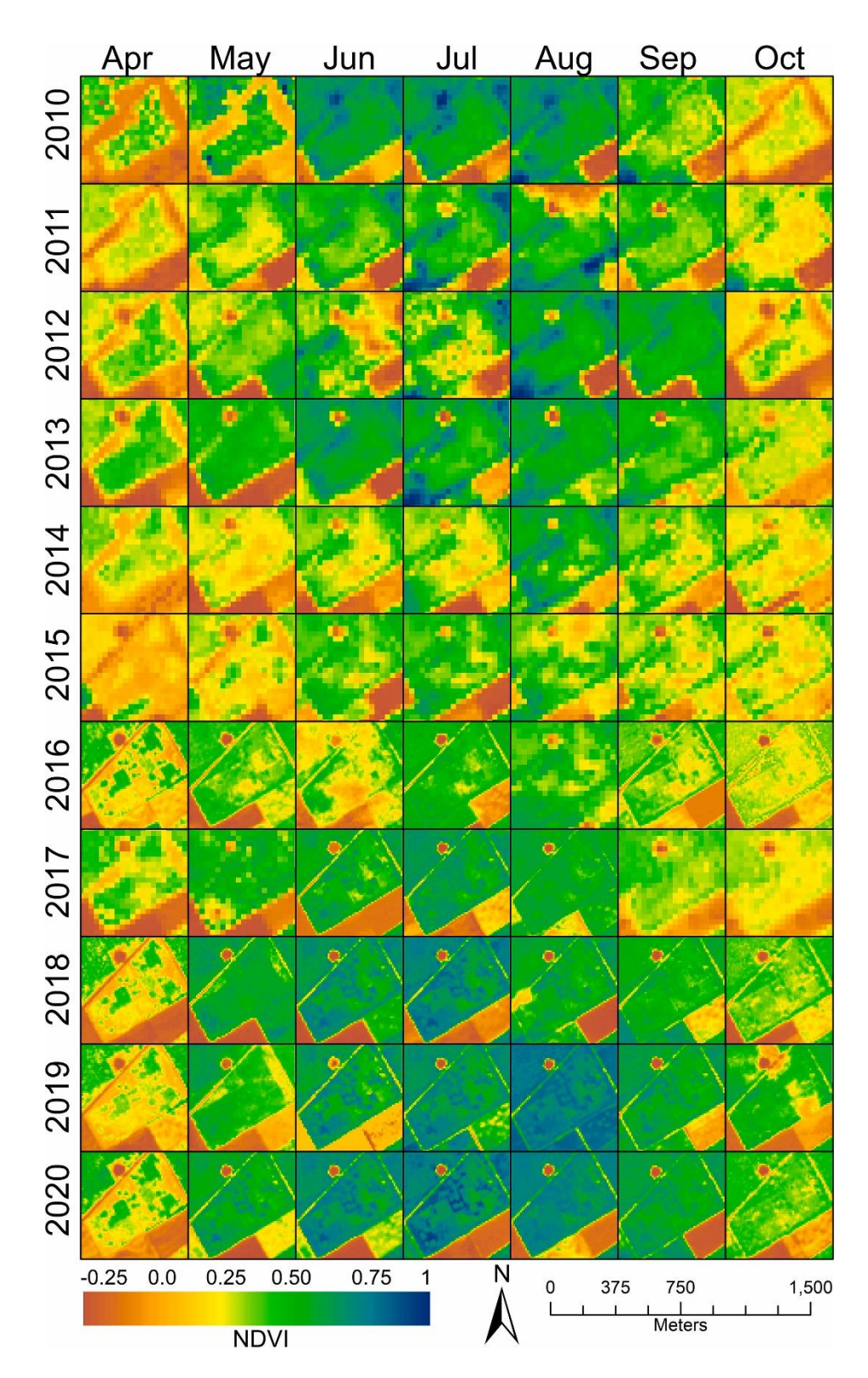


Figure 3.5. Spatiotemporal patterns of mean daily normalized difference vegetation index (NDVI) by moth over the growing season (April to October) for each variable retention harvesting treatment, the missing data filled from available nearest satellite observation from Landsat and Sentinel-2.

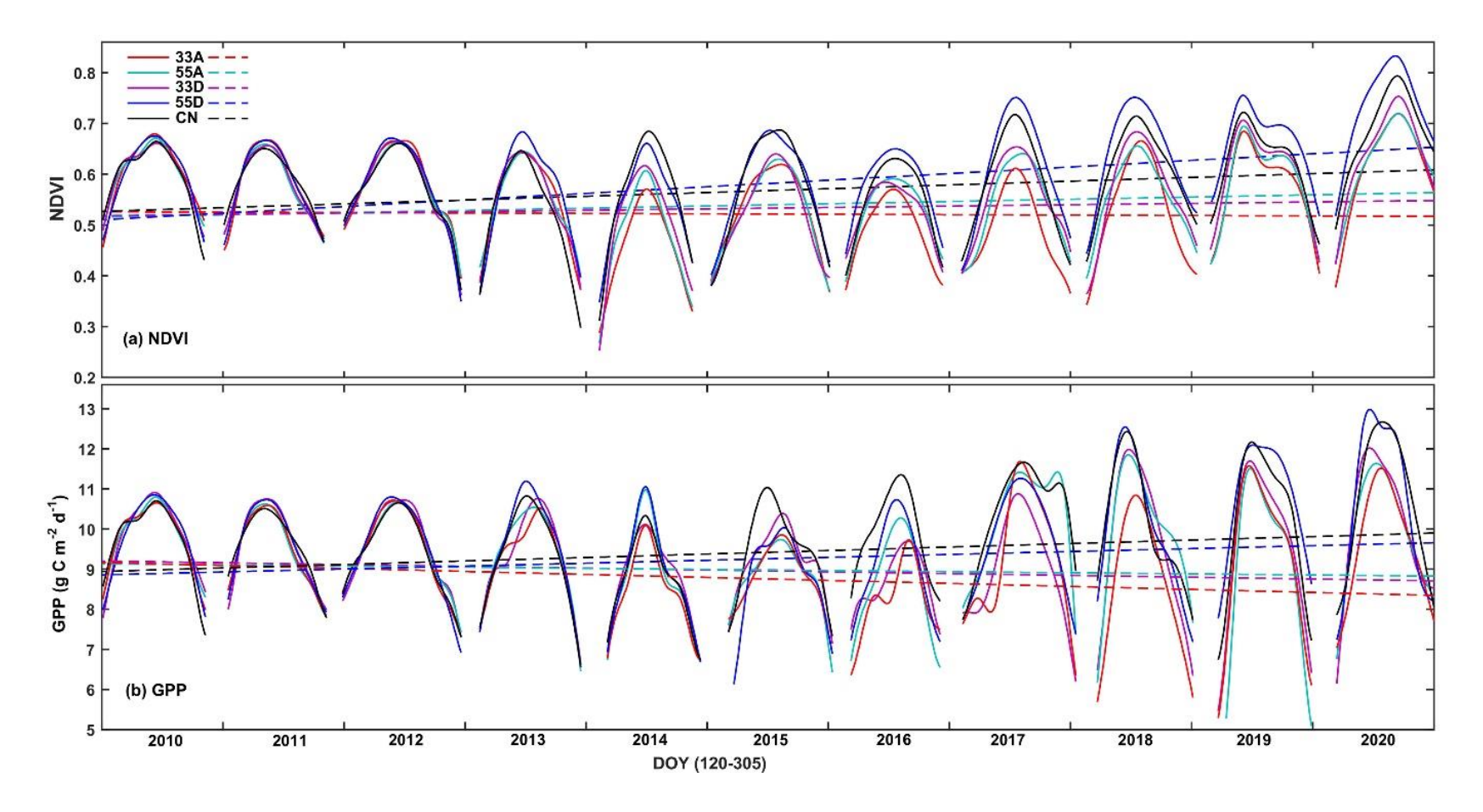


Figure 3.6. (a) Time series of mean daily normalized difference vegetation index (NDVI) for each variable retention harvesting treatment over the growing season (April to October) from 2010 to 2020 and (b) time series of mean daily gross primary productivity (GPP) trajectory from 2010 to 2020 for each treatment. Fitted trend lines (dashed lines) to daily mean NDVI of each treatment from 2010 to 2020 are also shown.

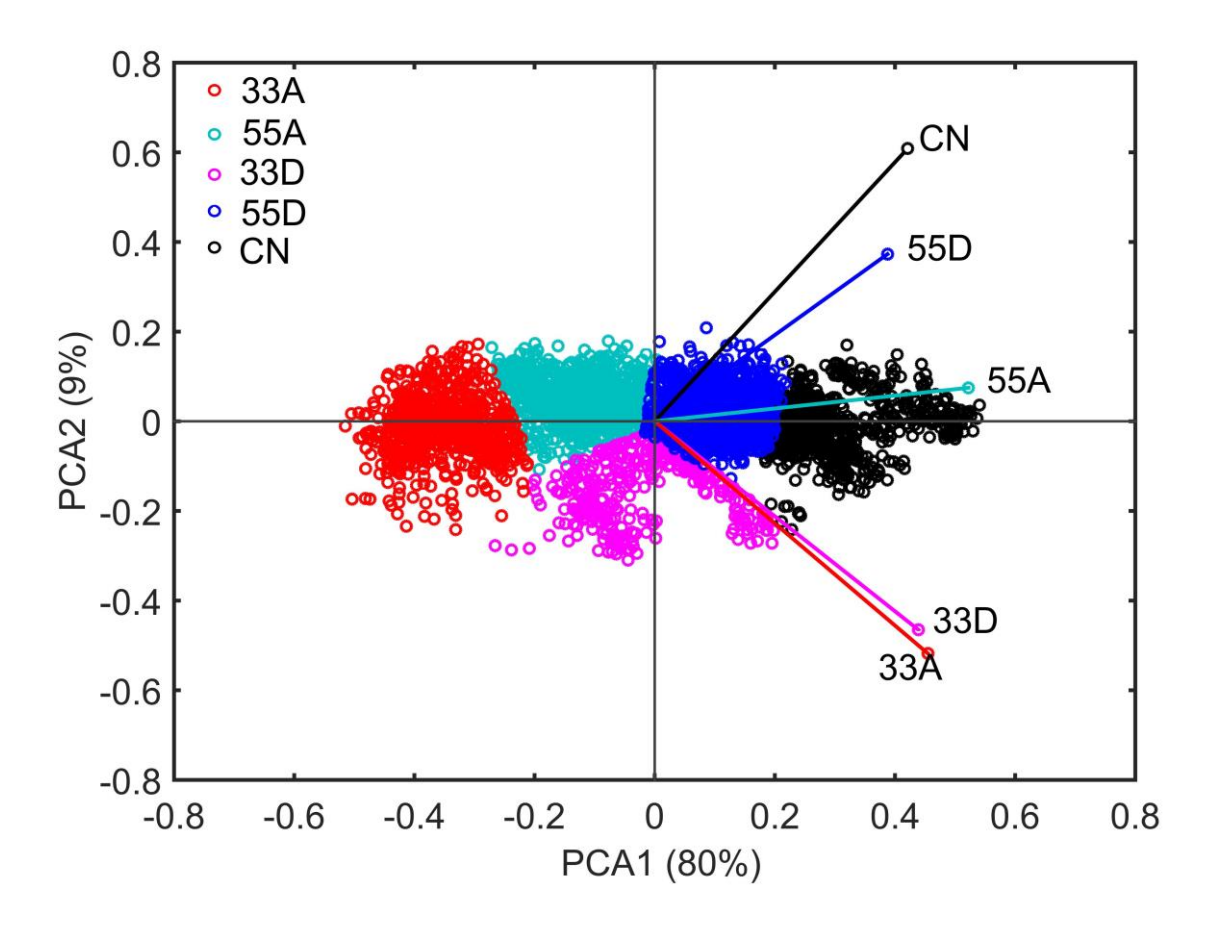


Figure 3.7. Normalized difference vegetation index (NDVI) contribution to principal component analysis (PCA) for each variable retention harvesting treatment from 2014 to 2020.

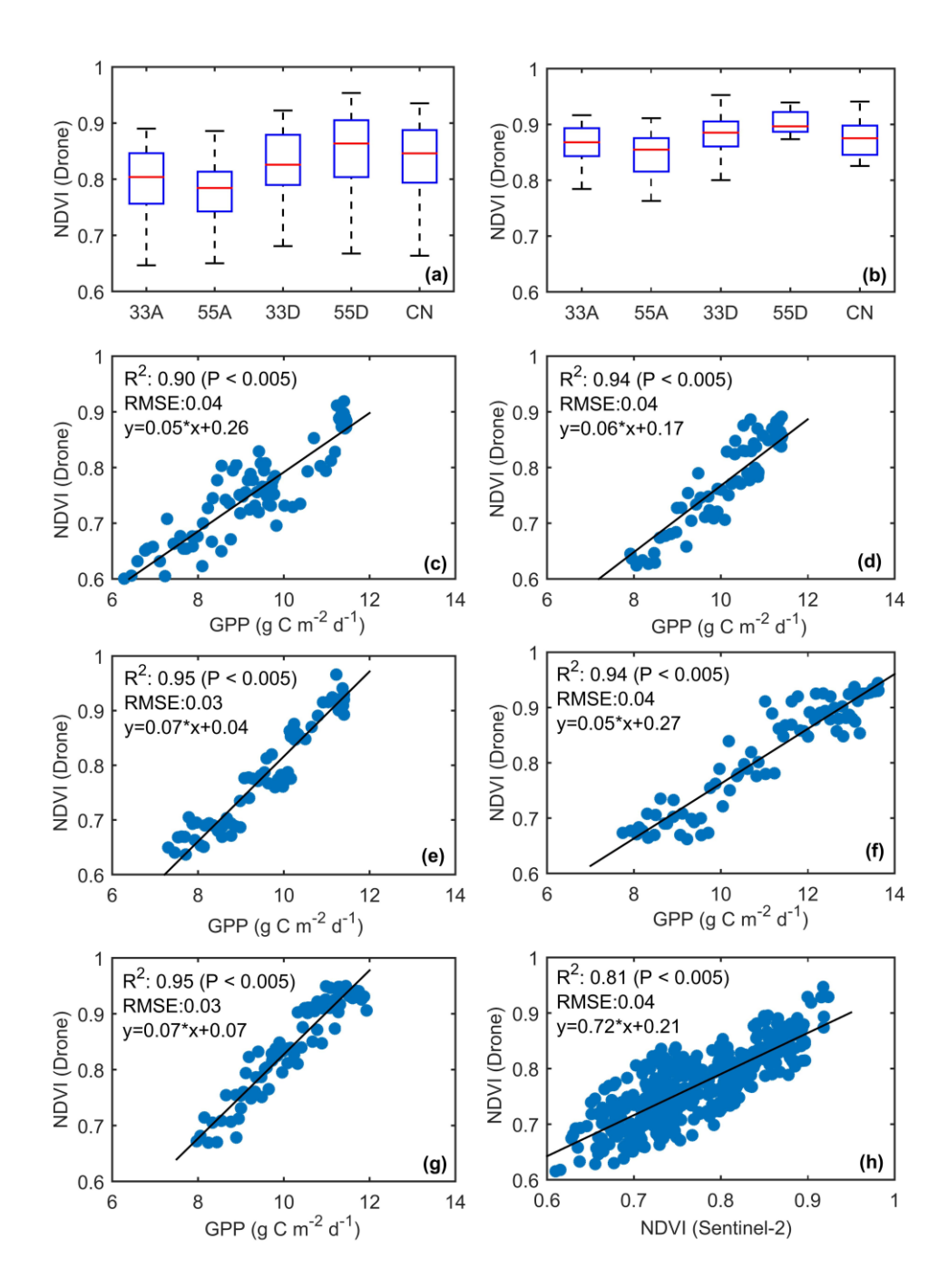


Figure 3.8. Comparison of mean daily normalized difference vegetation index (NDVI) values for all variable retention harvesting treatments on (a) 25 June 2019 and (b) 17 July 2020. The linear relationship between satellite-retrieved GPP and drone-measured NDVI in panel c-g respectively for 33A, 55A, 33D, 55D and CN treatment. The relationship between satellite and drone observation of NDVI in (h). Linear regression equation, R2 and RMSE are shown in each panel of c to h.

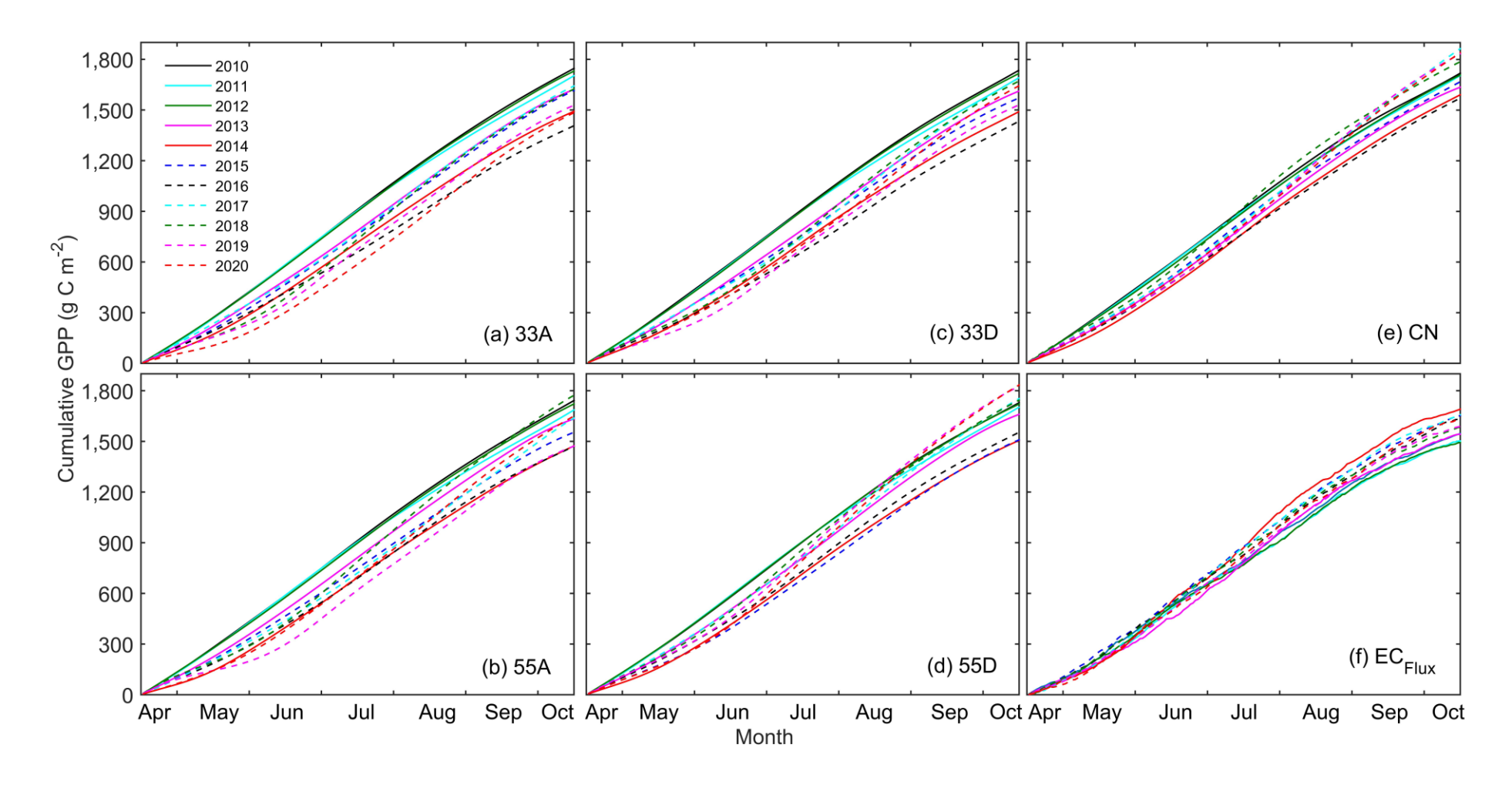


Figure 3.9. (a-e) Satellite-derived gross primary productivity (GPP) from 2010 to 2020 for each variable retention harvesting treatment and (f) GPP from eddy covariance flux measurements over the entire study period.

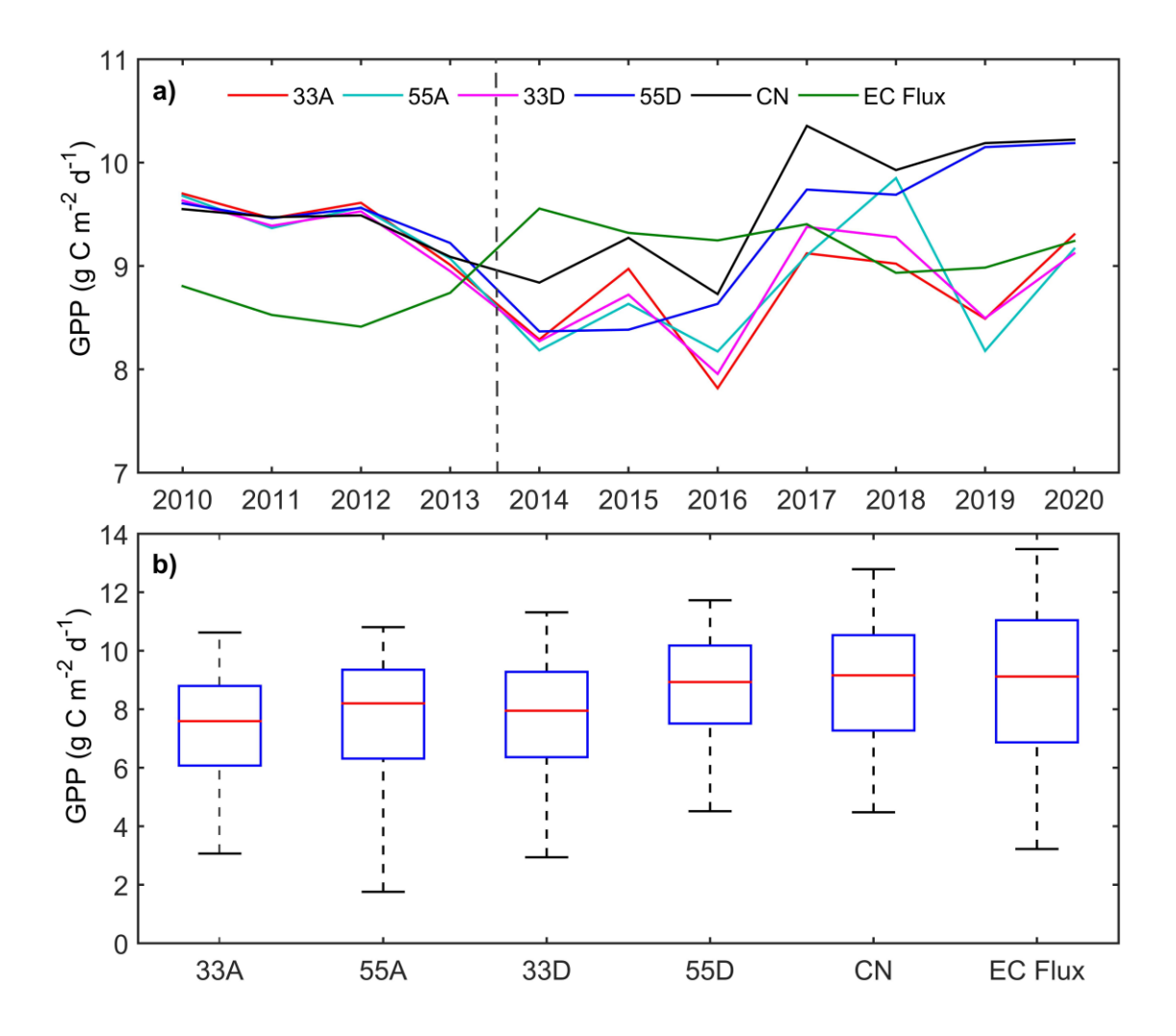


Figure 3.10. (a) Mean daily gross primary productivity (GPP) for each variable retention harvesting treatment from remote sensing data and adjacent white pine forest using eddy covariance flux observations from 2010 to 2020 and (b) box plot of post-harvest daily mean GPP for each variable retention harvesting treatment and adjacent white pine forest from 2014 to 2020.

CHAPTER 4

ASSESSMENT OF SPONGY MOTH INFESTATION IMPACTS ON FOREST PRODUCTIVITY AND CARBON LOSS USING THE SENTINEL-2 SATELLITE REMOTE SENSING AND EDDY COVARIANCE FLUX DATA

4.1 Abstract

Deciduous forests in eastern North America experienced a widespread and intense spongy moth (Lymantria dispar) infestation in 2021. This study quantified the impact of this spongy moth infestation on carbon (C) cycle in forests across the Great Lakes region in Canada, utilizing high-resolution ($10 \times 10 \text{ m}^2$) Sentinel-2 satellite remote sensing images and eddy covariance (EC) flux data. Study results showed a significant reduction in leaf area index (LAI) and gross primary productivity (GPP) values in deciduous and mixed forests in the region in 2021. Remote sensing derived, growing season mean LAI values of deciduous (mixed) forests were 3.66 (3.18), 2.74 (2.64), and 3.53 (2.94) m² m⁻² in 2020, 2021 and 2022, respectively, indicating about 24 (14)% reduction in LAI, as compared to pre- and post-infestation years. Similarly, growing season GPP values in deciduous (mixed) forests were 1338 (1208), 868 (932), and 1367 (1175) g C m⁻², respectively in 2020, 2021 and 2022, showing about 35 (22)% reduction in GPP in 2021 as compared to pre- and post-infestation years. This infestation induced reduction in GPP of deciduous and mixed forests, when upscaled to whole study area (178,000 km²), resulted in 21.1 (21.4) Mt of C loss as compared to 2020 (2022), respectively. It shows the large scale of C losses caused by this infestation in the Canadian Great Lakes region. The methods developed in this study offer valuable tools to assess and quantify natural disturbance impacts on the regional C balance of forest ecosystems by integrating field observations, high-resolution remote sensing data and models. Study results will also help in developing sustainable forest management practices to achieve net-zero C emission goals through nature-based climate change solutions.

4.2 Introduction

Forest ecosystems cover more than 30% of the terrestrial area and play a crucial role in the global carbon (C) cycle through the processes of photosynthesis and respiration (FAO, 2010; Ahmed, 2018). The balance between these two opposing fluxes determines whether the forest ecosystem is C sink or source (DeLucia et al., 2007; Litton et al., 2007; Schmid et al., 2016; Chi et al., 2021). Forests have consistently demonstrated higher levels of gross primary productivity (GPP) and established the Earth's most substantial C pools (Peters et al., 2007). Forests in North America are estimated to contribute approximately 76% of the region's net terrestrial C sequestration (Zhao et al., 2021). In Canada, forest ecosystems have accumulated on average 173 million tons of C per year over much of the past century (Gray et al., 2006; Hengeveld et al. 2008). However, this rate of C sequestration can be influenced by natural disturbances such as wildfires and insect infestations (Kurz et al., 2002; Kalamandeen et al., 2023).

In North America, frequent outbreaks of insect infestations including mountain pine beetle (*Dendroctonus ponderosae*) infestation in western parts and spongy moth (*Lymantria dispar*) infestations in eastern regions have been the major factors impacting forest growth, health and C balance (Kurz et al., 2002). The spongy moth is a non-native species originally from Europe and Asia (Joria et al. 1991; Wang et al., 2022), that was first accidentally introduced in Boston area in USA in 1869 (Williams et al., 1985; Picq et al., 2023). Since then, it has expanded its range from New England to southward in Virginia to North Carolina and westward in Wisconsin, Michigan and the Great Lakes regions in USA and Canada (De Beurs and Townsend, 2008; Hajek et al., 2021). Spongy month causes defoliation of various deciduous and mixed forests, including oak (*Quercus*), birch (*Betula*), aspen (*Populus*), sugar maple (*Acer saccharum*), American beech (*Fagus grandifolia*), balsam fir (*Abies balsamea*), and in sever

infestation cases eastern white pine (*Pinus strobus*) and Colorado blue spruce (*Picea pungens*). The spongy moth's life cycle involves egg dispersion before April, with early-stage caterpillars persisting until mid-May, late-stage caterpillars emerging in June, pupae developing in mid-July, and adult moths appearing by mid-August (Government of Ontario, 2024). Defoliation typically begins in the early caterpillar stage and intensifies throughout the late caterpillar stage from June to August.

In Eastern North America, spongy moth outbreaks have occurred roughly every seven to ten years with the past major or significant infestations recorded in 1981, 1985, 1991, 2002, 2008 and 2021 (ONDMNRF, 2021; OMNRF, 2024). Since 1970, it is estimated that over 30 million hectares of forest have experienced defoliation due to spongy moth infestation (De Beurs and Townsend, 2008; Hajek et al., 2021). The spongy moth outbreak of 2021 was the largest on record in the region where almost 1.78 million hectares of forests were impacted in the province of Ontario, Canada and 2.5 million hectares affected in the United States (USDA, 2023; OMNRF, 2024). In Ontario, 17,797 km² forest area was severely impacted by the infestation (OMNRF, 2024). The large-scale 2021 spongy moth defoliation severely impacted C sequestration capabilities of forest ecosystems in both Canada and the USA and posed a considerable challenge for the health and growth of forests (Chung et al., 2021). With about 595 million hectares of non-affected forests in North America that are climatically suitable habitats for spongy moth expansion, future outbreaks may potentially pose a major challenge for forest growth, health and C uptake in the region (Gray, 2004; Kalamandeen et al., 2023). Therefore, there is a need to develop effective forest monitoring and management strategies and develop integrated methods to quantify the loss of C caused by these infestations, which are expected to become more widespread, intense and frequent in future due to climate change (De Beurs and Townsend, 2008; Harvey et al., 2022).

Remote sensing techniques have been effectively employed for estimating spongy moth defoliation areas since the mid-1980s utilizing Earth observatory satellite imagery from platforms such as Landsat (Williams et al., 1985; Joria et al., 1991; White et al., 2017), SPOT-1 (Ciesla et al., 1989), and MODIS (De Beurs and Townsend, 2008). These satellite systems typically classify regions impacted by spongy moth infestations into different categories, including light, moderate, and heavy defoliation, while also identifying regions of healthy forests (Williams et al., 1985; Ciesla et al., 1989; Joria et al., 1991; Kovalev et al., 2023). However, the precise categorization of the intensity of spongy moth infestation has been challenging, primarily due to the shorter duration of spongy moth outbreak and low or moderate resolution of satellite imagery (e.g. from MODIS, SPOT, and Landsat Satellites). Recent advances in high-resolution remote sensing techniques have significantly improved the accuracy of remote sensing images, enabling not only the detection of defoliation areas but also providing capabilities for the precise measurements of the extent of these events and quantifying defoliation impacts on C sequestration (Townsend et al., 2004; Kovalev et al., 2023). It allows systematic assessment of the influence of spongy moth infestations on forest ecosystems and their C balances.

Sentinel-2A and 2B satellites provide high-resolution (10 × 10 m²) images that are very suitable for monitoring insect infestation such as spongy moth defoliation and for quantifying forest C losses through the exploration of vegetation indices (VIs), and estimation of GPP (Hussain et al., 2024). Several studies in the literature have successfully estimated infestation impact on forest growth and health by utilizing VIs such as the normalized difference vegetation index (NDVI) and the enhanced vegetation index (EVI) (Carter and Knapp, 2001; Fraser & Latifovic, 2005; Eklundh et al., 2009). However, studies focusing on the

quantification of the effects of insect defoliation on forest C dynamics has been limited (De Beurs and Townsend, 2008; Senf et al., 2017; Kovalev et al., 2023).

The primary aim of this study is to determine the impact of 2021 spongy moth (*Lymantria dispar*) infestations on forest growth and productivity in the Great Lake region in Canada using high-resolution (10 × 10 m²) Sentinel-2 satellite remote sensing data and eddy covariance (EC) flux observations from 2020 to 2022. The specific objectives of this study are to: (i) estimate seasonal variations and trends in the leaf area index (LAI) using high resolution remote sensing data; (ii) determine forest photosynthetic uptake and gross primary productivity (GPP) using observed eddy covariance flux and remote sensing data; and (iii) quantify carbon (C) losses across the region because of this wide spread and server spongy moth infestation. To delineate distinct vegetation categories within the study area, the study employed a machine learning-based land use/land cover (LULC) classification scheme using Sentinel-2 data in the Google Earth Engine (GEE) platform. An examination of the suitability of utilizing LAI to measure the biomass and GPP of various affected vegetation cover types across the region was also conducted. These assessments will contribute to the development of sustainable forest management strategies and help to achieve net zero carbon goals through nature-based climate change solutions.

4.3 Materials and Methods

4.3.1 Study area

The study area covers a region from 75° W to 84° W longitude and 42° N to 48° N latitude, situated along the shores of Lake Ontario, Lake Erie, and Lake Huron, encompassing approximately 178,000 km² in southern and central Ontario, Canada (Figure. 4.1). Much of this

area is part of Great Lakes-St. Lawrence forest is dominated by different ages of hardwood forests including a variety of tree species such as sugar maple (*Acer saccharum*), red maple (*Acer rubrum*), white oak (*Quercus alba*), red oak (*Quercus rubra*), yellow birch (*Betula alleghaniensis*), basswood (*Tilia americana*), white pine (*Pinus strobus*), red pine (*Pinus resinosa*), Eastern hemlock (*Tsuga canadensis*) and white cedar (*Thuja occidentalis*). Deciduous, conifer and mixed forests cover up to 62% land of this area. The southern latitudes of the study area are dominated by cropland such as corn, soybean, and forage for livestock production, as well as deciduous forests which cover about 10% of the area (OMNRF, 2024). The remaining land is categorized as primary wetlands or urban areas. The northern parts of study area is part of the Boreal forest and the Georgian Bay lowlands forest, while the central and southern forests are also characterized as Carolinian forests. The southern region is more conducive to agriculture, more densely populated, and urbanized. In contrast, the central and northern regions of the study areas are mountainous terrain covered with forests and have a relatively untouched environment (Baldwin et al., 2000; Shah et al., 2022).

The climate of the study area is characterized as cool continental, which is influenced by regional factors due to area's proximity to the Great Lakes. The mean annual precipitation of 786 mm year⁻¹ based on observations recorded at the Toronto Pearson Airport Weather Station during the normal climate period from 1991 to 2020 (Environment and Climate Change Canada, 2023) where 14% of the precipitation fell as snow. The mean annual temperature varies across the region depending on latitude, with mean annual temperature of 8.2 °C from 1991 to 2020 at the Toronto Pearson airport weather station (Environment and Climate Change Canada, 2023). Additionally, mean temperature during the growing season fluctuates between 15 and 30 °C (Wazneh et al., 2017).

4.3.2 Remote sensing and observed eddy covariance flux datasets

Sentinel-2A and Sentinel-2B (S2) satellites of the COPERNICUS satellite systems of the European Union's earth observation program (Drusch et al., 2012) provide high-resolution datasets for terrestrial ecosystem monitoring (Löw & Koukal, 2020). The Sentinel-2 multispectral instrument (MSI) system delivers 13 spectral bands, including $10 \times 10 \text{ m}^2$ spatial resolution of visible and near-infrared (NIR) and $20 \times 20 \text{ m}^2$ spatial resolution of short-wave infrared (SWIR) spectrum with up to five-day revisiting time (Drusch et al., 2012; Sun et al., 2021). This study used Sentinel-2 data to calculate vegetation indices (VIs) such as normalized difference vegetation index (NDVI), and leaf area index (LAI) for biomass estimation. Sentinel-2 satellite datasets were downloaded from https://earthexplorer.usgs.gov/. Sentinel-2 (S2) data was also used to estimate GPP while utilizing radiative model and observed eddy covariance (EC) flux data.

The observed EC flux data were obtained from Turkey Point Environmental Observatory (Arain et al., 2022; Beamesderfer et al., 2020; Latifovic and Arain, 2024). These sites are known as the Canadian Turkey Point deciduous forest sites (CA-TPD) including four different EC flux stations (TP-Ag, TP39 TP02and TPD) and associated with the Global Water Futures Observatory Program, Ameriflux and Global Fluxnet network (Arain, 2018). Although EC flux and meteorological variables have been continuously measured at this site since 2012, CO₂ fluxes for three years, i.e. 2020 (pre-infestation), 2021 (infestation) and 2022 (post-infestation) were used in the analysis presented in this study. In 2021 spongy month infestation was quite severe at our forest site where majority of deciduous trees were defoliated as shown in Figure 4.2 and further discussed in Latifovic and Arain (2024). The quality control of EC

flux and meteorological data was conducted utilizing the Biometeorological Analysis, Collection, and Organizational Node (BACON) software, which was developed by our lab (Brodeur, 2014). Outliers within the dataset were detected and eliminated through the BACON software and small gaps in the dataset were filled through linear interpolation from the onsite data. Further details of EC fluxes and meteorological measurements, data gap filling and partitioning of observed CO₂ flux in ecosystem respiration and GPP are given in Latifovic and Arain (2024). In addition, no forest management activity had taken place at the forest in recent years.

4.3.3 Land use and land cover (LULC) classification

The GEE platform's machine-learning approach was utilized to create cloud-free Sentinel-2 data for the LULC analysis (Nasiri et al., 2022). The GEE cloud computing approach was utilized to collect images and process data for the growing season of 2020 (Figure 5.1). GEE-based machine learning classifier, support vector machine (SVM) was used to classify six primary land cover categories, namely water bodies, urban areas, agricultural land, coniferous forest, deciduous forest and mixed forest (Sheykhmousa et al., 2020). Each land cover category was assessed using 650 ground point samples to extract per-band pixel values from the Sentinel-2 dataset, ensuring that the data used had minimum cloud cover (less than 5%). The evaluation of classification accuracy provided a comparison between LULC classes derived from the training point and data obtained during the testing phase (Nasiri et al., 2022), which involved a total of 3900 ground point samples. This accuracy assessment was performed using confusion matrices (Table 4.1). The overall accuracy based on these confusion matrices was 95.7%.

The analysis revealed that coniferous forests occupied the largest land area, covering 43,017 km², which represents 24.29% of the total studied area. Agriculture was the second-largest land cover category, covering 42,294 km², accounting for 23.88% of the total area. Deciduous forests covered 36,574 km², constituting 20.64% of the total area and mixed forests occupied 23,936 km², making up to 13.51% of the total area. Additionally, water bodies and wetlands covered 13,053 km², covering 7.37% of the total area, while the urban areas occupied 19,256 km², covering 10.87% of the total area.

4.3.4 Retrieval of leaf area index (LAI)

LAI was calculated using the Sentinel-2 data and the PROSAIL model which is the combination of PROSPECT (Jacquemoud and Baret, 1990; Feret et al., 2008) and SAIL model (Verhoef, 1984). The PROSPECT model provides leaf optical properties and the SAIL model provides plant canopy reflectance (Sun et al., 2021). The PROSPECT model measures leaf hemispherical reflectance and transmittance to define leaf optical elements at 400–2500 nm through six input parameters: leaf structure parameter (N, unitless), leaf chlorophyll content (Cab), carotenoid content (Car), brown pigment content (Cbrown), equivalent water thickness (Cw) and dry matter content (Cm) (Xu et al., 2019). The SAIL model calculates canopy reflectance as a function of leaf optical elements obtained from PROSPECT and six input parameters: leaf inclination distribution function (LIDF), LAI, hot spot parameter (hspot), solar zenith angle (tts), view zenith angle (tto), relative azimuth angle (psi) (Sun et al., 2021). All input parameters for the PROSAIL model are shown in Table 4.2.

The spectral response function for Sentinel-2 satellite data is used from band effective reflectance. The band reflectance was calculated based on the measured canopy hyperspectral

reflectance and simulated reflectance from the PROSAIL model. The band reflectance was calculated by Wang et al. (2015) as follows:

$$\rho_{s}(\lambda) = \frac{\int_{\lambda_{min}}^{\lambda_{max}} \rho_{s}(\lambda_{i}) \psi(\lambda_{i}) d\lambda}{\int_{\lambda_{min}}^{\lambda_{max}} \psi(\lambda_{i}) d\lambda}$$
(4.1)

This derivative follows,

$$\rho_{s}(\lambda) = \frac{\int_{400}^{2500} \rho_{s}(\lambda_{i})\psi(\lambda_{i})d\lambda}{\int_{400}^{2500} \psi(\lambda_{i})d\lambda} \approx \frac{\sum_{400}^{2500} \rho_{s}(\lambda_{i})\psi(\lambda_{i})}{\sum_{400}^{2500} \psi(\lambda_{i})}$$
(4.2)

where $\rho_s(\lambda)$ is the simulated band reflectance of the sensor, $\rho_s(\lambda_i)$ is the simulated reflectance of the PROSAIL model, which is coded in MATLAB. λ_{min} is equal to 400 nm the minimum value of wavelength limit and λ_{max} is 2500 the maximum value of the wavelength limit, $\psi(\lambda_i)$ is the spectral response coefficient of Sentinel-2.

4.3.5 Remote sensing-based gross primary productivity (GPP) estimation

GPP was estimated using the Sentinel-2-based light use efficiency (LUE) model to quantify the CO₂ uptake from different vegetation cover types. LUE model has the empirical capability to estimate GPP (Zhang et al., 2017; Sun et al., 2019) using remote sensing data. Observed air temperature (T_a) and photosynthetically active radiation (PAR) data were used with satellite data in the LUE model to calculate GPP (Hussain et al., 2024). The following equations were used as part of the LUE model (Table 4.3).

In Table 5.3, APAR_{chl} is absorbed photosynthetically active radiation (PAR); fPAR_{chl} is the fraction of PAR estimated by chlorophyll or linear function of EVI, which is modified following Xiao et al. (2004). 0.1 and 1.25 are constants to adjust for vegetated land and were validated from solar-induced chlorophyll fluorescence (SIF); ε_g is the light use efficiency (LUE), ε_0 is the apparent quantum yield or maximum light use efficiency (μ mol CO₂ per μ mol photosynthetic photon flux density (PPFD)); T_{scalar}, W_{scalar} are the downward-parameter scalars for the effects of temperature and water respectively on LUE by C3/C4 photosynthesis pathways; Ta, Tmin, Tmax, and Topt refer to the mean, minimum, maximum, and optimum temperature for photosynthesis, respectively; LSWI is the land surface water index. Model estimated daily GPP values were compared with the observed GPP values for 2020 and 2021 as shown in Figure 4.3. There was a strong correlation between satellite-derived and observed daily GPP values for agricultural lands, conifer forests and deciduous forests, respectively (Figure 4.3a–c).

4.3.6 Statistical analysis

Weighted double logistic (WDL) function was used to fit the daily time series of VIs as described in Yang et al., (2019). WDL consists of two logistic functions based on the vegetation growth activity, including the growing part (f_1) and the declining part (f_2) to set the model parameters which can provide the daily time series using following equations (Yang et al., 2019).

$$y = f_1 + f_2 + e (4.3)$$

$$f_1 = \frac{c_1}{1 + e^{a_1 + b_1 t}} + d_1 \tag{4.4}$$

Ph.D. Thesis – Nur Hussain

$$f_2 = \frac{c_2}{1 + e^{a_2 + b_2 t}} + d_2 \tag{4.5}$$

$$e = max (c_1 + d_1, c_2 + d_2)$$
(4.6)

where y is the time series of variable, d and c+d denote the minimum value (min(f)) and maximum value (max(f)), respectively; c indicates the local amplitude; and a and b determine the shape and slope of the logistic function, respectively. The subscripts I and 2 identify the parameters of the growing and declining parts, respectively. In the retrieval of these unknown parameters, the initial d and c are assigned as min(f) and max(f)-min(f), respectively. Thus, the principal problem is to derive parameters a and b. Considering the different weights of each of the data points, we transformed the non-linear fitting problem into a linear one by a function transformation as a_1+b_1 $t=In(c_1f_1-d_1-1)$. Furthermore, the WLS method is applied to solve the analytic expression of the logistic function for each part $(f_1$ and $f_2)$.

We also utilize standardized anomalies to understand temporal variations and deviations from normal growth trends over the study period. We calculated these anomalies by subtracting the mean GPP during three growing periods from the daily GPP values and then dividing it by the standard deviation observed over the same periods. These calculations followed equations 5.7 and 5.8 as shown by Zhao et al. (2022).

$$y_{sd} = \frac{y_d - \overline{y_d}}{\sigma} \tag{4.7}$$

$$y_d = x - \bar{x} \tag{4.8}$$

where, y_{sd} is standardized anomaly, y_d is daily anomaly and x is daily GPP and \bar{x} is the threeyear mean GPP estimated from Sentinel-2.

4.4 Results

4.4.1 Climatic conditions

The meteorological variables measured at our site from 2020 to 2022 are shown in Figures 4.4 and 4.5. The mean annual Ta was 10.6, 11.3, and 10.6 °C for 2020, 2021, and 2022, respectively. The daily maximum Ta was observed during July–August periods, while minimum Ta values were observed during January–February, reflecting the typical seasonal patterns in the Great Lakes region (Figure 4.4b). At the same time, Ts was 9.7, 10.3, and 9.6 °C. Temporal variability in Ts closely followed the temporal variability of Ta, with a correlation coefficient of 0.89 (P<0.001). Additionally, photosynthetically active radiation (PAR) exhibited similar patterns to temperature variations (Figure 4.4a, b), with respective daily values of 317, 321, and 343 µmol m⁻² d⁻¹ for 2020, 2021, and 2022.

The daily mean values of VPD were 0.37, 0.38, and 0.38 kPa for 2020, 2021, and 2022, respectively. The similarity between VPD values across the years indicates overall relatively stable atmospheric moisture conditions during the study period. Additionally, VWC during the same period was 0.11, 0.12, and 0.11 m³ m⁻³. The temporal variations in VWC reflected changes in soil moisture following large precipitation events throughout the year (Figure 4.4d). The annual total precipitation values were 1127, 1009, and 960 mm for 2020, 2021, and 2022, respectively (Figure 4.5). 2021 showed a dry period with low precipitation values in 2021 from early March to mid-June. This dry and rain-free period in the early parts of the growing season in 2021 may have helped the spongy moth to establish and thrive. Overall, observed meteorological conditions during the study period showed similarities with long-term observed weather conditions at this site.

4.4.2 Dynamics of remote sensing-based leaf area index (LAI)

Remote sensing-based monthly mean LAI values for major land cover types including deciduous, conifer and mixed forests and agricultural lands over the growing season are shown in Figure 4.6. Deciduous forests had mean LAI values of 3.66 ± 1.6 , 2.74 ± 1.1 , and 3.53 ± 1.5 m² m⁻², conifer forests had LAI value of 4.34 ± 1.6 , 4.28 ± 1.6 , and 4.26 ± 1.5 m² m⁻² and mixed forest had LAI value of 3.18 ± 1.4 , 2.64 ± 1.1 , and 2.94 ± 1.3 m² m⁻² for 2020, 2021, and 2022, respectively. Mean LAI values for agricultural lands were 3.31 ± 2.2 , 3.25 ± 2.3 , and 3.11 ± 2.2 m² m⁻² for respective years. The highest LAI values were observed for agricultural lands and conifer forests in July, followed by deciduous and mixed forests. These satellite-derived LAI values showed a large decline for deciduous and mixed forests in 2021, when these forests were impacted by spongy moth infestations (Figure 4.6c, d).

Mean LAI values for deciduous and mixed forests declined by 25 (22)% and 17 (10)% in comparison to the pre-infestation (post-infestation) values recorded in 2020 (2022). LAI values recovered to almost normal levels in 2022 for deciduous forests after the infestation, while LAI for mixed forests showed relatively lower recovery values.

4.4.3 Impact of spongy moth infestation on gross primary productivity (GPP)

The satellite-derived daily GPP values showed similar trends as observed for LAI, with much lower daily GPP values for deciduous and mixed forests in 2021 due to spongy moth infestation (Figure 4.7). In deciduous forests, photosynthetic C uptake usually started in mid-May and peaked in July with typical maximum daily GPP values of about 14 to 16 g C m⁻² d⁻¹. However, in 2021, GPP values rapidly declined at the start of June when spongy moth

defoliation intensified. Daily GPP values reached as low as 3.0 g C m⁻² d⁻¹ in July in 2021. Similar low GPP values were also observed for mixed forests. GPP saw a rebound in late July and August when the short-lived spongy moth infestation started to end due to the transformation of leaf-eating larvae (caterpillars) to pupa and adult stages. In addition, these decreasing trends of GPP were well aligned with the spongy moth life cycle, where the late caterpillar stage occurs from mid-May to the end of July, causing extensive leaf damage. However, after this period, daily GPP values showed some recovery but only reached up to 7 to 8 g C m⁻² d⁻¹ before the usual autumn photosynthetic decline started to take effect in late September. In general, rebounded daily GPP values were even lower for mixed forests due to the combined effects of infestation for deciduous forests and usual seasonal low soil moisture from late July to August in the region, which typically causes lower GPP values in conifer trees. However, overall the soil moisture was sufficient for ecosystem production in 2021 (Figure 4.4d). In 2020 and 2021, the active period of growth for deciduous forests ended by the end of October, while in 2022 deciduous forests experienced an earlier end of growing season (Figure 4.7c).

In contrast, photosynthetic C uptake in coniferous forests began earlier in April as compared to other vegetation types and continued until the end of October. The maximum daily GPP in conifer forests was observed in June, with maximum daily GPP values of about 10 to 14 g C m⁻² d⁻¹. In agricultural lands, daily GPP was almost zero in April but it started to increase in mid-May and peaked in July and August, with maximum daily GPP values reaching about 20 to 23 g C m⁻² d⁻¹ (Figure 4.7a). These trends were also clearly shown in the standardized daily GPP anomaly values, where GPP in deciduous and mixed forests showed a large decline, while GPP in conifer forests and agricultural lands were not impacted (Figure

4.8). In 2022, the forest appeared to be fully recovered with a notable increase in both the daily mean and seasonal total GPP values as compared to 2021.

Overall, growing season mean daily GPP values in deciduous forests were 6.83±4.1, 4.43±2.5, and 7.77±5.4 g C m⁻² d⁻¹ for 2020, 2021 and 2022, respectively. Corresponding GPP values for coniferous forests were 6.87±3.5, 7.10±2.7, and 6.86±2.7 g C m⁻² d⁻¹ and for mixed forests were 6.45±4.2 g C m⁻² d⁻¹, 4.81±2.2 g C m⁻² d⁻¹, and 6.12±2.3 g C m⁻² d⁻¹. Agricultural lands had growing season mean daily GPP values of 9.65±5.4, 8.45±6.1, and 9.55±6.2 g C m⁻² d⁻¹ in 2020, 2021, and 2022, respectively (Figure 4.7; Table 4.4). The highest cumulative GPP values over the growing season were observed in the coniferous forest in all three years, followed by deciduous forests, agricultural lands, and mixed forests (Figure 4.7e–h and Table 4.4). Maximum GPP estimates for conifer forests highlighted their optimum photosynthetic activity and proficiency for C uptake. Deciduous forests had total growing season GPP values of 1338, 869, and 1367 g C m⁻² in 2020, 2021 and 2022, respectively, while coniferous forests photosynthesized 1443, 1475, and 1438 g C m⁻² and mixed forests exhibited GPP values of 1208, 932, and 1175 g C m⁻² for the same years (Figure 4.7e–h and Table 4.4). Agricultural lands showed cumulative GPP values of 1235, 1266, and 1241 g C m⁻² over the same period (Figure 4.7e–h and Table 4.4).

Spatial patterns of total GPP over the growing season (April—October) for 2020, 2021 and 2022 are shown in Figure 4.9. These spatial patterns of GPP clearly showed the severely impacted areas and extent of decline in photosynthetic C update in the region where almost all deciduous and mixed forests were impacted. Southern areas which had a higher proportion of deciduous tree species were more severely impacted. These areas were in the north of Lake Erie and west

of Lake Ontario (Figure 4.9c). However, low values of GPP as shown by yellow color were prevalent almost all over the study region, except in the central and far northwestern parts that were dominated by conifer species. Overall, these results showed 35 (36)% decrease in total GPP over the growing season for deciduous forests in 2021 when compared to pre-infestation (post-infestation) years. A similar GPP decline for mixed forests was 23 (21) % in 2021 when compared to pre-infestation (post-infestation) years (Table 4.4).

4.5 Discussion

Remotely sensed LAI measurements have been widely used to observe the intensity and extent of defoliation in deciduous and mixed forests (De Beurs and Townsend, 2008). LAI measurements also provide direct quantification of leaf properties, photosynthetic activity, C uptake (Jarlan et al., 2008; Boussetta et al., 2013; Alton, 2016; Brown et al., 2020) and are often used to estimate vegetation biomass utilizing remote sensing-based models (Zolles et al., 2021). Our study results showed that the mean LAI values for deciduous forests decreased by about 25% in 2021 as compared to the pre-infestation LAI values in 2020, and by about 22% as compared to the post-infestation LAI values in 2022. It provided an indication of the severity of the impacts of spongy moth infestation on forest growth and productivity. We used these LAI values as a key indicator to observe the spatial patterns and the extent of spongy moth infestation. It helped us to observe the trajectory and dynamics of defoliation and to determine the timing and extent of canopy recovery when larvae or caterpillars were transformed into pupa and adult moths after a few weeks (Latifovic and Arain, 2024). We also used these LAI values to calculate remote sensing based GPP across the region (Sun et al., 2021). We found a strong positive correlation between LAI and remote sensing based GPP values with R^2 values of 0.90, 0.76, 0.86 and 0.67 for agricultural lands, coniferous forests, deciduous forests and mixed forests respectively and significance level (p) values of ≤ 0.005

(data not shown). Similar strong correlations between LAI and GPP have also been found by other researchers (e.g. Qu et al., 2018; Zhang et al., 2021; Chen et al., 2023).

Our analysis showed the intense and widespread nature of the 2021 spongy moth infestation in the region where deciduous and mixed stands experienced large-scale defoliation resulting in 35% and 22% decrease in mean daily GPP values as compared to 2020 and 2022, respectively. Our study not only supported the earlier inferences that 2021 infestation was as record disturbance event in North America (Embrey et al., 2012; CFIA, 2021; Chung et al., 2021; Gooderham et al., 2021; Government of Canada, 2021; MNRF, 2021; MNDMNRF, 2022; TRCA, 2022; Clark et al., 2022; Foster et al., 2022; Coleman and Liebhold, 2023; Latifovic and Arain, 2024), but it also provides quantitative assessment of the photosynthetic C uptake reduction across the region due to defoliation (Dymond et al., 2010; Medvigy et al., 2012; Kretchun et al., 2014). These C uptake reduction estimates have significance because in recent years most of the terrestrial C cycle studies in the literature have been reporting an increase in vegetation C uptake due to warmer temperatures, longer growing seasons and CO₂ fertilization effects (Goodale et al., 2002; Harris et al., 2016; Birdsey et al., 2019; Fei et al., 2019; Ameray et al., 2021; Quirion et al., 2021). Our study has highlighted how C sequestration of deciduous and mixed forest ecosystems in eastern North America, specifically in the Great Lakes region, might be impacted by a major natural disturbance event. Such natural disturbance events are expected to increase in frequency and intensity in the future due to climate change (Pureswaran et al., 2018; IPCC, 2021; Harvey et al., 2022; Kalamandeen et al., 2023). They will have adverse consequences for biological C sinks to offset greenhouse gases (GHG) emissions to achieve net zero C emission goals.

Our study also showed that in the Great Lakes region, conifer forests have a much greater capacity for C sequestration as compared to deciduous and mixed forests due to their longer growth period and conducive environmental conditions in the region (Payne et al., 2019; Beamesderfer et al., 2020). Sustainable management of both deciduous and conifer forests may help to conserve and further enhance C uptake capacity of these forests. In this regard, our study provides the systematic methodology and road map to monitor and quantify the growth and C sequestration of all major vegetation ecosystems in the region, including conifer, deciduous and mixed forests as well as agricultural lands at high $(10 \times 10 \text{ m}^2)$ spatial resolution. Because most inset infestations are species-specific and some of them occur for short periods such as spongy moth infestations, it becomes very challenging to accurately quantify their impacts. Our utilization of high-resolution Sentinel-2 satellite imagery and a light use efficiency (LUE) model to estimate GPP for the whole region was a unique effort which provided a quantitative assessment of the photosynthetic C uptake loss because of the largescale nature of this infestation. It showed that 2021 infestation caused 4.84 and 2.6 t C ha⁻¹ reduction of C uptake in deciduous and mixed forests, respectively. This was a substantial potential C sequestration loss, considering the mean annual GPP of 14.0 t C ha⁻¹ for Canada (Gonsamo et al., 2013; Chen et al., 2020) and 12.25 t C ha⁻¹ for the USA (Turner et al., 2003; Tang et al., 2010). Our estimated total C uptake loss for the whole study area of 178,000 km² in 2021 was 21.1 (21.4) megatons of carbon (Mt C) when compared to 2020 (2022). This C loss amounted to ~11.5 (11.7)% of Canada's national GHG emission of 182.7 Mt C eq (670 Mt CO₂ eq) or 52.3 (52.1)% of the Province of Ontario's GHG emissions of 41.1 Mt C eq (150.6) Mt CO₂ eq). However, the reader is cautioned about these extrapolated results because the defoliation is tree species dependent and there may be areas which many have not been severely impacted as well as the uncertainty associated with the remote sensing derived GPP values. Our study has also highlighted the importance of future forest conservation and management practices that should account for climatic and disturbance stresses and help to enhance the sustainability and resilience of forests to these stresses.

4.6 Conclusion

This study quantified the impact of a severe spongy moth infestation on C sequestration in deciduous and mixed forest ecosystems in the Great Lakes region in Canada. By utilizing remotely sensed LAI as a key indicator, the study assessed the onset and progression of spongy moth infestation in 2021. Study results showed a substantial decline in GPP in deciduous and mixed forests in 2021 when compared to pre- and post-infestation years i.e. 2020 and 2022. Total growing season GPP values were 1338, 868, and 1367 g C m⁻² in deciduous forests over the study area from 2020 to 2022, respectively. Corresponding mean total growing season GPP values in mixed forests were 1208, 932, and 1175 g C m⁻² and in coniferous forests, they were 1443, 1475, and 1438 g C m⁻² in 2020, 2021 and 2022, respectively. It showed 35 (36)% reduction in mean total growing season GPP in deciduous forests in 2021 as compared to preinfestation (post-infestation) years. Corresponding decline in mixed forests was 23 (21)% in 2021. The whole study area (178,000 km²) experienced the total photosynthetic C uptake loss of 21.1 (21.4) Mt C when compared to 2020 (2022). Study results also displayed that coniferous forests consistently exhibited higher GPP values, indicating their efficient C sequestration capabilities. The methods developed in our study and their application using high resolution remote sensing data will help to improve our understanding of C dynamics of forest ecosystems in response to natural disturbances. Our results also emphasize the vulnerability of deciduous and mixed forests to insect infestations and signify the need to develop proactive and adaptive forest management practices that can enhance forest resilience to climate change. They will help to quantify regional-scale C balance and develop sustainable forest management practices to contribute to net zero C emission goals through nature-based solutions to mitigate climate change.

4.7 Acknowledgement

This study was funded by the Natural Sciences and Engineering Research Council (NSERC) grants, including Discovery and Alliance Mission grants, Global Water Futures Program (GWF)—Southern Forests Water Future and GWF Observatory grants awarded to M.A Arain as well as US National Science Foundation (NSF)—Social Science and Humanities Research Council (SSHRC) of Canada funded Global Centre for Climate Change Impacts on Transboundary Waters Grant (P.I. Gail Krantzberg, CoPI. M.A Arain). In kind support from the Ontario Ministry of Natural Resources and Forestry (OMNRF), Ontario Ministry of Environment, Conservation and Parks, Long Point Region Conservation Authority (LPRCA) and the St. Williams Conservation Reserve Community Council (SWCRCC) is gratefully acknowledged. We thank our Lab group members (specially Lejla Latifovic) for their contributions to flux data measurements.

4.8 References

- Ahmed, I. U. (2018). Forest soil C: Stock and stability under global change. In *New Perspectives in Forest Science*, (pp. 37–67). https://doi.org/10.5772/intechopen.74690
- Alton, P. B. (2016). The sensitivity of models of gross primary productivity to meteorological and leaf area forcing: A comparison between a Penman-Monteith ecophysiological approach and the MODIS light-use efficiency algorithm. *Agricultural and Forest Meteorology*, 218, 11–24.
- Ameray, A., Bergeron, Y., Valeria, O., Montoro Girona, M., & Cavard, X. (2021). Forest carbon management: A review of silvicultural practices and management strategies across boreal, temperate and tropical forests. *Current Forestry Reports*, 7, 245–266.
- Arain, M. A. (2018). AmeriFlux BASE CA-TPD Ontario—Turkey Point Mature Deciduous, Ver. 2–5, AmeriFlux AMP. https://doi.org/10.17190/AMF/1246152
- Arain, M. A., Xu, B., Brodeur, J. J., Khomik, M., Peichl, M., Beamesderfer, E., Restrepo-Coupe, N., & Throne, R. (2022). Heat and drought impact on carbon exchange in an age-sequence of temperate pine forests. *Ecological Processes*, 11, 7.
- Baldwin, D. J., Desloges, J. R., & Band, L. E. (2000). Physical geography of Ontario. In Ecology of a managed terrestrial landscape: Patterns and processes of forest landscapes in Ontario (pp. 12–29). UBC Press.
- Beamesderfer, E. R., Arain, M. A., Khomik, M., & Brodeur, J. J. (2020). The impact of seasonal and annual climate variations on the carbon uptake capacity of a deciduous forest within the Great Lakes Region of Canada. *Journal of Geophysical Research: Biogeosciences*, 125(9), e2019JG005389.
- Birdsey, R. A., Dugan, A. J., Healey, S. P., Dante-Wood, K., Zhang, F., Mo, G., & McCarter, J. (2019). Assessment of the influence of disturbance, management activities, and environmental factors on carbon stocks of US national forests. *General Technical Report*, RMRS-GTR-402.
- Boussetta, S., Balsamo, G., Beljaars, A., Kral, T., & Jarlan, L. (2013). Impact of a satellite-derived leaf area index monthly climatology in a global numerical weather prediction model. *International Journal of Remote Sensing*, 34(9–10), 3520–3542.

- Brodeur, J. (2014). Data-driven approaches for sustainable operation and defensible results in a long-term, multi-site ecosystem flux measurement program (Doctoral dissertation). McMaster University, Hamilton.
- Brown, L. A., Meier, C., Morris, H., Pastor-Guzman, J., Bai, G., Lerebourg, C., Gobron, N., Lanconelli, C., Clerici, M., & Dash, J. (2020). Evaluation of global leaf area index and fraction of absorbed photosynthetically active radiation products over North America using Copernicus Ground Based Observations for Validation data. *Remote Sensing of Environment*, 247, 111935.
- Carter, G. A., & Knapp, A. K. (2001). Leaf optical properties in higher plants: Linking spectral characteristics to stress and chlorophyll concentration. *American Journal of Botany*, 88(4), 677–684.
- CFIA. (2021). Lymantria dispar dispar (LDD moth)—Fact sheet. Canadian Food Inspection Agency. https://inspection.canada.ca/plant-health/invasive-species/insects/ldd-moth-and-agm/fact-sheet/eng/1330355335187/1335975909100 (Accessed 19 January 2023).
- Chen, B., Arain, M. A., Chen, J. M., Wang, S., Fang, H., Liu, Z., Mo, G., & Liu, J. (2020). Importance of shaded leaf contribution to the total GPP of Canadian terrestrial ecosystems: Evaluation of MODIS GPP. *Journal of Geophysical Research: Biogeosciences*, 125(10), 5917.
- Chen, X., Cai, A., Guo, R., Liang, C., & Li, Y. (2023). Variation of gross primary productivity dominated by leaf area index in significantly greening area. *Journal of Geographical Sciences*, 33(8), 1747–1764.
- Chi, J., Zhao, P., Klosterhalfen, A., Jocher, G., Kljun, N., Nilsson, M. B., & Peichl, M. (2021). Forest floor fluxes drive differences in the carbon balance of contrasting boreal forest stands. *Agricultural and Forest Meteorology*, 306, 108454.
- Chung, E., Hopton, A., & Singh, I. (2021). Why an invasive moth caterpillar infestation is breaking records in central Canada. CBC News. https://www.cbc.ca/news/science/invasive-moths-ldd-canada-infestation-1.6078864 (Accessed 26 June 2021).
- Ciesla, W. M., Dull, C. W., & Acciavatti, R. E. (1989). Interpretation of SPOT-1 color composites for mapping defoliation of hardwood forests by gypsy moth. *Photogrammetric Engineering & Remote Sensing*, 55, 1465–2147.

- Clark, K. L., Aoki, C., Ayres, M., Kabrick, J., & Gallagher, M. R. (2022). Insect infestations and the persistence and functioning of oak-pine mixed wood forests in the mid-Atlantic region, USA. *PLOS ONE*, 17(5), e0265955.
- Coleman, T. W., & Liebhold, A. M. (2023). Slow the spread: A 20-year reflection on the national *Lymantria dispar* integrated pest management program. *General Technical Report*, NRS-256.
- De Beurs, K. M., & Townsend, P. A. (2008). Estimating the effect of gypsy moth defoliation using MODIS. *Remote Sensing of Environment*, 112(10), 3983–3990.
- De Lucia, E. H., Drake, J. E., Thomas, R. B., & Gonzalez-Meler, M. (2007). Forest carbon use efficiency: Is respiration a constant fraction of gross primary production? *Global Change Biology*, 13(6), 1157–1167.
- Drusch, M., Del Bello, U., Carlier, S., Colin, O., Fernandez, V., Gascon, F., Hoersch, B., Isola,
 C., Laberinti, P., & Martimort, P. (2012). Sentinel-2: ESA's optical high-resolution
 mission for GMES operational services. *Remote Sensing of Environment*, 120, 25–36.
- Dymond, C. C., Neilson, E. T., Stinson, G., Porter, K., MacLean, D. A., Gray, D. R., Campagna, W. A., & Kurz, W. A. (2010). Future spruce budworm outbreak may create a carbon source in eastern Canadian forests. *Ecosystems*, 13, 917–931.
- Eklundh, L., Johansson, T., & Solberg, S. (2009). Mapping insect defoliation in Scots pine with MODIS time-series data. *Remote Sensing of Environment*, 113(7), 1566–1573.
- Embrey, S., Remais, J. V., & Hess, J. (2012). Climate change and ecosystem disruption: The health impacts of the North American Rocky Mountain pine beetle infestation. *American Journal of Public Health*, 102(5), 818–827.
- Environment and Climate Change Canada. (2023). National Inventory Report 1990–2021: Greenhouse gas sources and sinks in Canada: Canada's submission to the United Nations Framework Convention on Climate Change, part 3. https://publications.gc.ca/collections/collection_2023/eccc/En81-4-2021-1-eng.pdf (Accessed 28 January 2024).
- FAO (Food and Agriculture Organization of the United Nations). (2010). Global forest resources assessment 2010: Main report. FAO Forestry Paper 163, FAO, Rome.

- Fei, S., Morin, R. S., Oswalt, C. M., & Liebhold, A. M. (2019). Biomass losses resulting from insect and disease invasions in US forests. *Proceedings of the National Academy of Sciences*, 116(35), 17371–17376.
- Feret, J. B., François, C., Asner, G. P., Gitelson, A. A., Martin, R. E., Bidel, L. P., Utsin, S. L., Le Maire, G., & Jacquemoud, S. (2008). PROSPECT-4 and 5: Advances in the leaf optical properties model separating photosynthetic pigments. *Remote Sensing of Environment*, 112(6), 3030–3043.
- Foster, A. C., Wang, J. A., Frost, G. V., Davidson, S. J., Hoy, E., Turner, K. W., ... & others. (2022). Disturbances in North American boreal forest and Arctic tundra: Impacts, interactions, and responses. *Environmental Research Letters*, 17(11), 113001.
- Fraser, R. H., & Latifovic, R. (2005). Mapping insect-induced tree defoliation and mortality using coarse spatial resolution satellite imagery. *International Journal of Remote Sensing*, 26(1), 193–200.
- Gonsamo, A., Chen, J. M., Price, D. T., Kurz, W. A., Liu, J., Boisvenue, C., Hember, R. A., Wu, C., & Chang, K. H. (2013). Improved assessment of gross and net primary productivity of Canada's landmass. *Journal of Geophysical Research: Biogeosciences*, 118(4), 1546–1560.
- Goodale, C. L., Apps, M. J., Birdsey, R. A., Field, C. B., Heath, L. S., Houghton, R. A., ... & others. (2002). Forest carbon sinks in the northern hemisphere. *Ecological Applications*, 12(3), 891–899.
- Gooderham, M., Haq, M., Beecker, J., & O'Toole, A. (2021). *Lymantria dispar* (Gypsy in present Spongy moth) moth dermatitis. *Journal of Cutaneous Medicine and Surgery*, 25(5), 555–556.
- Government of Canada. (2021). Gypsy moth. Retrieved January 19, 2023, from https://www.canada.ca/en/health-canada/services/pest-control-tips/gypsy-moths.html
- Government of Ontario. (2024). Spongy moth: information about the spongy moth, a forest-defoliating insect found in Ontario. Retrieved January 9, 2024, from https://www.ontario.ca/page/spongy-moth
- Gray, D. R. (2004). The gypsy moth life stage model: landscape-wide estimates of gypsy moth establishment using a multi-generational phenology model. *Ecological Modelling*, 176(1–2), 155–171.

- Gray, D. R., & MacKinnon, W. E. (2006). Outbreak patterns of the spruce budworm and their impacts in Canada. *The Forestry Chronicle*, 82(4), 550–561.
- Hajek, A. E., Diss-Torrance, A. L., Siegert, N. W., & Liebhold, A. M. (2021). Inoculative releases and natural spread of the fungal pathogen Entomophaga maimaiga (Entomophthorales: Entomophthoraceae) into US populations of gypsy moth, Lymantria dispar (Lepidoptera: Erebidae). *Environmental Entomology*, 50(5), 1007–1015.
- Harris, N. L., Hagen, S. C., Saatchi, S. S., Pearson, T. R. H., Woodall, C. W., Domke, G. M., ... & others. (2016). Attribution of net carbon change by disturbance type across forest lands of the conterminous United States. *Carbon Balance and Management*, 11(1), 1–21.
- Harvey, J. A., Tougeron, K., Gols, R., Heinen, R., Abarca, M., Abram, P. K., ... & others. (2022). Scientists' warning on climate change and insects. *Ecological Monographs*, 93(1), e1553.
- Hengeveld, H., Braithwaite, L., Desjardins, R., Gorjup, J., & Hall, P. (2008). Enhancement of greenhouse gas sinks: a Canadian science assessment, atmospheric science assessment and integration. Environment Canada, Toronto, Ontario.
- Huete, A., Didan, K., Miura, T., Rodriguez, E. P., Gao, X., & Ferreira, L. G. (2002). Overview of the radiometric and biophysical performance of the MODIS vegetation indices. *Remote Sensing of Environment*, 83(1–2), 195–213.
- Hussain, N., Arain, M. A., Wang, S., Parker, W. C., & Elliott, K. A. (2024). Evaluating the effectiveness of different variable retention harvesting treatments on forest carbon uptake using remote sensing. *Remote Sensing Applications: Society and Environment*, 33, 101124.
- IPCC. (2021). Climate Change 2021: The physical science basis. In Contribution of working group I to the sixth assessment report of the intergovernmental panel on climate change. Cambridge and New York, NY: Cambridge University Press. Retrieved from https://www.ipcc.ch/report/ar6/wg1/
- Jacquemoud, S., & Baret, F. (1990). PROSPECT: A model of leaf optical properties spectra. *Remote Sensing of Environment*, 34(2), 75–91.

- Jarlan, L., Balsamo, G., Lafont, S., Beljaars, A., Calvet, J. C., & Mougin, É. (2008). Analysis of leaf area index in the ECMWF land surface model and impact on latent heat and carbon fluxes: Application to West Africa. *Journal of Geophysical Research: Atmospheres*, 113, D24117. https://doi.org/10.1029/2007JD009370
- Joria, P. E., Ahearn, S. C., & Connor, M. (1991). A comparison of the SPOT and Landsat Thematic Mapper satellite systems for detecting gypsy-moth defoliation in Michigan. *Photogrammetric Engineering and Remote Sensing*, 57(12), 1605–1612.
- Kalamandeen, M., Gulamhussein, I., Castro, J. B., Sothe, C., & Gonsamo, A. (2023). Climate change and human footprint increase insect defoliation across central boreal forests of Canada. Frontiers in Ecology and Evolution, 11, 1293311. https://doi.org/10.3389/fevo.2023.1293311
- Kovalev, A., Soukhovolsky, V., Tarasova, O., Akhanaev, Y., & Martemyanov, V. (2023). Remote sensing indicators of spongy moth (*Lymantria dispar L*.) damage to birch stands in Western Siberia. *Forests*, 14(12), 2308.
- Kretchun, A. M., Scheller, R. M., Lucash, M. S., Clark, K. L., Hom, J., & Van Tuyl, S. (2014). Predicted effects of gypsy moth defoliation and climate change on forest carbon dynamics in the New Jersey Pine Barrens. *PLOS ONE*, 9(8), e102531.
- Kurz, W. A., Apps, M., Banfield, E., & Stinson, G. (2002). Forest carbon accounting at the operational scale. *The Forestry Chronicle*, 78(5), 672–679.
- Latifovic, L., & Arain, M. A. (2024). The impact of spongy moth (*Lymantria dispar*) defoliation on carbon balance of a temperate deciduous forest in North America. *Agricultural and Forest Meteorology*. [Accepted manuscript]
- Litton, C. M., Raich, J. W., & Ryan, M. G. (2007). Carbon allocation in forest ecosystems. *Global Change Biology*, 13(10), 2089–2109.
- Löw, M., & Koukal, T. (2020). Phenology modelling and forest disturbance mapping with Sentinel-2 time series in Austria. *Remote Sensing*, 12(24), 4191.
- Medvigy, D., Clark, K. L., Skowronski, N. S., & Schäfer, K. V. R. (2012). Simulated impacts of insect defoliation on forest carbon dynamics. *Environmental Research Letters*, 7(4), 045703.
- MNDMNRF. (2022). Forest Health Conditions in Ontario 2021, Ministry of Northern Development, Mines, Natural Resources and Forestry (MNDMNRF), Ontario, Canada.

- https://www.ontario.ca/files/2022-07/mnrf-srb-forest-health-conditions-ontario-2021-en-2022-07-20.pdf
- MNRF. (2021). Gypsy moth. Online access from the Ministry of Natural Resources and Forestry (MNRF). https://www.ontario.ca/page/gypsy-moth. Accessed 19 Jan 2023.
- Monteith, J. L. (1972). Solar radiation and productivity in tropical ecosystems. *Journal of Applied Ecology*, 9(3), 747–766.
- Nasiri, V., Deljouei, A., Moradi, F., Sadeghi, S. M. M., & Borz, S. A. (2022). Land use and land cover mapping using Sentinel-2, Landsat-8 Satellite Images, and Google Earth Engine: A comparison of two composition methods. *Remote Sensing*, 14(9), 1977.
- OMNRF. (2024). Ontario Ministry of Natural Resources and Forestry (OMNRF). https://www.ontario.ca/page/forest-regions. Accesses 5 Jan 2024.
- ONDMNRF. (2021). Ministry of Northern Development, Mines, Natural Resources and Forestry. https://www.ontario.ca/files/2022-07/mnrf-srb-forest-health-conditions-ontario-2021-en-2022-07-20.pdf. Accessed 25 Jan 2024.
- Ontario GeoHub. (2022). Land Information Ontario Data Description: Forest Insect Damage Event. https://geohub.lio.gov.on.ca/documents/lio::forest-insect-damage-event/about
- Payne, N. J., Cameron, D. A., Leblanc, J. D., & Morrison, I. K. (2019). Carbon storage and net primary productivity in Canadian boreal mixed wood stands. *Journal of Forest Research*, 30(5), 1667–1678.
- Peters, W., Jacobson, A. R., Sweeney, C., Andrews, A. E., Conway, T. J., Masarie, K., ... Tans,
 P. P. (2007). An atmospheric perspective on North American carbon dioxide exchange:
 Carbon Tracker. *Proceedings of the National Academy of Sciences*, 104(48), 18925–18930.
- Picq, S., Wu, Y., Martemyanov, V. V., Pouliot, E., Pfister, S. E., Hamelin, R., & Cusson, M. (2023). Range-wide population genomics of the spongy moth, *Lymantria dispar* (Erebidae): Implications for bio-surveillance, subspecies classification and phylogeography of a destructive moth. *Evolutionary Applications*, 16(3), 638–656.
- Pureswaran, D. S., Roques, A., & Battisti, A. (2018). Forest insects and climate change. *Current Forestry Reports*, 4, 35–50.

- Qu, Y., & Zhuang, Q. (2018). Modeling leaf area index in North America using a process-based terrestrial ecosystem model. *Ecosphere*, 9(1), e02046.
- Quirion, B. R., Domke, G. M., Walters, B. F., Lovett, G. M., Fargione, J. E., Greenwood, L., ... Campbell, J. L. (2021). Insect and disease disturbances correlate with reduced carbon sequestration in forests of the contiguous United States. *Frontiers in Forests and Global Change*, 4, 716582.
- Rouse, J. W., Haas, R. H., Schell, J. A., & Deering, D. W. (1974). Monitoring vegetation systems in the Great Plains with ERTS. *NASA Special Publication*, 351(1), 309.
- Schmid, A. V., Vogel, C. S., Liebman, E., Curtis, P. S., & Gough, C. M. (2016). Coarse woody debris and the carbon balance of a moderately disturbed forest. *Forest Ecology and Management*, 361, 38–45.
- Senf, C., Seidl, R., & Hostert, P. (2017). Remote sensing of forest insect disturbances: Current state and future directions. *International Journal of Applied Earth Observation and Geoinformation*, 60, 49–60.
- Shah, L., Arnillas, C. A., & Arhonditsis, G. B. (2022). Characterizing temporal trends of meteorological extremes in Southern and Central Ontario. *Canada Weather and Climate Extremes*, 35, 100411.
- Sheykhmousa, M., Mahdianpari, M., Ghanbari, H., Mohammadimanesh, F., Ghamisi, P., & Homayouni, S. (2020). Support vector machine versus random forest for remote sensing image classification: A meta-analysis and systematic review. *IEEE Journal of Selected Topics in Applied Earth Observations and Remote Sensing*, 13, 6308–6325.
- Sun, Z., Wang, X., Zhang, X., Tani, H., Guo, E., Yin, S., & Zhang, T. (2019). Evaluating and comparing remote sensing terrestrial GPP models for their response to climate variability and CO₂ trends. *Science of the Total Environment*, 668, 696–713.
- Sun, B., Wang, C., Yang, C., Xu, B., Zhou, G., Li, X., ... Xu, G. (2021). Retrieval of rapeseed leaf area index using the PROSAIL model with canopy coverage derived from UAV images as a correction parameter. *International Journal of Applied Earth Observation and Geoinformation*, 102, 102373.
- Tang, G., Beckage, B., Smith, B., & Miller, P. A. (2010). Estimating potential forest NPP, biomass and their climatic sensitivity in New England using a dynamic ecosystem model. *Ecosphere*, 1(6), 18.

- Townsend, P. A., Eshleman, K. N., & Welcker, C. (2004). Remote estimation of gypsy moth defoliation to assess variations in stream nitrogen concentrations. *Ecological Applications*, 14, 504–516.
- TRCA (2022). The rise and fall of the spongy moth, Toronto Region Conservation Authority (TRCA). https://trca.ca/conservation/environmental-monitoring/terrestrial-habitat-species/spongy-moth-update-2023/. Accessed 19 Jan 2024.
- Turner, D. P., Ritts, W. D., Cohen, W. B., Gower, S. T., Zhao, M., & Running, S. W. et al. (2003). Scaling gross primary production (GPP) over boreal and deciduous forest landscapes in support of MODIS GPP product validation. *Remote Sensing of Environment*, 88(3), 256–270.
- USDA (2023). Major Forest Insect and Disease Conditions in the United States: 2022. U.S. Department of Agriculture, Forest Service FS–1219 (November 2023). Retrieved from https://www.fs.usda.gov/sites/default/files/fs_media/fs_document/Major-Forest-Conditions-2022.pdf
- Verhoef, W. (1984). Light scattering by leaf layers with application to canopy reflectance modeling: The SAIL model. *Remote Sensing of Environment*, 16(2), 125–141.
- Wang, L., Yang, R., Tian, Q., Yang, Y., Zhou, Y., Sun, Y., & Mi, X. (2015). Comparative analysis of GF-1 WFV, ZY-3 MUX, and HJ-1 CCD sensor data for grassland monitoring applications. *Remote Sensing*, 7(2), 2089–2108.
- Wang, Y. M., Sparks, M. E., Harrison, R. L., & Shi, J. (2022). Analyses of adult transcriptomes from four different populations of the spongy moth, Lymantria dispar L., from China and the USA. *Scientific Reports*, 12(1), 18232.
- Wazneh, H., Arain, M. A., & Coulibaly, P. (2017). Historical spatial and temporal climate trends in southern Ontario, Canada. *Journal of Applied Meteorology and Climatology*, 56(10), 2767–2787.
- White, J. C., Wulder, M. A., Hermosilla, T., Coops, N. C., & Hobart, G. W. (2017). A nationwide annual characterization of 25 years of forest disturbance and recovery for Canada using Landsat time series. *Remote Sensing of Environment*, 194, 303–321.

- Williams, D. L., Nelson, R. F., & Dottavio, C. L. (1985). A georeferenced LANDSAT digital database for forest insect-damage assessment. *International Journal of Remote Sensing*, 6, 643–656.
- Xiao, X., Zhang, Q., Braswell, B., Urbanski, S., Boles, S., & Wofsy, S. (2004). Modeling gross primary production of temperate deciduous broadleaf forest using satellite images and climate data. *Remote Sensing of Environment*, 91(2), 256–270.
- Xu, X. Q., Lu, J. S., Zhang, N., Yang, T. C., He, J. Y., Yao, X., ... Zhou, L. M. (2019). Inversion of rice canopy chlorophyll content and leaf area index based on coupling of radiative transfer and Bayesian network models. *ISPRS Journal of Photogrammetry and Remote Sensing*, 150, 185–196.
- Yang, Y., Luo, J., Huang, Q., Wu, W., & Sun, Y. (2019). Weighted double-logistic function fitting method for reconstructing the high-quality Sentinel-2 NDVI time series data set. *Remote Sensing*, 11(20), 2342.
- Zhang, Y., Xiao, X., Jin, C., Dong, J., Zhou, S., Wagle, P., ... Chen, J. M. (2016). Consistency between sun-induced chlorophyll fluorescence and gross primary production of vegetation in North America. *Remote Sensing of Environment*, 183, 154–169.
- Zhang, Y., Xiao, X., Wu, X., Zhou, S., Zhang, G., Qin, Y., & Dong, J. (2017). A global moderate resolution dataset of gross primary production of vegetation for 2000–2016. *Scientific Data*, 4(1), 170165.
- Zhang, Z., Xin, Q., & Li, W. (2021). Machine learning-based modeling of vegetation leaf area index and gross primary productivity across North America and comparison with a process-based model. *Journal of Advances in Modeling Earth Systems*, 13(10), e2021MS002802.
- Zhao, B., Zhuang, Q., Shurpali, N., Köster, K., Berninger, F., & Pumpanen, J. (2021). North American boreal forests are a large carbon source due to wildfires from 1986 to 2016. Scientific Reports, 11(1), 7723.
- Zhao, H., Jia, G., Xu, X., & Zhang, A. (2022). Contrasting responses of vegetation production to rainfall anomalies across the Northeast China Transect. *Journal of Geophysical Research: Biogeosciences*, 127(6), 6842.

Zolles, A., Schueler, S., Gartner, K., & Scheifinger, G. (2021). Continuous parameterization of leaf area index and phenological phases within deciduous forests based on temperature measurements. *Frontiers in Forests and Global Change*, 4, 768085.

Table 4.1. Confusion matrices-based accuracy assessment of land use and land cover (LULC) classification.

Class	Water	Unban	Agriculture	Deciduous	Coniferous	Mixed forest	Producer accuracy	User accuracy
Water	627	1	0	0	0	2	98.4%	99.4%
Unban	1	617	0	6	2	2	96.7%	98.0%
Agriculture	3	1	622	8	6	10	97.2%	96.2%
Deciduous	3	9	12	606	22	12	96.4%	94.2%
Coniferous	4	12	7	16	610	11	95.5%	94.7%
Mixed forest	12	10	9	14	10	613	94.7%	94.1%

Overall accuracy: 95.7%

Table 4.2. Input parameters set for the PROSAIL model. The fixed value is used in this study.

Model	Input Parameters	Symbol	Unit	Range	Fixed value
	Leaf structure	N	dimensionless	1.5 – 3.0	1.5
	Chlorophyll content	Cab	μg.cm-2	10 - 80	40
PROSPECT	Carotenoid content	Car	μg.cm-2		10
PROSPECT	Brown pigment	Cbrown	arbitrary units		0
	Equivalent water thickness	Cw	cm		0.01
	Dry matter content	Cm	g.cm-2		0.009
	Loof inclination distribution	LIDF	shape	spherical	spherical
	Leaf inclination distribution	LIDFa	slope	-1 to 1	-0.35
	function	LIDFb	Kind of distortion	-1 to 1	-0.15
SAIL	Leaf Area Index	LAI	m2/m2	0 - 8	
SAIL	Hot spot parameter	hspot	m/m	0.03 - 0.1	0.01
	Solar zenith angle	tts	(°)	20 -70	30
	View zenith angle	tto	(°)	0 - 30	10
	Relative azimuth angle	psi	(°)		0

Table 4.3. Equations have been used for ecosystem properties.

Variables	Equation	References
GPP	$GPP = APARchl \times \epsilon g$	Monteith, 1972
	$APARchl = PAR \times fPARchl$	Xiao et al., 2004
	$fPARchl = (EVI - 0.1) \times 1.25$	Zhang et al., 2017
LUE	$\varepsilon g = \varepsilon 0 \times Tscalar \times Wscalar$	Zhang et al., 2017
	$T_{\text{scalar}} = \frac{(T - T_{\text{max}}) \times (T - T_{\text{min}})}{(T - T_{\text{max}}) \times (T - T_{\text{min}}) - (T - T_{\text{opt}})^2}$	Zhang et al., 2016
	$W_{scalar} = \frac{1 + LSWI}{1 + LSWI_{max}}$	Zhang et al., 2016
Indices	NDVI = (RNIR - RRed)/(RNIR + RRed)	Rouse et al., 1974
	$EVI = 2.5 \times \frac{R_{NIR} - R_{Red}}{R_{NIR} + 6 \times R_{Red} - 7.5 \times R_{Blue} + 1}$	Huete et al., 2002
	LSWI = (RNIR - RSWIR) / (RNIR + RSWIR)	Xiao et al., 2004

Table 4.4. Mean daily gross primary productivity (GPP) of different vegetation types in the growing season (g C m⁻²)

Vegetation Type	2020		2021		2022	
	Daily mean	Seasonal Total	Daily mean	Seasonal Total	Daily mean	Seasonal Total
Agriculture land	9.65±5.4	1235	8.45±6.1	1266	9.55±6.2	1242
Conifer forest	6.87±3.5	1443	7.10±2.7	1475	6.86±2.7	1438
Deciduous forest	6.83±4.1	1338	4.43 ±2.5	868	7.77±5.4	1367
Mixed forest	6.45±4.2	1208	4.81±2.2	932	6.12±2.3	1175
Mean	7.45	1306	6.20	1135	7.58	1305

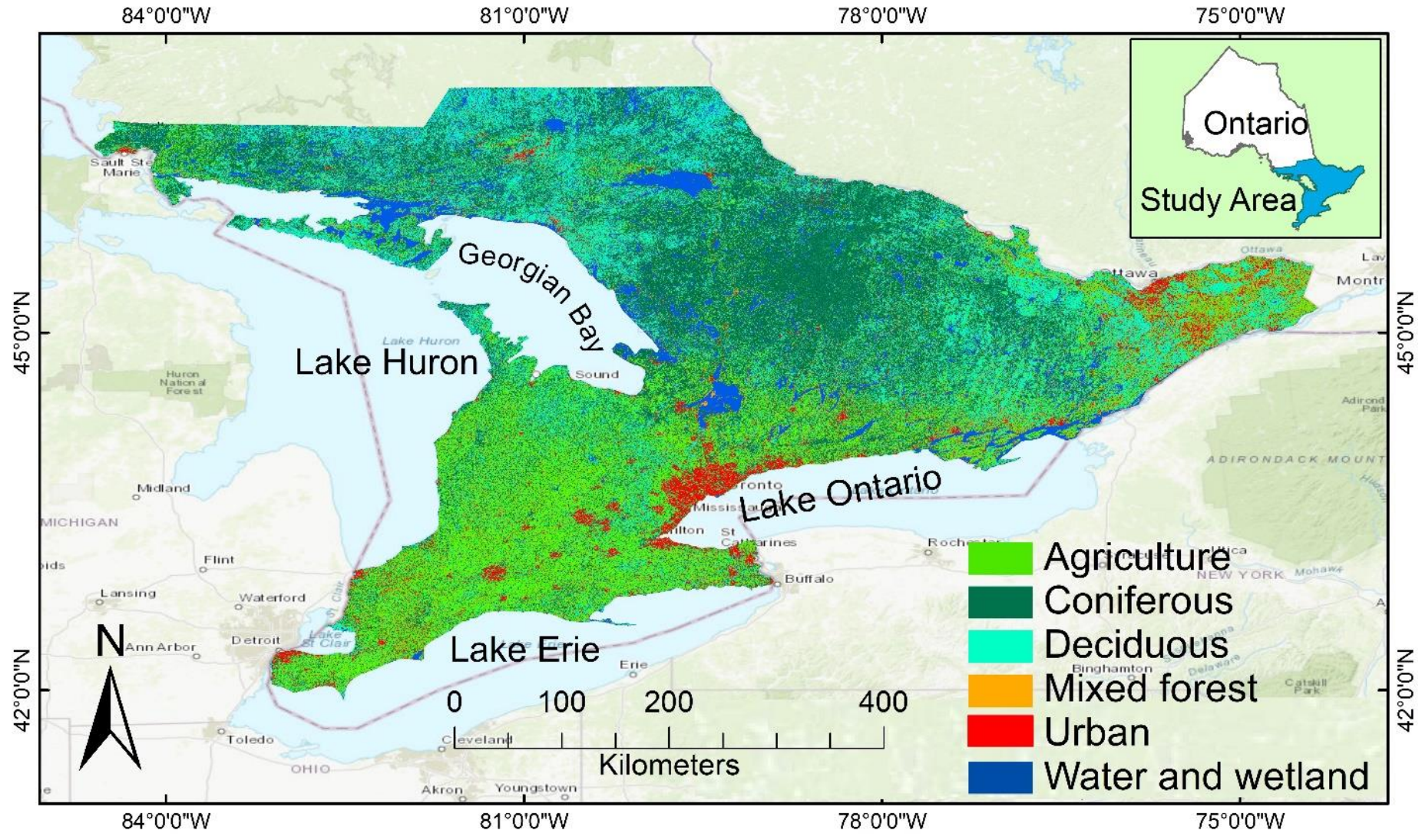


Figure 4.1. Study area map. The LULC map was generated by machine learning-based Google Earth Engine (GEE) using Sentinel-2 remote sensing data from the composite images of the growing season of 2020.



Figure 4.2. Defoliated tree due to spongy moth infestation at the Turkey Point Environmental Observatory's deciduous forest site on 21 June 2021

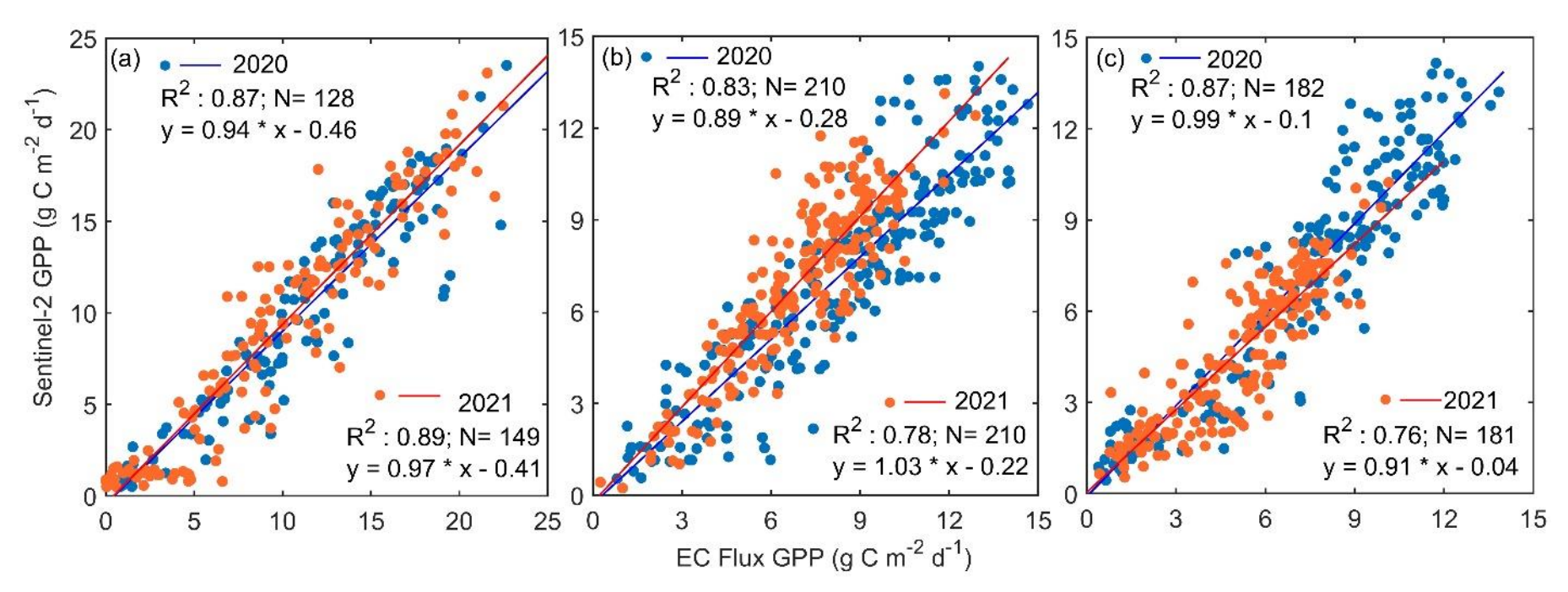


Figure 4.3. The relationship between Satellite-derived and Eddy Covariance (EC) flux tower-based observed daily gross primary productivity (GPP) values for (a) agriculture areas, (b) conifer forests and (c) deciduous forests, respectively from 2020 to 2021.

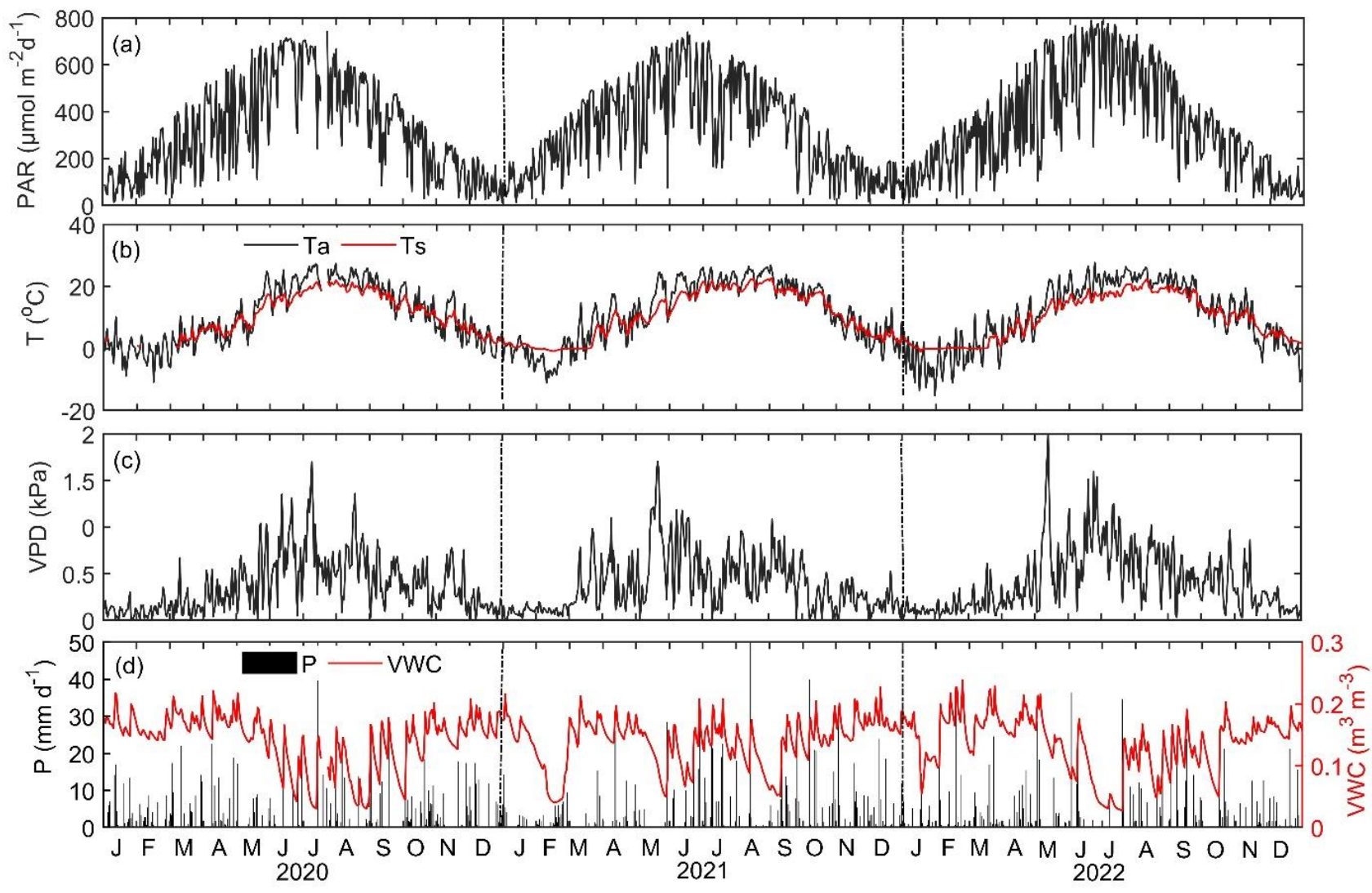


Figure 4.4. Daily mean values of (a) photosynthetically active radiation (PAR), (b) air temperature (Ta) and soil temperature (Ts) at 5cm depth, (c) vapor pressure deficit (VPD), (d) precipitation (P) and volumetric water content (VWC) from 2020 to 2022.

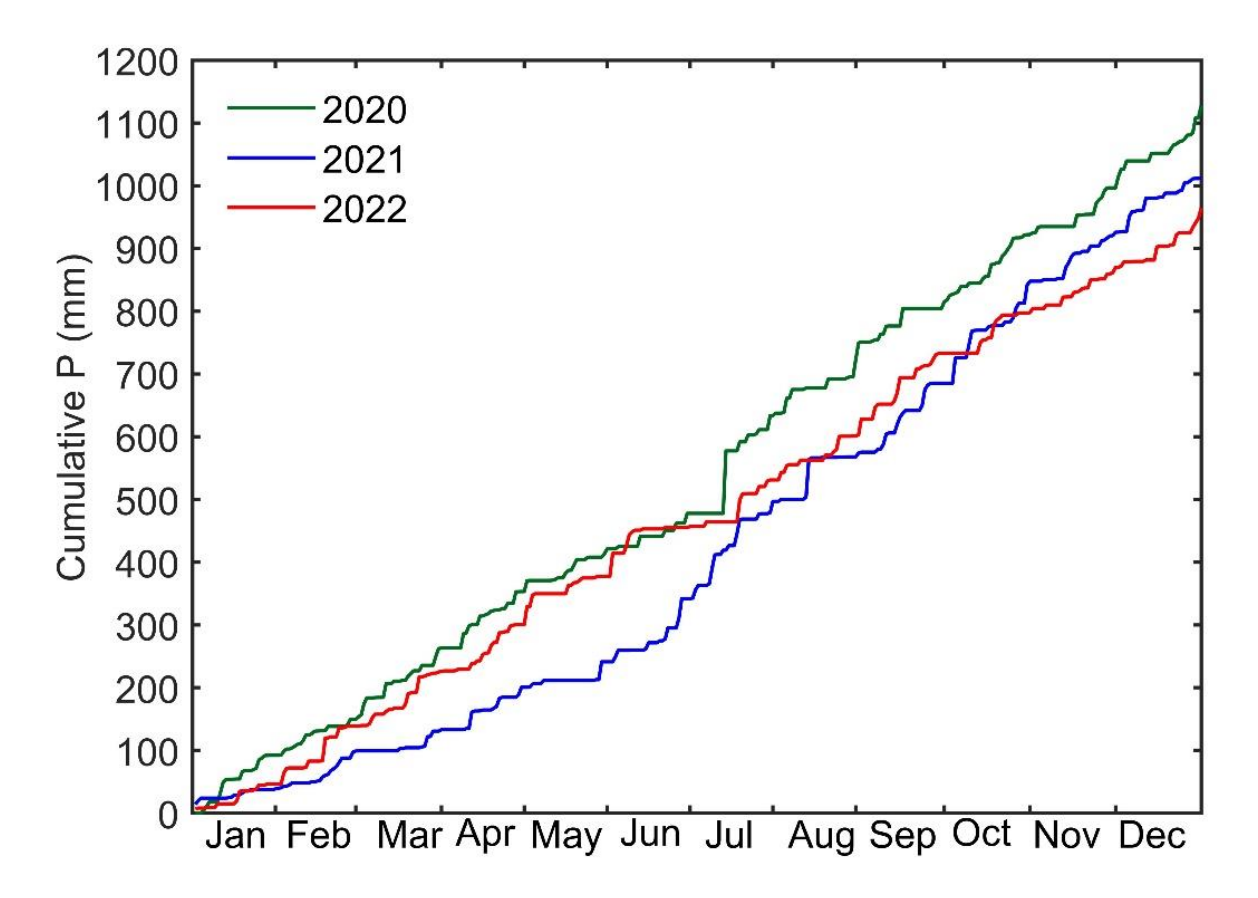


Figure 4.5. Daily cumulative precipitation (P) from 2020 to 2022.

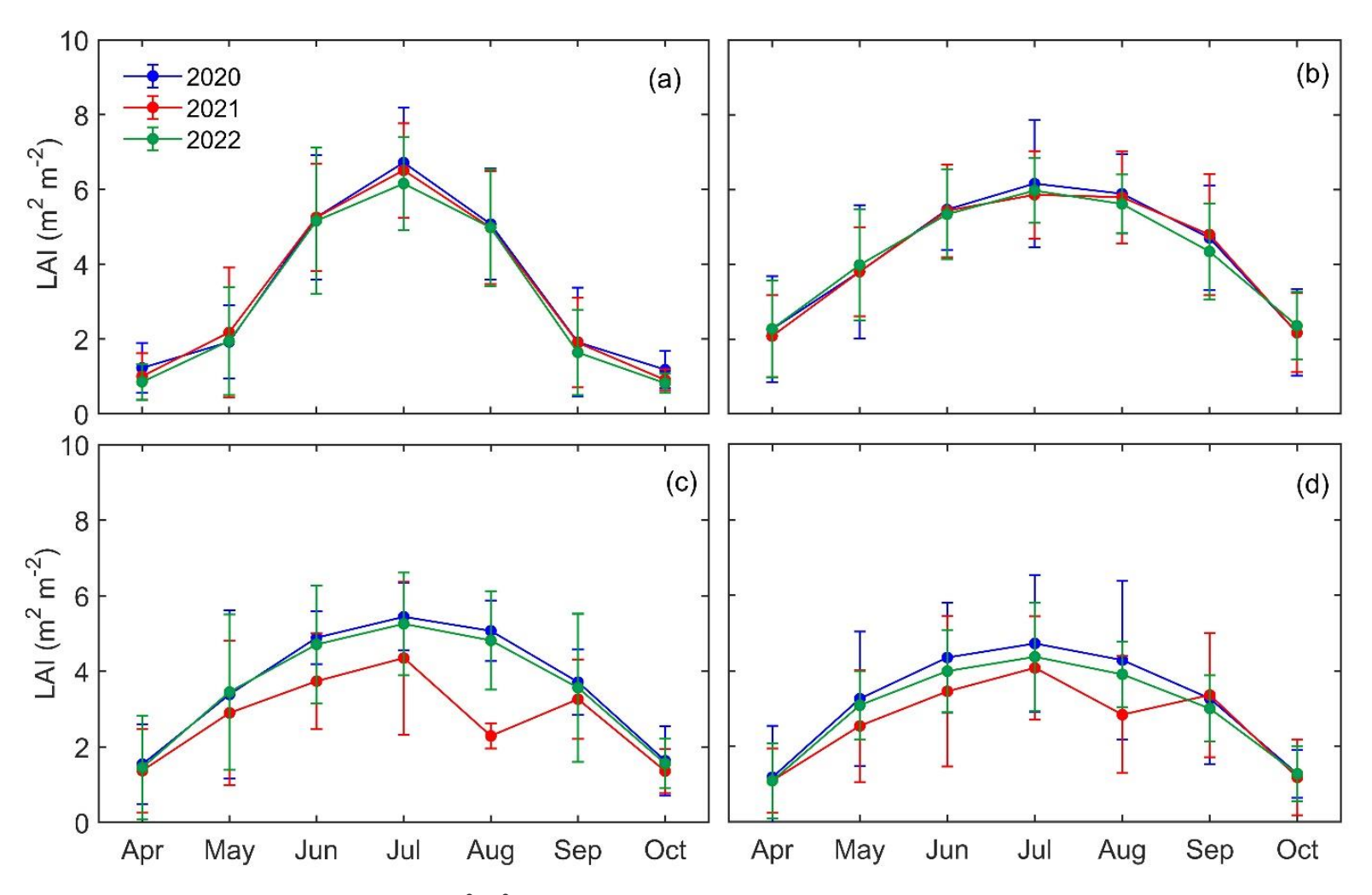


Figure 4.6. Monthly mean leaf area index, LAI (m²m⁻²) values over the study area for (a) agricultural lands, (b) conifer, (c) deciduous and (d) mixed forests, respectively from 2020 to 2022.

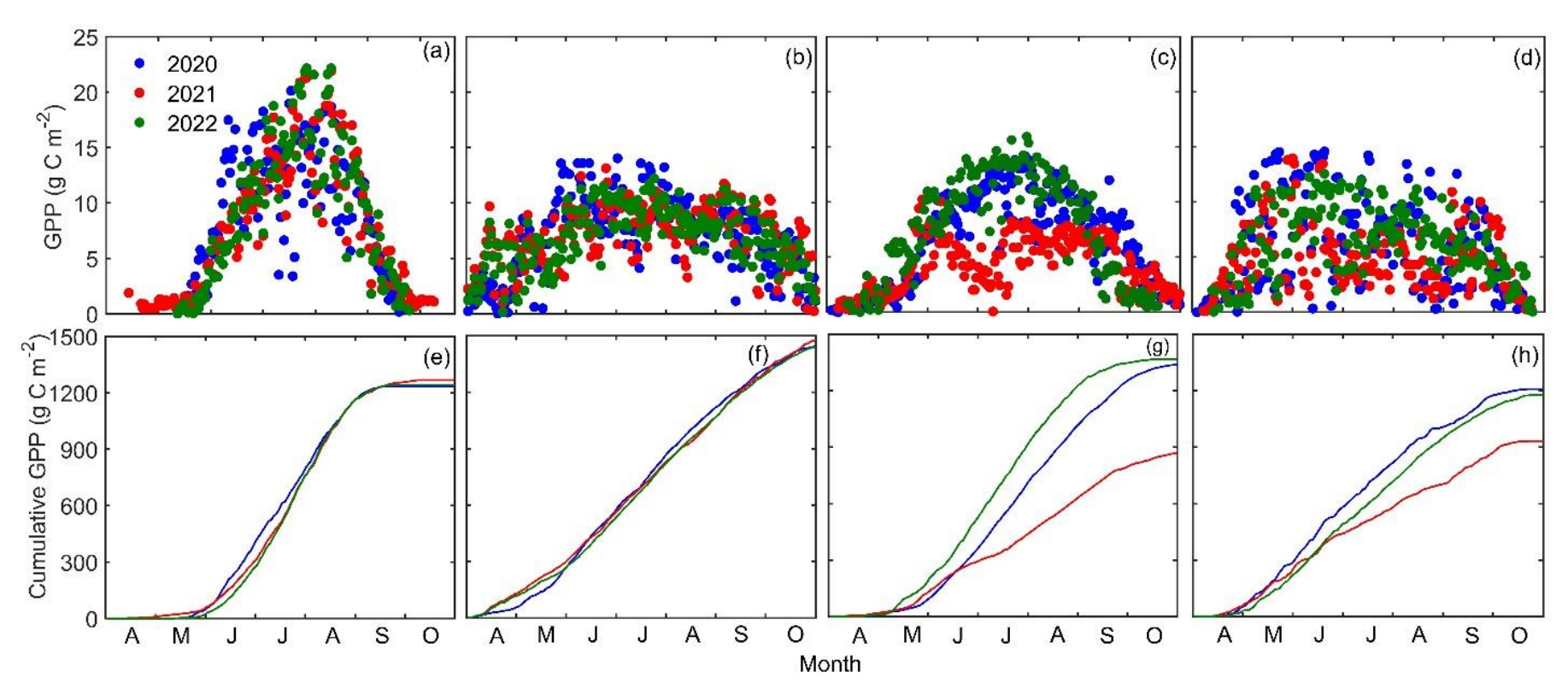


Figure 4.7. Daily gross ecosystem productivity, GPP values (g C m⁻² d⁻¹) for (a) agricultural lands, (b) conifer, (c) deciduous and (d) mixed forests, respectively, from 2020 to 2022. Similarly, cumulative GPP values over the growing season for (e) agricultural lands, (f) conifer, (g) deciduous and (h) mixed forests, respectively from 2020 to 2022.

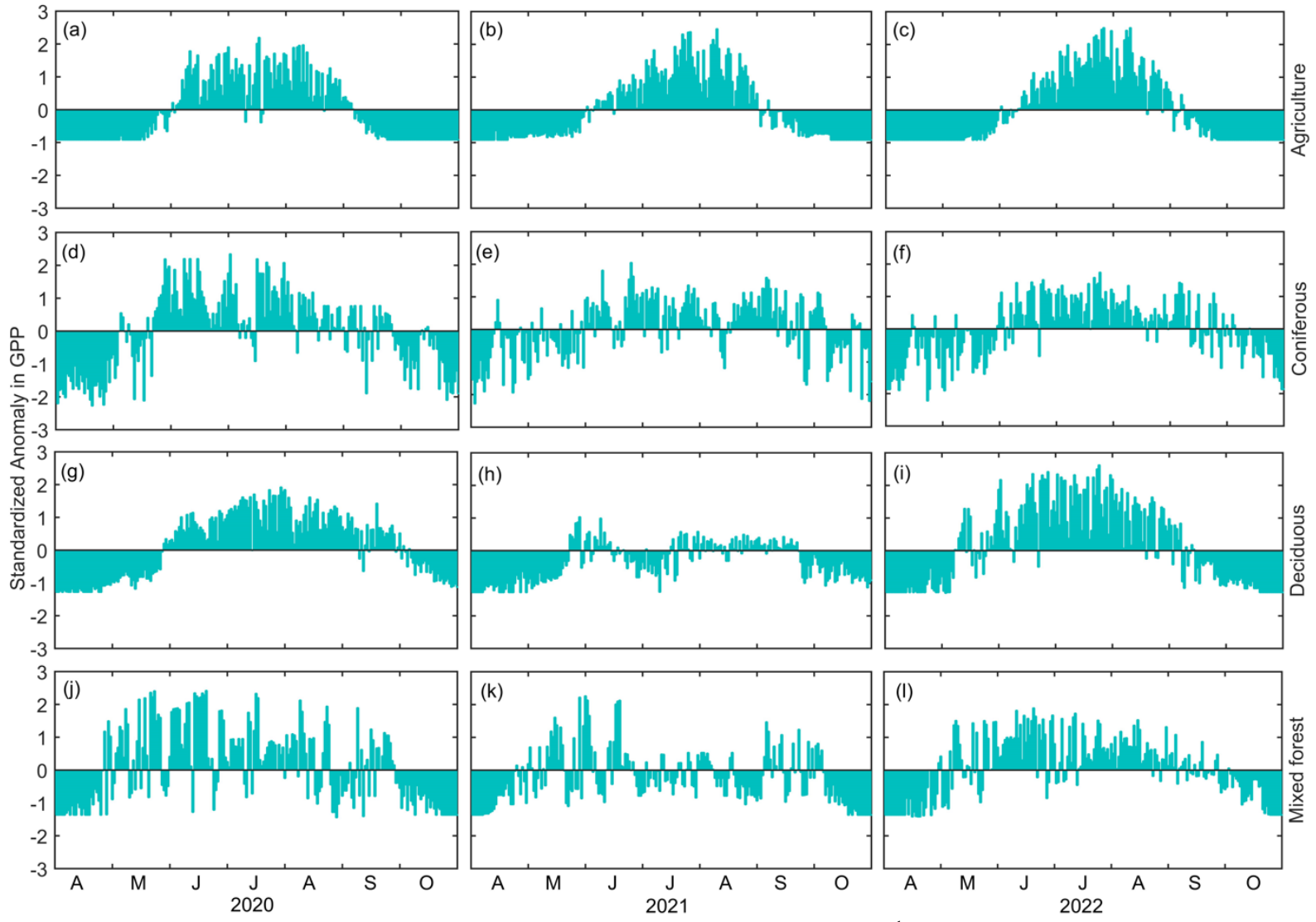


Figure 4.8. The daily standardized anomaly in gross ecosystem productivity, GPP (g C m^{-2} d^{-1}) for agricultural areas (a,b,c), conifers forests (d, e, f); deciduous forest (g, h, i) and mixed forests (j, k, l) for 2020, 2021 and 2022.

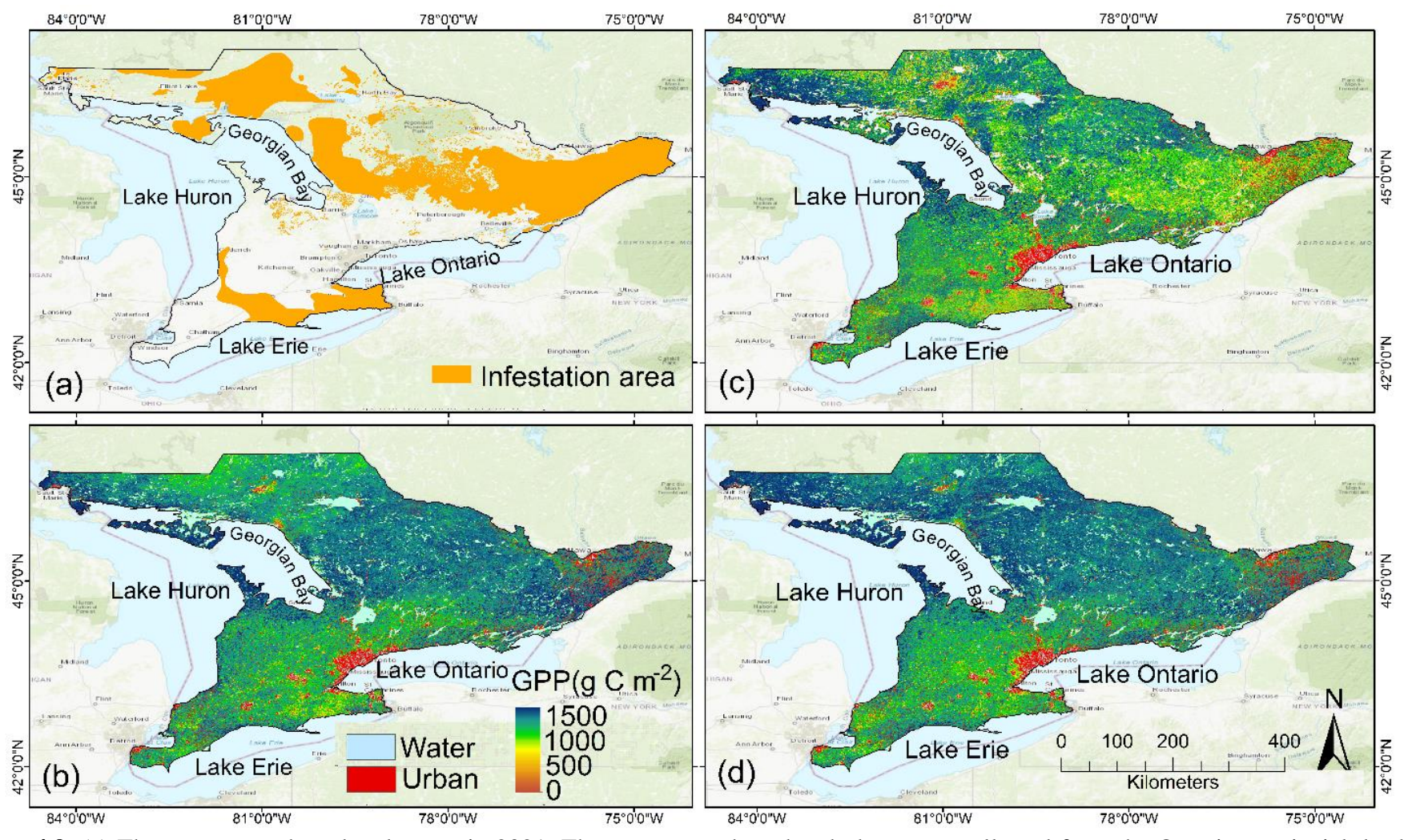


Figure 4.9. (a) The spongy moth outbreak areas in 2021. The spongy moth outbreak data were collected from the Ontario provincial database (Ontario GeoHub, 2022). The LULC map was generated by machine learning-based GEE using Sentinel-2 remote sensing data from the composite images of the growing season of 2020. The spatial pattern of total gross ecosystem productivity, GPP (g C m⁻²) over the growing season (April-October) for (b) 2020, (c) 2021 and (d) 2022.

CHAPTER 5

SUMMARY AND CONCLUSIONS

5.1 Summary of Results and Their Significance

This study examined the influence of climate variability, extreme weather events and natural and human-induced disturbances or management practices on C exchanges in agricultural and forest ecosystems in southern Ontario in the Great Lakes region. As part of this study continuous measurements of C, water and energy fluxes and meteorological variables were made in an agricultural site from 2020 to 2023. This agriculture flux site is part of the Turkey Point Environmental Observatory (TPEO), where EC flux, meteorological and ecological variables are being continuously made in three different ages (84-, 49- and 21-yr old as of 2023) of conifer forest since 2002 and a deciduous (>90-yr old) forest since 2012. The establishment of the agricultural site has allowed TPEO to become representative of the major biomes in the Great Lakes region, encompassing coniferous and deciduous forests, as well as agricultural crops. The agricultural site was planted with corn in 2020 and 2021, sweet potato in 2022 and tobacco in 2023. Study results showed that annual NEP values were 485±3.7 and $249\pm3.5~g~C~m^2~yr^{-1}$ for the corn in 2020 and 2021, respectively, $-120\pm2.1~g~C~m^2~yr^{-1}$ for sweet potato in 2022 and 7 g C m² yr⁻¹ for tobacco in 2023. It showed that site was C sink for corn, C source for sweet potato and C neutral for tobacco. The grain yields (GY) were 537, 491, 90 and 124 g C m⁻² in 2020, 2021, 2022 and 2023 resulting in annual net ecosystem carbon balance (NECB) of -52 (corn), -242 (corn), -210 (Sweet potato) and -117 (tobacco) g C m⁻² year⁻¹. This study helps to enhance our understanding of C and water flux dynamics in agricultural fields in the Great Lakes region and provides valuable data for flux up-scaling, remote sensing applications, and ecosystem modeling.

For the forest ecosystem, study utilized high resolution Sentinel-2 satellite ($10 \times 10 \text{ m}^2$) and drone-observed remote sensing data along with EC fluxes data to evaluate the effects of five different variable retention harvesting (VRH) treatments on the growth and C uptake of a 90-year-old red pine (*Pinus resinosa Ait.*) plantation (1931) forest, in Southern Ontario, Canada. CN and 55D plots consistently showed higher daily GPP values post-harvest, with CN exhibiting the highest annual GPP followed by 55D, 55A, 33D, and 33A treatments. Overall, the mean annual GPP for this 20-ha experimental site was $1651 \pm 89 \text{ g C m}^{-2}$ year⁻¹, ranging from 1407 to 1864 g C m⁻² year⁻¹. The study indicated that VRH treatment with dispersed residual canopies retaining over half of the initial basal area (i.e 55D) was the most optimized management strategy that enhanced forest growth and C uptake. Study will help forest managers to develop forest management pathways to enhance forest C uptake for nature-based climate solutions.

The study also used high-resolution satellite remote sensing and EC fluxes to investigate the impact of 2021 spongy moth (*Lymantria dispar*) infestation on forest productivity and C losses in the deciduous and mixed forests across Southern Ontario. Results showed significant (i.e 24(14)%) reduction in leaf area index (LAI) for deciduous (mixed) forests across the region with LAI values of 3.66 (3.18), 2.74 (2.64), and 3.53 (2.94) m² m² in 2020, 2021, and 2022, respectively. Similarly, growing season GPP values in deciduous (mixed) forests across the region were 1338 (1208), 868 (932), and 1367 (1175) g C m², respectively in 2020, 2021, and 2022, indicating about 35 (22)% reduction in GPP in 2021 compared to pre- and post-infestation years. It showed the large scale of C losses caused by 2021 infestation in Canadian Great Lakes region. The study emphasized the severe consequences of spongy moth infestations on forest C budget. The methods developed in the study offer valuable tools to

assess and quantify natural disturbance impacts on the regional C balance of forest ecosystems by integrating field observations, high-resolution remote sensing data and models. Study results will help in developing sustainable forest management practices in changing climate where forest infestation may be more prevalent.

5.2 Study Limitations

This research focused on to determine how plants grow and absorb atmospheric CO₂ in both agriculture and forest ecosystems using advanced remote sensing and EC flux measurements. However, there are challenges when using these techniques, like scarcity of data availability, atmospheric noise, cloudy conditions affecting data quality and differences in the timing of satellite overpasses. In forests, the accusation of understory data using both remote sensing and EC flux techniques is a major challenge (Zhang et al., 2016; Fratini et al., 2018; Xie et al., 2019; Sun et al., 2021; Wang et al., 2021). Figuring out how much understory vegetation contributes to the total C uptake of the forest is important (Thrippleton et al., 2016; Landuyt et al., 2018, Kaarakka et al., 2021). EC flux data has its own limitations such as instrument and power failures, various corrections required to process data and the inability of the sensors to capture flux data under low turbulence conditions (Fratini et al., 2018; Reitz et al., 2022). It causes gaps in data which are filled using different gap-filling methods as described in detail in individual chapters. Data gap-filling introduces uncertainties, which should be accounted while interpreting and using study results.

5.3 Suggestions for Future Research

This study helped in advancing the understanding of C exchange processes in different crops and managed forest ecosystems. It provided insight into various forest management (partial

thinning) techniques and identified appropriate harvesting density and composition that can be utilized to enhance forest growth and C sequestration. It also provided regional estimates of net C loss from deciduous and mixed forests in southern Ontario that experienced a major Spongy Moth infestation in 2021. It would be interested to observed health, growth and C exchanges of these forests over the post infestation years. There are many questions that can be further explored such as (i) how quickly these forests recovered from the infestation in terms of their C uptake and was there any changes in the balance between photosynthetic uptakes and ecosystem respiration and (ii) was there any increase in the tree mortality in the post infestation years. It would be very important to develop a mechanism to further explore the contribution of forest understory in the overall C budget for both deciduous and conifer forests. It is vital because remote sensing data mainly captures information from the canopy level. This highlights the importance of the integration of ground observation and remote sensing techniques. There is also a need to further explore the performance of VRH treatments over multiple years under different extreme weather events such as heat, drought or combined occurrence of both heat and drought events. After the application of VRH treatments, the species composition and biodiversity of the forest starts to change. These changes have impact on the key climate controls and C, water and energy exchanges. Therefore, observation and documentation of these changes is also important for future forest management regimes. In the agriculture field long term flux and remote sensing data in replicated crops will be very valuable for researchers and users. It will help to explore the potential contributions of different crops for C sequestration as part of climate mitigation efforts. Study results and long-term datasets will help in the calibration and validation of ecosystem models, remote sensing algorithms as well as developing sustainable forest and agricultural management practices to achieve net-zero C emission goals through nature-based climate change solutions.

5.4 Conclusions

This study explores the critical role of forests and agricultural ecosystems in C sequestration, offering actionable understandings for developing climate-resilient land management strategies to mitigate C losses and enhance ecosystem productivity amid ongoing climate change. It provides a significant contribution to the understanding of C exchange dynamics in the Great Lakes region, focusing on the impacts of climate variability, extreme weather, and disturbances. By integrating advanced remote sensing with continuous EC flux measurements, the study identifies crop-specific C sequestration capabilities and demonstrates how VRH enhances forest C uptake. It also quantifies the severe C losses caused by the 2021 spongy moth infestation, emphasizing the vulnerability of forests to natural disturbances.

The integration of high-resolution satellite and drone data with EC fluxes enables precise, real-time monitoring, offering crucial methodologies for upscaling carbon flux measurements and improving ecosystem modeling. These findings are essential for designing climate-adaptive management practices, particularly in enhancing carbon sequestration across forest and agricultural landscapes and advancing net-zero carbon emission goals through nature-based solutions.

5.5 References

- Fratini, G., Sabbatini, S., Ediger, K., Riensche, B., Burba, G., Nicolini, G., ... & Papale, D. (2018). Eddy covariance flux errors due to random and systematic timing errors during data acquisition. *Biogeosciences*, *15*(17), 5473-5487.
- Kaarakka, L., Cornett, M., Domke, G., Ontl, T., Dee, L E. (2021). Improved forest management as a natural climate solution: A review. *Ecol. Solut. Evid.* 2, e12090.
- Landuyt, D., Perring, M. P., Seidl, R., Taubert, F., Verbeeck, H., Verheyen, K., 2018.
 Modelling understorey dynamics in temperate forests under global change—Challenges and perspectives. Perspect. *Plant Ecol. Evol. System.* 31, 44-54.
- Reitz, O., Graf, A., Schmidt, M., Ketzler, G., & Leuchner, M. (2022). Effects of measurement height and low-pass-filtering corrections on eddy-covariance flux measurements over a forest clearing with complex vegetation. *Boundary-Layer Meteorology*, 184(2), 277-299.
- Sun, Y., Qin, Q., Ren, H., & Zhang, Y. (2021). Decameter cropland LAI/FPAR estimation from sentinel-2 imagery using google earth engine. *IEEE Transactions on Geoscience and Remote Sensing*, 60, 1-14.
- Thrippleton, T., Bugmann, H., Kramer-Priewasser, K., & Snell, R. S., 2016. Herbaceous understory: an overlooked player in forest landscape dynamics? *Ecosys.* 19, 1240-1254.
- Wang, M., Wang, S., Zhao, J., Ju, W., & Hao, Z. (2021). Global positive gross primary productivity extremes and climate contributions during 1982–2016. *Science of The Total Environment*, 774, 145703.
- Xie, X., Li, A., Jin, H., Tan, J., Wang, C., Lei, G., ... & Nan, X. (2019). Assessment of five satellite-derived LAI datasets for GPP estimations through ecosystem models. *Science of The Total Environment*, 690, 1120-1130.
- Zhang, Y., Xiao, X., Wu, X., Zhou, S., Zhang, G., Qin, Y., & Dong, J. (2017). A global moderate resolution dataset of gross primary production of vegetation for 2000–2016. *Scientific data*, 4(1), 1-13.